THE UNIVERSITY OF ADELAIDE
AUSTRALIA

Cu Mineralisation in the Middleback Ranges:

Conditions of Mineralisation.

Ryan Jones

10/25/2010

onesteel

Table of Contents

1 Abstract

The Moola Prospect situated within the Middleback Ranges on the northern Eyre Peninsula, South Australia, is comprised of potential IOCG-style, Cu mineralisation which appears to share some geological and mineralogical affinities with other IOCG deposits throughout the Gawler Craton. This recently identified mineralisation represents a new exploration region within the southern extent of the Olympic Cu-Au province which has proven to be highly lucrative with the recent discovery of the Hillside deposit in the neighbouring Yorke Peninsula. A broad investigation into host rock lithology, alteration and mineralisation paragenesis, as well as paleotemperature-pressure conditions of the deposit was carried out on drill core from OneSteel's inaugural exploratory diamond drill hole.

The mineralisation is hosted within the Paleoproterozoic Myola Volcanics, a package of rhyolites, rhyodacites and felsic gneisses which are intruded by amphibolite sills and granitic intrusives, assumed to be the neighbouring Wertigo granite. Prominently vein hosted, the mineralisation is localised around a north-northeast trending shear zone inferred to be an expression of the Kimban aged, Kalinjala shear zone which is located ~60 Km west of the Middleback Ranges. The alteration mineralogy present is divisible into two main assemblages, an early albite-epidote assemblage which has experienced extensive overprinting by the main mineralising phase associated with a quartz-carbonate-sericite± hematite-sulphide assemblage. Ore mineral paragenesis occurs as a transition of overlapping minerals that record coprecipiation. The first mineral to form was magnetite which was later extensively martitised during the transition to hematite precipitation which is preceded by a transition to pyrite, then finally chalcopyrite. A later phase of native copper mineralisation is recorded within the transecting shear zone which represents a supergene enrichment interpreted to have occurred as meteoric water gained access to depth via the structural weakness of the shear zone and remobilised any sulphides present, which were redeposited as native copper.

The temperature of mineralisation was established by TitaniQ thermometry which provided a precise temperature range between 415-530 °C with the peak at ~475 °C, which represents the conditions at which the paragenically linked quartz and mineralisation formed. Chlorite thermometry was also performed to obtain a temperature of mineralisation, with a few samples corresponding with the conditions established by the TitaniQ thermometer; however a majority of the data overestimates the temperature range by an unacceptable amount. Pressure conditions were reconstructed using the much more reliable TitaniQ temperature range inconjuntion with fluid inclusion data to establish the pressure conditions of mineralisation which ranged between ~5-7 kbar, and indicated mineralisation occurred at a deep crustal setting.

Fluid and mineralisation characteristics indicate a moderate salinity inferred from the fluid inclusions study, with NaCl ranging between 27.5-7.5 equiv wt%, along with a sulphur isotopic signature corresponding with magmatically derived fluids with the $\delta^{34}S$ ranging between -10.5 and -1.2 ‰. Which corresponds with other IOCG style mineralisation present throughout the Craton, with the Moola Prospect also being spatially associated to the interpreted source of these fluids within the Galwer Craton, the Hiltaba Suite granitoids? Even though the Moola Prospect shares affinities with IOCG style mineralisation this study cannot definitively identify its model of genesis as it also comprises characteristics that contradict this model, indicating that further study is required to better understand the extent and nature of this mineralising system.

2 Introduction

The Moola Prospect is a recently discovered, Cu mineralisation hosting, tenement located approximately 60 Km southwest of Whyalla (Fig.1), within the historically renowned iron ore mining district of the Middleback ranges, which is situated in the north-eastern corner of the Eyre Peninsula, South Australia. The prospect and the surrounding region has been the focus of recent exploration programs, by multiple companies, targeting iron-oxide copper gold (IOCG)-style mineralisation within this extent of the Olympic Cu-Au province, a highly prospective metallogenic belt of the Gawler Craton (Fig.2) which hosts some of the world's most significant IOCG deposits. ML001, the focus of this project, is the inaugural exploratory diamond drill hole put in place by OneSteel within the Moola Prospect, as part of their maiden venture into copper exploration within their existing tenements along the Middleback Ranges. Targeted within the Myola Volcanics along a strong structural shear zone running parallel to the range front, IOCG style mineralisation and alteration was predicted to occur within the area. As it contains all of the structural and geological criteria shared by other economical deposits of the Olympic Cu-Au province and was highlighted during previous RAB drilling programs as having an anomaly in the region. Despite the possible economic significance of Cu mineralisation throughout the northern Eyre Peninsular, very little has been published about the host rock geology, alteration, mineralisation or structural controls of both recent and historic discoveries. Including Rex Minerals' exploratory efforts at Cowell ~60 km south of the Middleback ranges or the old workings of the Murninnie Mine situated ~10 km south of the Moola Prospect on an adjacent structural shear zone, with no information regarding the pressure-temperature conditions of formation or a model of genesis ever being developed for any Cu mineralisation within the region. This lack of understanding promotes a considerable need to determine these characteristics in order to access the existence of IOCG mineralisation within the region and evaluate the IOCG potential of the rest of the northern Eyre Peninsula.

The Iron Oxide Copper Gold (IOCG) class of deposits encompasses a wide range of loosely related hydrothermally derived deposits ranging from the barren 'Kiruna style' magnetite-apatite deposits of Sweden to the highly enriched polymetallic deposits of the Gawler Craton, which form the two defining end members of the class. Exploration for IOCG deposits has come to the forefront in many regions throughout the world, including the Gawler Craton, due to the potential for economic grade and tonnage amongst the larger deposits. Many reviews in recent years (Groves et al.. 2010; Williams *et al.* 2005) have attempted to better define IOCG deposits in order to develop a superior exploration model for the traditional Olympic Dam style of deposit, IOCG *sensu strict (Groves et al.. 2010)*, for which the IOCG classification was initially created (Hitzman et al. 1992). These deposits generally involve highly saline, magmatically derived fluids, with some meteoric or metamorphic intermixing (Barton & Johnson 2004), and support economic Cu and Au grades along with a distinctive suit of minor element including Ag, U and REE (Hitzman & Valenta 2005). Most deposits are hosted within hydrothermal breccias, vein stockworks and disseminated throughout the host rock, whilst all under strong structural control (Hitzman 2000; Hitzman & Valenta 2005). With mineralisation consisting of predominately low S sulphides, lacking in abundant pyrite and generally not associated with abundant syn-mineralisation quartz veining or silicification (Groves et al. 2010). Extensive alteration is strongly associated with this style of mineralisation, including potassic, hydrolytic and massive, generally low-Ti iron oxide alteration focused around the major mineralising zone with a larger sodic-calcic footprint forming a regional alteration halo (Skirrow et al. 2002; Barton & Johnson 2004). From the IOCG deposits of the Gawler Craton a temporal and spatial, though only proximal, relationship has been established with the Mesoproterozoic Hiltaba Suite Granitoids (Groves et al. 2010), an extensive series of granitic intrusions which are often inferred as the source of metals and fluids for IOCG deposits. Host rock packages and tectonic setting are not defining characteristic for IOCG style mineralisation though they can affect the chemistry, mineralogy and behaviour of the hydrothermal system (Hitzman et al. 1992).

Since the discovery of the world renowned Olympic Dam deposit, the Gawler Craton has been the focus of extensive exploration programs targeting IOCG style mineralisation. These early programs lead to the establishment of the Craton's second operating IOCG mine, Prominent Hill, and the discovery of several prospective and sub economic IOCG style occurrences throughout the northern and central craton including Oak Dam, Emmie Bluff, Carapateena and Punt Hill (Brastrakov et al. 2007). From these successful discoveries, targeted IOCG exploration has expanded to cover all of the Olympic Cu-Au province including the southern extent that comprises both the Eyre and Yorke Peninsulas, which has been proven to be highly prospective with the recent discovery of the Hillside deposit (Cerlienco 2009) in the Moonta-Wallaroo district, which is about to enter into its feasibility assessment.

2.1 Geological Setting

The Middleback Ranges are located within the eastern Gawler Craton, a large and complex Precambrian basement crustal block (Fig.3). The craton records several phases of rifting and collision dating back to the Late Achaean (2560-2500 Ma) (Hand et al. 2007) and is subdivided into several tectonic subdomains based upon the variable structural and tectonic history experienced within each domain (Ferris et al. 2002). The Moola Prospect falls within the Cleve Domain, a region comprised of Paleoproterozoic metasediments, volcanics and plutonic rocks deformed into the north to northeast trending fold belt which comprises the Middleback Ranges. The presence of the Mesoproterozoic Hiltaba suite granitoids within the northern Eyre Peninsular, along with being incorporated within the Olympic Cu-Au province, earmarked the region for IOCG exploration as these intrusives are genetically linked to IOCG mineralisation throughout the Gawler Craton (Ferris et al. 2002). As well as the Cleve domain the Olympic Dam Cu-Au province spans the Spencer Domain, Olympic Domain, Gawler Range Volcanics Domain along with part of the Mt Woods Inlier (Skirrow et al. 2002) and hosts two operational IOCG mines; the supergiant

Olympic Dam and Prominent Hill, which along with many prospective occurrences including Hillside, Oak Dam, Carrapateena and Emmie Bluff (Brastrakov et al. 2007) make it one of Australia's most prominent IOCG provinces.

2.1.1 Regional Geology

-Archaean-

The basement underlying the Moola Prospect has been inferred to be a series of highly deformed layered crystalline Archaean gneisses of the Sleaford Complex (Parker & Fanning 1998). Comprised of the Carnot Gneiss, Wanangary Gneiss and the Dutton Suite this package was deformed during the Sleaford orgeny (~2440 Ma) and is believed to extend north eastwards towards Whyalla underlying much of the Eyre Peninsular (Parker & Fanning 1998). Outcropping predominantly within the southern expanse of the peninsula the extent of the Sleaford complex is highly ambiguous due to the dominance of tertiary and quaternary sediments within the Pirie Basin, as such is only assumed to be underlying the Moola Prospect with no confirming outcrop existing within the region (Parker & Fanning 1998).

-Proterozoic-

The intrusion of the Miltalie Gneiss (~2000 Ma) within the Sleaford Complex marks the end of the Archaean basement development within the Eastern craton (Hand et al. 2007), transitioning into a period dominated by multiple rift basin formations along the margin of the late Archaean Gawler Craton in which the Hutchison Group (2000-1850 Ma) was unconformably deposited (Vassallo & Wilson 2001). The Hutchison Group metasediments are the major lithological units that comprises the Middleback Ranges, consisting of a massive, basal quartzite (Warrow Quartzite) overlain by an interlayered sequences of carbonates and iron formations (Katunga Dolomite, Upper and Lower Middleback Jasperlite) which are accompanied by the politic to semi politic Cleve and Yadnarie schists, to form the Middleback Subgroup (Parker & Fanning 1998).

Interrupting this extended period of rift basin formation is the syn-tectonic magmatism responsible for the formation of the Donnington Suite (1850 Ma) which outcrops east of the Moola prospect and is associated with the Cornian Orogeny which is responsible for the change to a compressional tectonic setting (Hand et al. 2007). Rifting along the craton's eastern margin resumed after the deposition of the Donnington Suite at approximately 1791± 4Ma which is recorded by the eruption of the bimodal Myola volcanics (Hand et al. 2007) and the associated clastic sediments of the Broadview Schist. The Myola Volcanics , the host rocks of the Cu mineralisation within the Moola Prospect, are classified as a sequence of deformed, strongly laminated, porphyritic rhyolite, interbanded with rhyodacite along with occurrences of amphibolites sills and fine-grained felsic gneisses, most of which has experienced upper greenschist → lower amphibolites facies metamorphism (Parker & Fanning 1998). Often intruding the Myola Volcanics is the moderately foliated Wertigo Granite, one of many igneous intrusives associated within the Lincon Complex. In conclusive dating of the Wertigo Granite provided an age of 1828±34 Ma (Parker & Fanning 1998) which does coincide with the uncertainty of the Myola Volcanics age (1791±4 Ma) but is poorly defined as most zircons experienced a loss of radiogenic lead during the Neoproterozoic (Parker & Fanning 1998).

Sedimentation and volcanism continued sporadically within the eastern Gawler Craton during the Paleoproterozoic with the extensive widespread extrusion of the McGregor Volcanics at ~ 1740 Ma (Fanning et al. 1988). The bimodal McGregor Volcanics outcrop ~10 Km south of the Moola Prospect, restricted to the Moonabie region, sandwiched between the range front and the intrusive Charleston Granite further to the south. The Charlseton Granite represents the intrusion of the Hiltaba suite granitoids (1600-1585Ma) within the region, which are spatially associated IOCG mineralisation and a vital piece of exploration models within the Gawler Craton. Dated at 1585±5 Ma the Charleston granite (Parker & Fanning 1998) is a massive, undeformed, homogeneous granites composed of dominant, K-feldspar phenocrysts within a course-grained matrix.

2.2 Structural setting

The Kalinjala shear zone is the dominant structural feature within the Middleback region, situated ~60 Km west of the Middleback ranges, this 4-6 Km wide sub-vertical high strain zone records granulite facies metamorphism and dextral transpressional movement over is ~200 Km long extent (Hand et al. 2007). Forming during the 1730-1690 Ma Kimban Orogeny (Vassallo & Wilson 2002), like much of the structural architecture and metamorphism recorded within the Palaeoproterozic metasediments, deformation throughout the region associated with the Kalinjala was not only confined to the main shear zone but also occurred within a 50 to 100Km wide area (Hand et al. 2007) adjacent to the major structure (Fig.4). Within the Middleback ranges this is expressed as the series of north-northeast trending shear zones running throughout the range front and surrounding depositional plains (Fig.5). The Moola Prospect is situated upon one of these major splays which run along the range front and was the reason for it being targeted for exploration due to the strong structural controls associated with IOCG style mineralisation.

2.3 Previous Studies

Previous geological studies of the Middleback Ranges and the greater Whyalla region stem largely from the early pioneering discoveries of such economically viable deposits as the Wallaroo-Moonta-Kadina copper prospects and the iron ore resources of the Hutchison group at Iron Knob in the mid to late 19th Century which were extremely important in establishing those regions mining history and highlighting them for potential future discoveries.

The iron ore deposits of Iron Duke, Iron Duchess and Iron Baron have been the focus of a majority of the Middleback Ranges ore deposit research targeting the structure, lithology and genesis of the banded iron formations within the Middleback subgroup. The Myola volcanic, the host rock for this project, has had very little research performed on it since their initial mapping by A.J. Parker during the late 1970's, whilst compiling data for the

construction of the Whyalla 1: 250 000 geological map sheet. Several papers do use the unit during geochronology (Fanning et al. 1988; Webb et al. 1986; Wyborn, Page & Parker 1987) in order to reconstruct and constrain ages for the formation of the Gawler Craton, via both direct and indirect dating of the volcanics and associated units such as the Broadview schist contained within the Myola Volcanics, but otherwise little is known about them.

-Project Aims-

The aim of this study is to investigate the fundamental properties of copper mineralisation identified within exploratory diamond drill core samples from the Moola Prospect obtained by OneSteel. Host rock identification along with alteration and mineralisation paragenesis will be the primary objectives to characterize the hydrothermal system involved. Whilst pressure-temperature conditions and fluid characteristics will be targeted for comparison against other major copper mineralising deposits throughout the Gawler Craton to reconstruct a possible model of genesis and gauge the proposed IOCG style system theorized by the exploration model.

3 Preliminary Study

3.1 Field Mapping

From the initial background research into the Moola Prospect the feasibility of a field mapping component to this research looked viable with multiple geological maps showing abundant outcrop in the area, including a detailed 1:20 000 construct map compiled by A.J Parker targeting the Myola Volcanics. Once in the field it became apparent that this portion of the project would have to be reconsidered as a brief traverse across project area and a visit to the ML001 drill site highlighting the dominance of the tertiary sedimentary cover and overall lack in out crop within the project area. After visiting the site of A.J Parker's map the decision was made to abandon this portion of the project as the limited outcrop available showed evidence of extensive deformation making the lithology hard to determine and any data obtained unreliable.

3.2 Core Logging Study

Preliminary core logging was undertaken with the specific objectives of classifying host rock units, identifying mineralisation and alteration present, as well as to determine the analytical procedures available for use upon the samples to establish the conditions of mineralisation.

3.2.1 Alteration

Much of the core recovered from ML001 show signs of alteration which makes reconstruction of the host rock types difficult and when combined with extensive weathering nearly impossible. The alteration sequence established from core logging is summarized below, in chronological order, and was derived from observational conclusions drawn from replacement patterns, mineral overprinting and cross cutting features within the core.

- Potassic ± sodic feldspar alteration
- Widespread green sericite alteration of feldspars

- Possible epidote
- Extensive, both large and small scale, quartz veining- Main mineralising phase
- Chlorite alteration
- Carbonate veining –Also hosts mineralisation

3.2.2 Host Rock

From ML001 approximately 249m were drill at a 60° angle reaching an estimated depth of ~215m , with a core recovery of ~90% , a majority of which was experienced in the initial 15m of Tertiary sediments and highly weathered parent rock due to the use of a precollar during drilling. Five distinctive host rock types were identified during core logging along with two additional intrusive units a majority of which were able to be classified.

The first drill core samples recovered consisted of a highly weathered, saprolitic felsic volcanic unit which is largely unstable and brittle (Fig.6A), with the original rock type unable to be determined due to the extent of weathering and alteration it has undergone. Composed predominantly of light brown to dark grey, quartz and remnant feldspar phenocrysts it also contains a significant clay component, a bi-product of feldspar weathering. Evidence of possible sodic and/or potassic feldspar alteration is present in sections as veins. With an increase of depth came a decrease in the amount of weathering affecting the felsic volcanic unit which extended to approximately 65m where there was a transition into a banded felsic gneiss unit.

This unit is composed of pink-grey, fine grained, strongly foliated, quartz and feldspar layers composed of elongate flattened aggregates which form the gneissic texture (Fig.6B). Along with feldspar rich bands which are highlighted by extensive sericite alteration of the feldspar phenocrysts, which gives these layers a distinctive green colouring.

Intrusive bodies are found cross cutting throughout the banded felsic gneiss, including a 1-2m thick fine grained, green-black amphibole-plagioclase-biotite massive amphibolite

(Fig.6C), which hosts possible magnetite mineralisation indicated to the strong magnetic response (108m). Other intrusive bodies include those found in the upper and lower extents of the banded felsic gneiss unit (85,135m), comprised of course grained pink K-feldspar- (plagioclase), quartz- muscovite granites, which displays a dominant equigranular texture (Fig.6D).

Interfingering of the banded felsic gneiss by the granite occurs within the proximity of these large intrusions, gradually decreasing in size and frequency the further away from the initial occurrence. This is most prevalent around the second intrusion at the bottom extent of the unit, which marks the transition into the rhyolite unit.

The rhyolite unit is composed of red/pink fine to medium grained quartz and feldspar dominant ground mass which supports K-feldspar phenocrysts, forming a porphyritic texture (Fig.6E). Interlayering of the rhyolite by the banded felsic unit was picked up during detailed logging for the collection of petrographic samples, which highlighted that the true extent of these units is highly ambiguous as they are compositionally similar and often mistakenly classified, with the possibility that more extensive interlayering of the units could have occurred but were not picked up in the initial core logging.

Marking the end of the rhyolite unit is a very distinct transition into an unconsolidated highly weather green/white to green/grey volcaniclastic unit (Fig.6F), comprised predominantly of a quartz matrix which houses large unidentifiable phenocrysts forming a porphyritic texture. Both large and small scale voids occur throughout the unit formed via the complete weathering of select minerals. Chlorite alteration is still seen throughout the matrix along with occurrences of native copper, malachite and a notable lack of any other mineralisation.

Preceding this highly weathered zone is a transition to a dark grey fine grain rhyodacite unit which houses extensive carbonate veining, along with chlorite alteration throughout (Fig.6G). Highly siliceous banding showing signs of possible tectonic fabrics become

prominent towards the bottom of the hole but gives way to the extensive brecciation and K-feldspar alteration which marks the end of the drill hole.

In summary most of the drill core is largely uniform across each rock type, with only slight variation in the dominance of structural features such as minor brecciation. Both large and small scale veining is also prominent throughout the core, typically quartz dominant, but with an exception within the rhyodacite which shows a preference for carbonate veining which still host mineralisation.

3.2.3 Mineralisation

Varying degrees of mineralisation were found across a majority of the drill core, excluding the felsic volacanic and volcaniclastic units. Chalcopyrite was found to be the dominant form of mineralisation, found across a majority of the lithologies hosted within both carbonate and quartz veins (Fig.7A-B) and to a lesser degree disseminated throughout the host rock, which is generally reflected in the amount of brecciation present. Pyrite occurs in much the same style but in significantly less quantities, generally accompanying chalcopyrite within quartz veins. Hematite is notably absent in large quantities, only found within isolated veins and brecciation, but red colouring throughout the host rocks does indicate it may still be present. And the use of a magnetometer also highlighted the possible presence of magnetite within certain sections of the drill hole but not in excessive amounts.

3.3 Preliminary Study Recommendations

From preliminary core logging we obtained the first overview of the host rock types and alteration present within the Moola Prospect allowing assessment of viable analytical procedures to classify the relic hydrothermal system present and establish the conditions at which it was active. Petrographic samples were taken for the production of both thin sections and polished block samples by Pontifex Petrographic Services Ltd, with the thin sections to be used in classifying the host rock types and to further define alteration paragenesis, while polished blocks are to be used in establishing the paragenesis of

mineralisation. The abundance of both quartz veining and chlorite alteration identified during logging allows the application of TitaniQ and chlorite geothermometry to obtain the temperature conditions of mineralisation and alteration. With the associated pressure conditions and relative salinity of the fluids to be established via fluid inclusion analysis performed by Dr. Andreas Schmidt Mumm upon thick sections of targeted quartz veins. The abundance of sulphide mineralisation throughout the drill hole also allows the application of sulphur isotope analysis to establish a possible temperature of mineralisation via the investigation of isotopic fractionation between co-precipitating minerals and to obtain information about the origin and composition of hydrothermal fluids

4 Analytical Procedures

4.1 Petrography

Following the initial core logging stage representative samples were taken from ML001, targeting alteration, mineralisation and each host rock unit, from which thin sections and polished block samples were produced for the identification of ore and alteration mineral assemblages. The polished block samples were studied via reflective light microscopy to identify the ore minerals incorporated in the mineralisation and to establish their paragenesis. Whilst the thin sections were studied via transmitted light microscopy to further classify the host rock units, identify the alteration minerals present and establish their paragenesis. Microprobe analysis was also used in conjunction with the microscope petrography to assist in the identification of unknown minerals present.

4.2 Chlorite Geothermometry

Throughout ML001 chlorite was identified as a prominent hydrothermal mineral on which geothermometry could be applied (De Caritat et al. 1993). Chlorite geothermometry is performed via analysis, using an electron microprobe, of the elemental composition of the chlorite present within the hydrothermal system, which can be highly variable, existing within a continuum between its four major end members. This change in composition is temperature dependent and is targeted around the systematic increase in Al^{IV} and decrease in Si^{IV} within chlorites tetrahedral sites along with the increase in total amount of Fe/Mg and decrease of Al^{VI} at the octahedral sites (De Caritat et al. 1993).

In this study three well accepted equations, designed around the identified temperature dependent compositional change in chlorite, were utilised to calculate the temperature at which the sampled grains formed.

(Cathelineau & Neiva 1985) $$T = -61.92 + 321.98\, Al^{IV}$$

(Kranidiotis & MacLean 1987) $$T = 106\, Al_C^{IV} + 18$$

* Where Al_C^{IV} is a corrected Al^{IV} value which accounts for variation in Fe/ (Fe + Mg) and is calculated according to:

$$Al_C^{IV} = Al^{IV} + 0.7\left(\frac{Fe}{[Fe + Mg]}\right)$$

(Jowett 1991) $$T = 319\, Al_C^{IV} - 69$$

* Where Al_C^{IV} is again a corrected Al^{IV} value which accounts for variation in Fe/ (Fe + Mg) and is calculated according to:

$$Al_C^{IV} = Al^{IV} + 0.1\left(\frac{Fe}{[Fe+Mg]}\right)$$

-Electron Microprobe-

To perform the necessary analysis, Adelaide Microscopy's Cameca SX51 Electron Microprobe was utilized to obtain non-destructive, high spectral resolution, compositional data of the targeted chlorite grains. An accelerating voltage of 15kV and a beam current of 20nA provided the appropriate spot size and beam strength to accurately sample the chlorite via the detection and interpretation of the multiple, unique x-ray wavelengths emitted by the sample whilst in contact with the beam. This data provides the necessary weight percentage of each compositional element within the chlorite, required to calculate its temperature of formation.

4.3 TitaniQ Thermometry

Identified during preliminary core logging, quartz veining is prominent throughout ML001, often associated with sulphide and oxide mineralisation, allowing the application of

Titanium-in-Quartz (TitaniQ) thermometry to obtain the temperature at which the quartz present formed. This technique is based upon the temperature dependent substitution of Si by Ti within quartz's crystal structure and is an accurate geothermometer operating in a ± 5°C range of error (Wark & Watson, 2006) due to the simple, one for one, balanced cation exchange that requires no additional elements involvement.

In this study the following equation, designed around the identified temperature dependent substitution within quartz's crystal structure, was utilized to calculate the temperature at which the sampled grains formed.

$$\mathrm{T}\ (^{\circ}\mathrm{C}) = \frac{-3756}{\log\left[\frac{\mathrm{X}_{\mathrm{Ti}}^{\mathrm{qtz}}}{\alpha_{\mathrm{TiO2}}}\right] - 5.69} - 273$$

*Where α_{TiO2} = 1 when Ti-bearing minerals are paragentically associated with the quartz (Wark & Watson, 2006)

There are some prerequisites and limitations to the application of this geothermometer, mainly based upon the need for Ti saturation during the phase of quartz formation, which is established via the coexistence of Ti-bearing minerals within these veins and was verified by the presence of fine grained rutile needles within multiple thick section (Fig.8) along with illmentite identified by Ben Cave during Microprobe analysis of the polished block samples (Cave 2010). Pressure is also a factor that can affect the temperatures obtained via this technique as methodological reviews have highlighted a systematic decrease in the solubility of Ti in quartz at higher pressures. The inaccuracy caused by this pressure effect is not fully defined but is stated to effect solubility between 5→20 kbar (Thomas et al. 2010).

-LA-ICP-MS-

To perform the necessary analysis, Adelaide Microscopy's New Wave Research Merchantex Products UP-213 Laser Ablation System in conjunction with an Agilent 7500 Series ICP-MS was utilized, due to its superior detection limit, for the acquisition of Ti

trace element concentrations within the sampled quartz grains. A continuous beam of 5Hz with a spot diameter of 65µm set at 75% power was used to ensure adequate sample is aerosoled, without contamination from underlying glass slide, for analysis by the ICP-MS. During analysis a suite of elemental isotopes, Na^{23}, Al^{27}, Si^{29}, Cl^{27}, K^{39}, Ca^{43}, Ti^{47}, Ti^{48}, Ti^{49}, $Fe^{57}$and Cu^{63}, were sampled for quality assurance of the data obtained, along with the careful selection of quartz grains prior to analysis which eliminates any chance of contamination from oxides or sulphides inclusions. Investigation into the different stages of quartz growth, represented by the transgression from a cloudy core to a clear rim in most grains, was also performed to access any possible transition in temperature conditions.

During analysis multiple standards were implemented in order to obtain the relevant data. External standard, Nist-612, was used for the qualification of the results, which is achieved via the comparison of its known values against the unknowns obtained during analysis. Nist-614 was implemented to monitor instrumental drift with its values put on a linear fit and the relevant corrections applied to the data, whilst internal standard Si^{29} was also implemented to account for the difference in ablation experienced between the standards and the sample spots during analysis.

4.4 Sulphur Isotope Analysis

Sulphur isotope analysis was undertaken with the objectives of establishing a possible temperature of mineralisation via the investigation of isotopic fractionation between co-precipitating minerals and to obtain information about the origin and composition of ore fluids via the investigation of the isotopic ratios between sulphurs two major stable isotopes, ^{32}S and ^{34}S. This ratio is obtained via the application of the following equation:

$$\delta^{34}S = \left\{ \frac{\left(^{34}S/^{32}S\right)sample}{\left(^{34}S/^{32}S\right)standard} - 1 \right\} \times 100$$

*Where the $\left(^{34}S/^{32}S\right)\ standard$ values represent the Vienna Cañon Diablo meteorite troilite (VCDT), used as a reference in the sulfur isotope scale.

Representative samples were identified through the preliminary core logging, covering the range of host rock types, styles of alteration and mineralisation types present in order to cover as much mineralogical variation as possible.

All samples were extracted using either a high powered mounted rotary tool with a tungsten carbide drill bit or for whole rock samples using a ceramic jaw crusher to reduce the size of the sample so individual sulphide grains could be hand sorted to reduce any possible contamination. If required the samples were powderised using a mortar and pestle to achieve the appropriate grain size for analysis.

- Mass Spectrometer-

All powdered samples were collected in 2ml vials ready for analysis, which due to technical difficulties with the University of Adelaide's Fusions Optima Mass Spectrometer was outsourced to GNS Science, a New Zealand government-owned research organization. Duplicates of each sample were weighed out and placed in tin capsules with equal amounts of V_2O_5 for analysis using GNS Science's EuroVector Elemental Analyser in conjunction with a GVI IsoPrime mass spectrometer to obtain the relevant sulphur isotope data targeted around the S^{32} and S^{34} relationship. The use of three independent internal standards, R18742, R2268 and R2298 was implemented to normalise the sample data against their known values to calibrate for any instrumental error.

4.5 Fluid Inclusion Study

The study of fluid Inclusion was undertaken with the objectives of establishing the temperature and pressure at which they formed along with their relative salinity composition. This technique is based around physical observations of the internal fluid component of the inclusions which is performed under a cooling and heating regime observing freezing point, eutectic melting stages and vapour phase behaviour. The temperatures at which these characteristics occur then indicate the approximate salinity and homogenization temperature (TH) of the fluid inclusions.

From the preliminary core logging, quartz veins were identified as the most likely medium in which fluid inclusions would occur and as such a total of 10 samples, representative of all mineralisation hosting quartz veins across each host rock type, were selected to gauge the extent of the fluid inclusions present within ML001. However only two samples were found to contain acceptable amounts of fluid inclusions for study, A1st01 and A1st03, the former of which was deemed the most suitable and selected for thermometric analysis.

-Fluid Inclusion Microscope-

In order to observe the fluid inclusions, the double polished thick section, approximately 300µm thick, was prepared for use on the University of Adelaide' Linkam THM600 Heating and Cooling stage, this was done by submerging the thick section in acetone for an extended period in order to dissolve the adhesive from backing glass slide. Meanwhile, calibration using four independent standards (H_2O-CO_2, H_2O-NaCl eutectic composition, pure H_2O and H_2O-KCl eutectic composition) was utilized to establish the appropriate corrections required for the quality assurance of the salinity and homogenization temperature obtained. Once separated the targeted section, identified during the petrography study to contained relatively large, fairly irregular inclusions, was fragmented into an appropriate chip size to fit in the microscope stage, ready for analysis.

With capabilities of reaching -190°C and upwards of 700°C, the Heating and Cooling stage was used to controllably cool the sample via the application of liquid nitrogen until the freezing point of the internal fluid (Tf) was reached at which the exact temperature was recorded. Switching the stage to heating the temperature was controllably increased and observations performed on the internal fluid for the first signs of eutectic melting (Te) at which the temperature was recorded along with the eutectic melting temperature of the individual solid phases (TmHH, TmICE) identified within the inclusion as heating was applied which are used to approximated the salinity of the inclusions. Once melted, the heating of the sample was increased until the vapour phase within the inclusion diffused with the fluids, which corresponds to the temperature of homogenisation (Th).

5 Results

5.1 Petrography

Full petrography report of thin sections can be found in Appendix.1

5.1.1 Host Rock

Five distinctive host rock types and two additional intrusive units have been identified during the initial core logging and petrographic study of the representative thin sections, all of which have undergone some extent of alteration making interpretation of the original lithology difficult.

The most affected by this was the felsic volcanic unit (Fig.9 A-B) which is comprised of remnant feldspar phenocrysts that have been fully replaced by sericite alteration forming pseudomorphs, which are hosted within extensive fine to medium grained platy chlorite. Distinct banding of epidote accompanies these phenocrysts along with occurrences of equant quartz. A large scale vein network cross cuts the unit which are comprised of illite, a clay bi-product of feldspar weathering which has also stained the chlorite surrounding the veins a distinctive yellow colour.

The felsic gneiss unit (Fig.9 C-D) consists of strongly foliated elongate flattened aggregates of quartz and feldspar which form the gneissic texture, along with feldspar rich bands which are highlighted by extensive sericite alteration. This sericite alteration of the predominantly plagioclase feldspar component varies between partial and full replacement, forming pseudomorphs. Accessory minerals present include fine grained muscovite present in and around the larger aggregates or as course grained tabular occurrences.

The Amphibolite unit (Fig.9 E-F) was composed of hornblende and relic plagioclase banding which has been extensively affected by sericite alteration having fully replaced the feldspar component of the sample. Chlorite alteration is also present effecting the hornblende, which is replace in the proximity of fine scale carbonate veining present

throughout the unit. Extensive opaques are housed throughout the unit, which were identified as the martitzation of magnetite by hematite which is present at varying stages from partial replacement to the full formation of martite. The textures indicate that this unit was most likely derived from either fine grained dolerite or course grained basalt (Parker & Fanning 1998).

The granite unit (Fig.9 G-H) was comprised of course grained feldspar phenocrysts housed within an interlocking quartz matrix forming equigranular texture. Both plagioclase and microcline were identified amounts the phenocrysts which have undergone varying degrees of sericite alteration from partial to full replacement forming pseudomorphs. Accessory minerals found within the unit include sparse tabular muscovite and dark green anhedral amphiboles.

The rhyolite unit (Fig.9 I-J) consists of large feldspar phenocrysts in fine grained matrix forming a porphyritic texture. The phenocrysts are comprised of both plagioclase and microcline which have undergone varying stages of sericite alteration from partial to full replacement forming psuedomorphs Accessory minerals found within the unit include some minor sparse tabular muscovite.

The volcanoclastic unit (Fig.9 K-L) represents a highly weathered fault zone which transects the upper portion of the rhyodacite unit and contains large relic phenocrysts of feldspar alteration which themselves have been fully replaced by sericite. These phenocrysts are housed within a fine grained quartz and sericite matrix which is cross cut by extensive quartz veining. Trace amounts of chlorite alteration is still present but appears highly weathered and there is a notable absence of mineralisation within the samples, which is due to the remobilization of the sulphides and oxides by meteoric water which gains access to depth via the structural weakness of the transecting shear zone. Occurrences of supergene native copper are found throughout the unit within the extensive brecciation or void space left by weathered minerals, which is the product of this remobilization and weathering of sulphide mineralisation.

The rhyodactie unit (Fig.9 M-N) consists of some highly variable sections but is predominantly comprised of fine grained quartz and sericite matrix with a dominant fine to medium grained platy chlorite component which along with the fine grained hematite mineralisation defines the linear foliation of the rock. Brecciation is variable throughout the unit, which gives rise to greater amount of disseminated mineralisation then seen elsewhere in the core, and is accompanied by deformation of the foliation. Highly siliceous banding also becomes prevalent toward the bottom of the hole which also records deformation in its fabric, which gives way to extensive potassic alteration which marks the end of the hole.

The host rock package found in ML001 corresponds with the expected Myola Volcanic suite targeted for exploration and the existence of a crosscutting shear zone within the core confirms presence of the structural control required for IOCG style mineralisation.

5.1.2 Alteration

The hydrothermal alteration present throughout the core samples appears to be dominated by one major assemblage which has overprinted or replaced pre-existing stages making the timing and extent of these assemblages difficult to reconstruct, which is compounded by only being present in a minimal selection of slides.

-Albite-Epidote -

The earliest alteration identified is an albite-epidote assemblage that was only observed in representative samples obtained from the weathered felsic volcanic unit at the top of the hole. Distinctive fine grained banding of epidote was seen throughout these samples in conjunction with large sericite pseudomorphs of feldspar phenocrysts, which are inferred to be relic albite alteration based on the simple twinning observed in a few partially intact phenocrysts. Though not seen in representative samples minor magnetite mineralisation does occur in proximity to this assemblage, which is supported by magnetic susceptibility measurements of the core. There is a distinct possibility that other occurrences of this

alteration assemblage could exist throughout the hole, however none were identified or sampled during core logging.

- Quartz-carbonate-sericite Assemblage-

The most widespread and dominant alteration identified is comprised of a quartz-carbonate- chlorite-sericite-K-Feldspar± hematite-sulphide assemblage which overprints and replaces previous alteration stages. Quartz-carbonate-sericite are the most prevalent components of this assemblage, with vein networks dominant throughout all of the core and sericite nearly fully replacing all pre-existing feldspar components of the host rock. There is an identified preference for carbonate veining toward the bottom of the hole, in the rhyodacite unit, with the upper portion generally quartz dominant. Mineralisation is hosted within both styles of veining which record multiple cross cutting generations. Extensive chlorite alteration is also preferential localised within the more mafic rhyodacite unit found throughout the host rock and incorporated within veins. K-feldspar alteration within this assemblage is easily identified by the minimal amount of sericite alteration it has undergone with some nearly fully intact phenocrysts present.

5.1.3 Mineralisation

Multiple types of mineralisation were identified during petrographic study of the core which include: sulphide mineralisation , both chalcopyrite and pyrite, which are predominantly hosted within both quartz and carbonate veins comprised of multiple crosscutting generations, though disseminated occurrences do coincide with the areas of minimal brecciation present throughout the core. Hematite mineralisation present within the core is not easily identified in rock sample but further investigation via the petrographic study does highlight its presence, both disseminated throughout the host rock and housed within veins. Limited occurrences of magnetite are also present throughout the core though the true extent is unknown as representative sampling did not effectively pick up this component of the mineralisation.

- paragenesis -

Ore mineral paragenesis was established via reflected light microscopy of representative polished block samples. The first possible ore mineral to have precipitated from this hydrothermal system is magnetite which is found prominently disseminated throughout the amphibolite unit, with minor occurrences experienced within a highly altered section of the rhyodactite. No petrographic evidence is found associating it to any alteration assemblage indicating that magnetite could in fact be pre-existing mineralisation. The second stage of mineralisation identified was hematite which was established via the martitisation of magnetite (Fig.10A) present as both advanced and total replacement. Hematite is then found co-precipitating with pyrite (Fig.10B) before pyrite become sole mineralising phase , where there is a transition from hematite and pyrite showing a cogenetic relationship to where only small hematite occurrences are found around the outer rims of larger pyrite growths (Fig.10C). Chalcopyrite was the final phase in mineralisation showing extensive infilling of fractures within the pyrite along with cogenetic relationships (Fig.10D). Native copper is found localised within the volcanoclastic unit (Fig.10E), disseminated throughout the extensive brecciation. Its presence is interpreted as a supergene enrichment as meteoric water gains access to depth via the structural weakness of the crosscutting shear zone, remobilising any sulphides present which are in turn redeposited as native copper. No gold or uranium bearing minerals were observed during the petrographic study but further investigation would be required to dismiss their presence.

5.2 Chlorite Geothermometry

Using reflected and transmitted microscopy during the petrography study, chlorite was found in equilibrium with at least one stage of quartz and often with sulphides and oxides, generally occurring along the outer extent of quartz veins, as growth rings around large phenocrysts or as a major component of the rhyodacite unit which appears to have undergone extensive chlorite alteration.

From the raw data, all ambiguous spots were filtered out for quality assurance of the temperatures calculated (Table.1), this is done by implementing several criteria upon the data collected including eliminating any data points with an abnormally high weight %, as chlorite contains a high percentage of water within its structure, which is excluded from the microprobe analysis, and as such should be reflected by a deficient weight%. Samples deficient in chlorites major compositional elements (Al, Fe, Mg) are also excluded , which indicates these spots were in fact not chlorite, whilst samples containing in excess of 0.5 total% Ca, Na and K, were also omitted as it indicates the sample is impure, probably containing inclusions of quartz, carbonate or interlayering of other sheet silica minerals (Cathelineau & Neiva 1985).

114 sample spots, from the five different thin selections, were deemed suitable for chlorite geothermometry with classification based upon the Si vs Fe/(Fe+Mg) ratio system (Hey, 1954) indicating that a majority of the chlorites sampled falls within the pycnochlorite field with the rest falling into the ripidolite, brunsvigite or diabantite fields (Fig.11).Temperature calculations were performed via the application of A.G Tindle's Chlorite Geothermomentry spreadsheet, which contains all of the previously stated equations and is based upon the assumption of 28 oxygens along with recalculated Fe^{2+} /Fe^{3+} ratio and OH^- concentrations assuming full site occupancy (Tindle 1999).

From the petrography study it can be assumed that chlorite alteration and mineralisation are paragenetically linked as they coexist exhibiting paragenetic relationships, though the relationship of chlorite is not as strong as quartz's as chlorite appears to occur early in the paragensis occurring along the margins of quartz veins. As such the temperature conditions established form the chlorite thermometer which depicts the temperature of chlorite formation can be inferred to represent the temperature conditions of mineralisation as they formed under the same conditions.

5.3 TitaniQ Thermometry

From the raw data, all ambiguous spots were filtered out for quality assurance of the calculated temperatures (Table.2), this is done by eliminating spots that contain anomalous levels of K, Ca or Na, (> 500, 300 and 300 ppm respectively), which usually indicate that the sample spot was either not a quartz grain or contained feldspar and/or carbonate inclusions. Fe and Cu concentrations (> 50 ppm) are similarly used to identify samples spots contaminated by oxide or sulphide inclusion and excessively high Ti levels(> 10ppm) were excluded as it indicates the spot was in the proximity of or in contact with sub-surface rutile needles and as such are invalid for thermometric calculation.

Three titanium isotopes were specifically during analysis to reduce the effect of polyatomic and molecular ion interference from the ICPMS on the temperatures obtained. There are several background molecule ions formed from argon plasma, nebulizer water and dissolved air during ICPMS analysis that can affect the concentration of the three most abundant Ti isotopes, ^{47}Ti, ^{48}Ti and ^{49}Ti (Fig.12). From which ^{47}Ti appeared to be the most reliable, which is supported by the quality of the data obtained, as it is effected by the least interference ions and not effected by any sulphur based interference (eg ^{48}Ti: $^{32}S^{16}O^{+}$, ^{49}Ti: $^{32}S^{17}OH^{+}$, $^{32}S^{16}OH^{+}$, $^{34}S^{15}N^{+}$, $^{33}S^{16}O^{+}$) which is most likely to occur due to the sulphide mineralisation present in the samples and as such was chosen for use in the thermometric calculations.

70 sample spots, from four different slides, were deemed suitable for TitaniQ thermometry with their Ti concentrations ranging between 1.58 and 9.97 ppm, summarized in Table.2. The temperature of quartz formation were calculated via the application of an Titanium-in-quartz thermometry spreadsheet which is based upon the previously stated equation and the trace element concentrations (ppm) of Ti within the sampled quartz, which averaged 4.86ppm with a 95% confidence interval of4.46ppm-5.27 ppm. A normal distribution of the trace concentrations was experienced, displayed in

Figure.13, which is comprised of a single peaks at ~4.5 ppm, with recognized outliers at both high and low concentrations.

From the petrography study it can be assumed that quartz and mineralisation are paragenically linked as they coexist together exhibiting coprecipitaion relationships. As such the temperature conditions established form the TitaniQ thermometry which depicts the temperature of quartz formation can be inferred to represent the temperature conditions of mineralisation as they formed under the same conditions.

5.4 Sulphur Isotope Analysis

From the petrographic study it became apparent that obtaining a temperature of mineralisation via sulphur isotope analysis would not be viable, as all samples identified for analysis were either pyrite or chalcopyrite with the numbers disproportionate towards the latter due to the lack of suitable pyrite samples. Chalcopyrite and pyrite are not the optimal minerals for the application of this technique, as seen in Figure 14, there is very little temperature dependent fractionation recorded between the two co-precipitating minerals. With no higher S sulphides present the temperature range obtained via this technique would be very broad and inaccurate due to the disproportionate numbers and as such the technique was reconsidered with the data obtain via isotope analysis to be concentrated on obtaining information on the composition and origin of the ore fluids.

The results obtained for each sample are averages of the duplicate analyses (Table.3), excluding sample #A11 which contained insufficient sample volume. The average standard deviation across all samples was ~0.1‰ with no analysis recording greater than 0.2‰ differentiation, making all variation accountable within the mass spectrometer's analytical precision of 0.2 ‰ for $\delta^{34}S$. The sulphides recorded a $\delta^{34}S$ range of -10.5 to -1.2‰ with an average -7.78‰ .The highest frequency of values falls between -8 and -9‰ which forms the single peak of the data from which a left skew emerges ending with an outlying value

of -1.2‰ (Fig.15) With the analytical procedure being outsourced there is no opportunity to resample this value and rule out experimental error. Also due to the small data set this value may represent an entirely different population of sulphide that was not properly sampled, as such it cannot be definitively excluded as an outlier.

The comparison between the two sulphide minerals present within ML001 does show a discrepancy in the $\delta^{34}S$ values, though due the limited amount of pyrite sampled the interpretation of this variance is quiet subjective. Overall chalcopyrite trend towards more negative values within a precise population, whilst pyrite is comprised of a much wider range of values consisting of the outlying heavier sulphur reading, -1.2‰

5.5 Fluid Inclusion

The selection of fluid inclusions for microthermometric analyses was done according to the criteria as published by Roedder (1984), with only inclusions classified as primary being analysed in this project. Present as single inclusions, isolated clusters or on linear arrays along crystal growth, all inclusions contained a vapour phase of ~15vol%. The quartz host mineral of these inclusions was tightly intergrown with sulphides (chalcopyrite) suggesting an equilibrium paragenesis of the two minerals (Fig.16A-B).

The inclusion hosting quartz was often idiomorphic with distinct crystal faces. The individual quartz crystallites were frequently internally zoned with cloudy of cores and distinctly clear rims (Fig.16C). Inclusions are abundant throughout the crystallites but the cloudiness in the central section's allowed easier determination of homogenization temperatures (Th). In the clearer rim zones of the quartz, commonly close to the sulphide grains, inclusions were generally larger (≤ 40µm) than their counterparts which ranged between 10-20µm (Fig.16D-E).

The investigated fluid inclusions revealed low to very low freezing temperatures (Tf) of -50 to -70 °C respectively, which indicates complex saline solutions. This was confirmed by the initial melting temperatures (Te) of -55 to -35°C which further indicated the presence of

bivalent cations (Ca^{2+}, Mg^{2+}, Fe^{2+}) within the solution. Melting of hydrohalite (TmHH) in the presence of ice, but with no discernable NaCl daughter minerals, occurred at -44 to -20 °C, confirming the fluid was enriched in bivalent cations over monvalent, hence not a simple NaCl rich fluid. Measurement of the ice melting temperature (Tmice) occurred between -15.8 to -13.6 °C which provided the key data for the bulk salinity of the fluid as displayed in Fig.17, which indicates a moderate salinity of combined NaCl +$CaCl_2$ equivalent ranging between 27.5-7.5 NaCl equiv Wt% and 72.5-92.5 $CaCl_2$ equiv Wt%. The recorded homogenisation temperature for the representative fluid inclusions range from 131ºC to 194ºC with an average of ~168ºC and represent the minimum temperature at which the inclusion could have formed irrespective to pressure. All high and low temperature data can be found in Table.4.

6 Interpretation of results

6.1 Alteration and Mineralisation Paragenesis

The paragenesis of both alteration and mineralisation reconstructed from the petrographic study provides an isolated assessment of the mineralising system responsible for its formation but cannot be applied for the interpretation of lateral or vertical extent as the data only represents one point of reference.

The petrographic study of representative samples does show at least two alteration assemblages, consisting of an early albite-epidote assemblage and a dominant, overprinting, quartz-carbonate-chlorite-sericite± hematite-sulphide assemblage, as previously described. Between these two alteration stages, or even preceding both, there is an identified discontinuity focused around a possible magnetite bearing stage. Petrographic relationships indicate magnetite precipitating prior to hematite, recorded in the martitisation of magnetite, which indicates that magnetite predates the major mineralising quartz-carbonate-sericite assemblage. This is supported by iron oxide mineral chemistry performed by Cave (2010) which shows magnetite being relatively deficient with respects to Cu and as such was not incorporated within the Cu mineralising stage, unlike hematite which contains significantly higher Cu concentrations confirming its involvement. Though spatially associated with the earlier albite-epidote assemblage, magnetite cannot be definitively interpreted within this assemblage as no sample records coexistence meaning there is still no obvious answer to how long magnetite precipitated before hematite or whether magnetite was an initial phase in quartz-carbonate-sericite assemblage, but petrographic relationships show no record of hematite being replaced or surrounded by magnetite, which subjects that magnetite occurred well before hematite.

The ore paragenesis of the mineralising stage in the quartz-carbonate-sericite assemblage suggests it was progressive and relatively straight foreword indicating a gradual change in fluid composition represented by the transition from one dominant mineral phase to the next with intermittent co-precipitation. Petrography indicates that chalcopyrite formed

after pyrite and as such could contain a heavier stable isotope signature. This is due to the preferential incorporation of light sulphur isotopes from the source early in the evolution of the hydrothermal fluid. As the source becomes depleted in lighter isotopes the heavier isotopes will become enriched within the fluid and minerals derived from this later stage will consist of a heavier isotopic signature. Sulphur isotope analysis generally supports this paragenesis seen in Figure.15, indicating that the majority of pyrite, on volume, formed during co-precipitation with chalcopyrite, with none of the earlier fine grained pyrite inclusions hosted within hematite being successfully analysed due to the grain size of these samples, but they are assumed to contain a significantly lighter signature. A singular anomalously heavy pyrite result does contradict this paragenesis either indicating another source of fluid was involved, that the fluid fluctuated during this stage of mineralisation or provides evidence for the theorised multiple generations of identified from crosscutting mineralisation hosting quartz veins within the core.

No gold, REE and uranium minerals were observed in representative samples, which does not directly indicate they are not present though whole rock geochemistry performed by Cave (2010) does show minimal enrichment or in some cases depletion within ML001 samples in comparison to unaltered samples.

6.2 TitaniQ Thermometry

The temperature of each quartz spot was calculated, under assumed titanium saturation, and summarized in Table.5. From the refined data set a mean temperature of 474.5ºC with a 95% confidence interval of 469.2ºC-479.87ºC was recorded. Investigation into the range of temperatures produced from each individual slide (Fig.18) did not highlight any unique populations, the same with the temperature comparison of the quartz growth rims targeted around the transgression from a cloudy core to a clear rim in most grains, which show no clear preferred temperature range in either of the two petrographic features (Fig.19).

Overall the TitaniQ temperatures are focused around a strong single peak at ~ 475ºC forming a normal distribution with only a small amount of outliers both in the high and low extremities of the data set. Elemental plots were produced to investigate whether these outliers are related to any other possible contamination elements via a systematic increase with Ti (Fig.20). Weak correlations were observed between Al, K and Na, the former of which was an expected relationship as aluminium in quartz is also a somewhat reliable thermometer based around the temperature dependent increase of Al within quartz's crystal structure (Dennen et al. 1970). Whereas the K and Na most probably related to contamination by minor crystalline or fluid inclusions which were not picked up during petrographic selection of the sample spots.

6.3 Chlorite Geothermometry

The calculated temperature results are summarised in Table 6, from which a strong correlation can be drawn between those derived via the Cathelineau and Jowett geothermometers which have nearly identical mean temperatures of 626.80ºC and 628.89ºC with standard deviations of 49.30ºC and 49.39ºC respectively. In stark contradiction the Kranidiotis geothermometer produced a significantly lower temperature range, recording a mean temperature of 280.89ºC with a standard deviation of 18.04ºC.

Overall, the chlorite temperatures had a strong single peak at ~ 640ºC with a slight negative skew in the Cathelineau (Fig.21) and Jowett (Fig.22) geothermometers ,with a majority of the values focused around the peak, whilst the highly constrained, normal distribution exhibited by the Kranidiotis recorded a peak of ~ 190ºC (Fig.23). When compared to the TitaniQ temperatures, the Cathelineau and Jowett geothermometer overestimated the temperatures by upwards of 242ºC, but the extremities of data from both techniques do marginally overlap (Fig.24). Whereas the Kranidiotis geothermometer underestimates the temperatures by 169-77ºC and records no overlapping with the TitaniQ temperatures. This affinity for low temperatures seen within the Kranidiotis can

be attributed to insufficient Al concentrations within the system as this geothermometer is designed for Al rich host rocks.

The inconsistency in the temperatures obtained via the other two thermometers can also be explained by the effect host rock types has on chlorite growth and composition (De Caritat et al. 1993) which was highlighted in the petrography report, as the highly felsic rhyolite unit did not contain any trace of chlorite alteration as it does not contain the necessary Fe/Mg required for chlorite growth. Both over and under estimation of known temperature conditions have been recorded during chlorite geothermometry reviews, (De Caritat et al. 1993, Cathelineau and Neiva 1985) showing that the values obtained via this technique are ambiguous unless conditions are ideal. These reviews also highlight the effect fO_2 has upon the Al: Fe/Mg ratio at the octahedral site as it controls the preference of Fe^{2+} over Fe^{3+} which can alter the results obtained from the thermometric calculation. Demonstrated during the petrographic study, fO_2 is interpreted to be along the magnetite-hematite redox boundary, recorded in the martitisation of magnetite, which promotes the Fe^{3+} oxidation state for all iron present within the system. As the Fe^{2+}: Fe^{3+} ratio cannot be determined with an electron microprobe the Fe^{3+} content is generally calculated as a percentage of the total FeO though in a setting with variable fO_2 this is rarely representative

6.4 Fluid Inclusions

The homogenisation temperature (Th) of the inclusions in conjunction with the low temperature data (Tf, Te, TmICE, TmHH) can then used to calculate the densities and isochors in PT space of the representative inclusions using R.J Bakker's Bulk and ISOC Fluids package (2009, 2003A,B). From this the combination of an independent temperature determination, in the form of the TitaniQ thermometer, can be used to establish the pressure conditions at which the inclusions formed. Displayed in Figure.25 an 40ºC temperature range containing >50% of the TitaniQ data was selected to represent the temperature conditions under which the fluid inclusions formed as they share the

same paragensis as the quartz phase hosting them. The intersection of this temperature range with P-T isochors is then used to project the range of pressure conditions at which these fluid inclusions formed. The pressure range calculated for these representative fluid inclusions is fairly broad, ranging between 5 and 6.8 kbar.

7 Discussion

IOCG style mineralisation is one the Gawler Craton's most prominent styles of copper mineralisation and was the target for OneSteel's exploration efforts within their Middleback tenements. Consisting of the spatially and temporally associated Hiltaba Suite granites along with the required strong structural control, the region was highlighted for potential IOCG mineralisation which lead to the inaugural exploratory diamond drill hole on which this project is based. Comparison between the findings of this project with existing data from IOCG style deposits throughout the Olympic Cu-Au province does identify some correlations between the Moola Prospect mineralisation and the current IOCG model of genesis.

-Alteration-

Mineralisation present within ML001 does display some affinity to alteration styles present throughout the neighbouring Yorke peninsular as well as the greater Gawler Craton. Outlined by Skirrow (2002) IOCG style mineralisation throughout the Gawler Craton is comprised of three broad scale groupings of alteration assemblages which represents the spectrum of associated alteration witnessed throughout the Olympic Cu-Au province.

The relic albite and epidote alteration assemblage identified within the core corresponds with components of one of these alteration groupings, the CAM (calcsilicate-alkali feldspar± magnetite) which encompasses the regional albite alteration halo and is present within several deposits throughout the Craton. Notable variance within alteration assemblages between deposits is experienced throughout the Gawler Craton, as not all minerals in each broad assemblage are necessarily present within all deposits.

The main alteration assemblage responsible for the extensive quartz and carbonate veining that hosts the mineralisation within the core (quartz-carbonate- chlorite- sericite- K-Feldspar- hematite- sulphide), also corresponds with one of these broad scale IOCG

alteration assemblages, the HSCC (hematite-sericite-chlorite-carbonate± Fe-Cu), which is commonly described to be late in the paragenetic sequences, often displaying dominant overprinting of earlier assemblages, in much the same way as witness in ML001. This assemblage is the major mineralising stage within Olympic Dam and is also present within Emmie Bluff, Hillside and possibly Prominent Hill, suggesting that prospects containing this assemblage have the potential for containing IOCG mineralisation. (Bastrakov, 2007)

The alteration assemblages recorded within the Moola Prospect do appear to be very similar to those described by Skirrow et al. (2002), however there is a notable lack of large scale iron oxides, though present in small quantities. This deficiency is anomalous to the IOCG model of genesis, with all major IOCG deposits containing extensive hematite and/or magnetite association. Also no U or REE minerals were observed within representative samples, though this may reflect upon the limits imposed upon this project by being focussed around a singular drill hole.

Notably absent from ML001 is the presence of MB (magnetite-biotite± sulphide) alteration which is the third of the broad scale assemblages associated with IOCG style mineralisation commonly found throughout the Gawler Craton. This assemblage has often been interpreted as a transition stage in alteration as the hydrothermal system moves from the high temperature CAM to the low temperature HSCC assemblage, which could have plausibly occurred within the Moola Prospect as both of the key assemblages appear to be present, which would explain the presence of magnetite within the core, though no petrographic evidence was found to definitively support the presence of this assemblage.

-*Temperature & Pressure Condition*-

Temperature ranges for the mineralising fluids within the Olympic Cu-Au province is quite limited, with the data available forming a high density, low distribution pattern focused upon Olympic Dam, which provides a range between 400 and 200°C which characterises the shallow, paleosurface style of deposit. Bastrakov et al. (2007) utilised several sub

economic prospects to establish a range between 250-800ºC which greater represents IOCG deposits throughout the Gawler Craton.

The temperature conditions calculated via chlorite and TitaniQ thermometry do show that there are some inconsistencies in the quality of the results obtained with the representative temperature conditions from all thermometers used occurring across 500 ºC range. Though successfully applied to the Olympic Dam deposit by Conan-Davies (1987) , chlorite geothermometry shows the largest discrepancy in its data, producing a broad temperature range between ~500-770 ºC (Cathelineau and Jowett thermometers) which is encroaching upon the upper extent of chlorites stability field indicating that the data is highly unreliable. Several reviews have highlighted that no single chlorite geothermometer performs satisfactory over the wide range of natural conditions possible throughout all hydrothermal systems and therefore should be used with caution and not as the sole temperature determination, but preferably in conjunction with alternative methods to establish reliable temperature conditions. This project has found this assessment to be true with methodological weaknesses identified within the technique when applied to IOCG deposits. These weaknesses are generally focused around the techniques reliance on the reconstruction of chlorites crystal structure form microprobe analysis which can lead to inaccurate results as the microprobe cannot differentiate between irons two major oxidation states with Fe^{3+} having to be recalculated as a set percentage of all iron present which is often not representative of the chlorites actual composition. Also the assumption of full site occupancy within chlorites octahedral and tetrahedral sites can cause inaccuracy, as full site occupancy does not consistently occur within the natural world. The effect oxygen fugacity (fO_2) has on chlorite composition is the major concerning factor with the application of chlorite thermometry within IOCG systems, as oxygen fugacity effects the oxidation state of the iron incorporated with the hydrothermal system. As seen within the Moola Prospect, oxygen fugacity can be highly variable as indicated by the transition from magnetite to hematite precipitation which is common throughout many IOCG deposits within the Gawler Craton. This effects the

Fe:Mg ratio which is part of the temperature dependent compositional change experienced at chlorites octahedral site and as such will give an inaccurate temperature because it is not solely the temperature effecting the total Fe/Mg but the oxygen fugacity of the host rock as well, which could explain the high temperatures established for the Moola Prospect.

The TitaniQ temperature data on the other hand produced a much more precise temperature range between ~415-530 ºC, forming a well defined normal distribution. Even though still in its developmental stages this thermometer was chosen to better represent the temperature conditions present within the Moola Prospect and as such was used in combination with the fluid inclusion data to establish the pressure conditions of mineralisation. The reconstructed pressure conditions range between ~5-7 kbar which indicates that the data could be affected by the recently identified influence pressure has on the solubility of Ti in quartz. Thomas et al. (2010) witnessed that between pressures of 5-20 kbar there is an apparent decrease in the solubility of Ti in quartz which would affect the temperatures obtained via TitaniQ thermometry, as the temperature dependent substitution of Ti for Si in quartz's crystal structure would no longer be systematic and inaccurate temperatures would be established. The exact effect this decrease in solubility has upon the thermometer cannot be quantified for the Moola Prospect as the Thomas et al. (2010) experiment was performed at much higher temperatures (700-940 °C) but it can be assumed that the temperatures conditions could have been slightly underestimated.

The temperature conditions of ~475ºC and pressure conditions of ~5-7 kbar obtained for the Moola prospect, via TitaniQ thermometry and the fluid inclusion study, do correspond with the mid to high end of the IOCG temperature range characterising the Gawler Craton. Though these conditions contradict, but don't disprove, the generally shallow, low temperature, low pressure conditions associated with occurrences of the HSCC alteration assemblage. The reconstructed pressure conditions indicate a deep crustal setting

(>10km) (Roeder & Bodnar 1980) like that seen at Ernest Henry in the Cloncurry district, Queensland but mineralisation at such a depth is generally characterised by the MB alteration assemblage (Skirrow 2002), which indicates that there is either some inaccuracy within the establishment of temperature and pressure condition or that alteration within the Moola prospect does not correspond with the HSCC assemblage.

-Fluid & Mineralisation Characteristics-

From the fluid inclusion study the salinity of the hydrothermal fluid was indicated to be moderately saline with NaCl ranging between 27.5-7.5equiv wt%. These levels do not correspond with the typical highly saline fluids that characterised IOCG deposits, with occurrence of fluid inclusions recording NaCl up to 42 equiv Wt% in halite-saturated inclusions form Olympic Dam (Oreskes & Einaudi 1992). Though not highly saline these fluid inclusions do not discredit the possible IOCG genesis for the Moola Prospect mineralisation as several fluid inclusions studies performed throughout the Gawler Craton and around the world have recorded widely varying salinities and complex solute chemistry, with some matching very closely to that established for the Moola Prospect (Oreskes & Einaudi 1992).

Sulphur isotope data in much the same way as temperature conditions is widely focused upon Olympic Dam and is used to characterise fluid source and compare it to mineralisation potential. Investigations into several significant prospects and deposits within the Gawler Craton provide a wide range of $\delta^{34}S$ values ranging from -14 to +12.5. The data obtained from the Moola Prospect is comprised of a predominantly light sulphur isotope signature between -10.5 and -1.2 ‰ which corresponds with those found at Olympic Dam (~-10 to -5‰ CDT) rather than the heavier signatures associated with sub economic or barren prospects (~ -5 to 10‰ CDT) (Brastrakov et al. 2007). This difference

in isotopic fractionation is due in part to the source of the mineralising fluids with Olympic Dam interpreted to consist of a more magmatically derived origin then other subeconomic prospects, with the Moola Prospect sharing a similar interpretation, as depicted in Figure.26.

IOCG style deposits are rarely homogeneous with Prominent Hill and especially Olympic Dam highlighting the discontinuity experienced at a deposit scale as both record vertical and lateral zonation of mineralisation and alteration. Often consisting of extensive hydrothermal activity localised around the main mineralisation zone, there is a distinct transition from high grade sulphides (chalcocite, bornite) at the core into lower quantities of low grade sulphides (chalcopyrite, pyrite) towards the outer extremities. This transition is also is accompanied by a reduction in brecciation and hydrothermal activity towards the outer extremities. From the petrographic study it can be interpreted that the Moola prospect is possibly situated within the outer extremities or in proximity of a major mineralisation zone as it contains both a lack of brecciation and the accompanying low grade sulphides, (pyrite and chalcopyrite) which characterise these proximal zones. The presence of albite alteration also supports this interpretation as a large scale regional sodic alteration halo is often found surrounding IOCG style mineralisation.

8 Conclusions

The genesis of the Moola Prospect mineralisation cannot be definitively identified even though this project was able to establish several fundamental parameters of the Cu mineralisation, including host rock lithology, alteration-mineralisation paragensis, salinity and geochemical signatures of the fluid as well as paleotemperature-pressure conditions. Several of these characteristics do show some affinities towards the geological and mineralogical frameworks that comprise other IOCG deposits of the Gawler Craton. Mineralisation paragenesis can be interpreted to correspond with the proximal or outlying extremities of an IOCG mineralising zone which is supported by a lack of brecciation typical as you move further away from the hydrothermal epicentre. The mineralisation is comprised of two phases: the primary stage and a later supergene enrichment to form native Cu within the transecting shear zone. The primary mineralisation shows an evolution in fluid composition from magnetite to hematite transitioning through pyrite and finally onto chalcopyrite. The sulphur isotope signature and salinity levels correspond with the magmatically derived fluids interpreted for most IOCG deposits, with the Moola Prospect also being spatially associated to the interpreted source of these fluids within the Galwer Craton, the Hiltaba Suite granitoids. Alteration also shares affinities with the characteristic IOCG alteration assemblages seen throughout the Gawler Craton, though due to the restricted scope of the project .

Some qualities of the Moola Prospect though do not support an IOCG model of genesis; this is mainly based around the general lack of large scale iron oxide associated with the Cu mineralisation which is a requirement for IOCG style mineralisation. The pressure and temperature conditions also contradict the interpretation that the main phase of Cu mineralisation is a HSCC assemblage which is typically characterised as a shallow, low temperature, low pressure assemblage.

There are clearly several unanswered questions in relation to the Moola Prospect the primary ones being the timing and genesis of mineralisation. Possible monazites and

zircons may provide dateable minerals to be used in conjunction with identified epidote in order to constrain the age of mineralisation. Dating will help identify if the Moola Prospect share the same temporal association with the emplacement Hiltaba Suite Granitoid, shared by all IOCG deposit within the Gawler Craton and to determine if magnetite represents a distinct stage of mineralisation or if it is incorporated within the identified alteration assemblages. Other questions relate to the spatial variation and extent of alteration, as well as whether the mineralisation within the Moola Prospect represents a vein hosted subeconomic, hydrothermal system that is focus around a strong structural control or if it is in fact a small portion of a much larger system related to an ore body.

Acknowledgements

I would like to first and foremost thank my supervisor Andreas Schmidt Mumm for his guidance throughout most of the year and David Giles for stepping in when Andreas had “Gone Fishin”. This project would not have been possible without the support of OneSteel, especially Geoff Johnson whose guided tour of what the Middleback’s have to offer and help in the core yard made the project a lot easier. I would also like to thank both Ben Wade and Angus Netting at Adelaide Microscopy for their guidance using the Electron Microprobe and LA-ICPMS, as well as Ben Cerlienco for answering all of my pestering little questions. Lastly I would like to thank Ben Cave and the rest of the OneSteel honours group for making this year what it was.

References

BAKKER, R. J. (2003). Computer modeling in fluid inclusion research. *Fluid inclusion., Reveiws in Mineralogy* **12** , 644.

BAKKER, R. J. (2003). Package FLUIDS 1. Computer programs for analysis of fluids inclusion data and for modelling bulk fluid properties. *Chemical Geology* **194** , 3-23.

BAKKER, R. J. (2009). Package FLUIDS part 3. Correlations between equations pf state. thermodynamics and fluid inclusions. *Geofluids* **9** , 63-74.

BARTON, M. D., & JOHNSON, D. A. (2004). Footprints of Fe-Oxide (-Cu-Au) Systems. *Predictive Mineral Discovery Under Cover. Centre for Global Metallogeny, Spec. Pub.* **33** , 112-116.

BASTRAKOV, E. N., SKIRROW, R. G., & DAVIDSON, G. J. (2007). Fluid evolution and origins of iron oxide Cu-Au prospects in the Olympic Dam district, Gawler Craton, South Australia. *Economic Geology* **102** , 1415-1440.

CATHELINEAU, M., & NEIVA, D. (1985). A chlorite solid solution geothermometer. The Los Azufres (Mexico) geothermal system. *Contributions to Minerology and Petrology **91***, 235-244.

CAVE, B. (2010). *Copper-Gold Exploration in the Middleback Ranges: Source(s) of Fluids and Metals.* Adelaide: University of Adelaide.

CERLIENCO, B. (2009). *Geological Setting and Alteation Characteristics of Hillside Mineralising System, Yorke Peninsula (Unpublished).* Adelaide: University of Adelaide.

CONAN-DAVIES, M. S. (1987). *A sheet silicate and fluid inclusion study of the mine area DNW, Olympic Dam, South Australia. Unbupl. Thesis.* Canberra, ACT: Australian National University.

DE CARITAT, P., HUTCHEON, I., & WALSHE, J. L. (1993). Chlorite Geothermometry: A Reveiw. *Clays and Clay Minerals* **41** , 219-239.

DENNEN, W. H., BLACKBURN, W. H., & QUESADA, A. (1970). Aluminum in quartz as a geothermometer. *Contributions to Mineralogy and Petrology* **27** , 332-342.

FANNING, C. M., FLINT, R. B., PARKER, A. J., LUDWIG, K. R., & BLISSETT, A. H. (1988). Refined proterozoic evolution of the Gawler Craton Craton, South Austalia, through U-Pb zircon geochronology. *Precambian Research 40/41* , 363-386.

FERRIS, G. M., SCHWARZ, M. P., & HEITHERSAY, P. (2002). The Geological Framework, Distribution and Controls of Fe-Oxide-Cu-Au Mineralisation in the Gawler Craton, South Australia. In Porter

T.M, *Hydrothermal Iron Oxide Copper-Gold & Related Deposits: A Global Perspective 2.* Adelaide: PGN Publishing .

GROVES, D. I., BIERLEIN, F. P., MEINERT, L. D., & HITZMAN, M. W. (2010). Iron Oxide Copper-Gold (IOCG) Deposits through Earth History: Implications for Origin, Lithospheric Setting, and Distinction from Other Epigenetic Iron Oxide Deposits. *Economic Geology,* **105** , 641–654.

HAND, M., REID, A., & JAGODZINSKI, L. (2007). Tectonic Framework and Evolution of the Gawler Craton, Southern Australia. *Economic Geology* **102** , 1377-1395.

HEY, M. H. (1954). A review of the chlorites. *Mineralogical Magazine* **30** , 227.

HITZMAN MW (2000) Iron oxide-Cu-Au deposits: what, where, when, and why. In: Porter TM (ed) Hydrothermal iron oxide copper-gold and related deposits: A global perspective. Australian Mineral Foundation, Adelaide, pp 9–25

HITZMAN, M. W., & VALENTA, R. K. (2005). Uranium in Iron Oxide-Copper-Gold (IOCG) Systems. *Economic Geology* **100** , 1657- 1661.

HITZMAN, M. W., ORESKES, N., & EINAUDI, M. T. (1992). Geological characteristics and tectonic setting of Proterozoic iron oxide (Cu-U-Au-REE) deposits . *Precambrian Research* **58** , 241–287.

HUNT, J. A., BAKER, T., & THORKESON, D. J. (2007). A Reveiw of Iron Oxide Copper Copper-Gold Depoists, with Focus on the Wernecke Breccias, Yukon, Canada, as a example of a example of a Non-magmatic end member and implications for IOCG Genesis and Classification. *Exploration and Mining Geology* **16** , 209-232.

JOWETT, E. C. (1991). Fitting iron and magnesium into hydrothermal chlorite geothermometry. *GAC/MAC/SEG Joint annual Metting (Toronto, May 27-29 1991)* , Program Abstracts 16.

KRANIDIOTIS, P., & MACLEAN, W. H. (1987). Systematics of chlorite alteration at the Phelps Dodge massive sulfide deposit, Matagami, Quebec. *Economic Geology* **82** , 1898-1911.

ORESKES, N., & EINAUDI, M. T. (1992). Origin of hydrothermal fluids at Olympic Dam: Preliminary results from fluid inclusions and stable isotopes. *Economic Geology* **87** , 64-90.

PARKER, A. J., & FANNING, C. M. (1983). *Whyalla, South Australia, 1:250 000 geological series map. Sheet SI/53-08 Zone 5, 1st edition.* Geological Survey of Australia.

PARKER, A. J., & FANNING, C. M. (1998). Explanatory Notes for the Whyalla 1:250 00 Geological Map. *Geological Suvey of Australia* .

PARKER, A. J., FANNING, C. M., FLINT, R. B., MARTIN, A. R., & RANKIN, L. R. (1989). *Early Proterozoic granitoids, metasediments and mylonites of southern Eyre Peninsula, South Australia. Field Guide.* Geological Society of Australia. Specialist Group in Tectonics and Structural Geology.

ROEDDER, E. (1984). Fluid Inclusions; Reviews in Mineralogy . *Fluid Inclusions, analysis and Interpretation (eds. Samson I, Anderson A, Marshall D), Short Course v32* , 175-212.

SKIRROW, R. G., BASTRAKOV, E. N., DAVIDSON, G. J., RAYMOND, O. L., & HEITHERSAY, P. (2002). The Geological Framework, Distribution and Controls of Fe-Oxide CU-Au Mineralisation in the Gawler Craton, South Austrlia Part II- Alteration and Mineralisation. In Porter. T.M, *Hydrothermal Iron-Oxide Copper-Gold & related Deposits: A Global Perspective* (pp. 33-47). Adelaide: PGC Publishing .

THOMAS, J. B., WATSON, E. B., SPEAR, F. S., SHEMELLA, P. T., NAYAK, S. K., & LANZIROTTI, A. (2010). TitaniQ under pressure: the effect of pressure and temperature. *Contributions Mineraology and Petrology* **160**, 12-33.

TINDLE, A. G. (1999). *Mineral Recalculation Software: Chlorite (Unpubl.) Online.* www.open.ac.uk/earth-research/tindle/AGTWebData/Chlorite.xls.

VASSALLO, J. J., & WILSON, C. J. (2001). Structuarl repetition of the Hutchison Group metasediments, Eyre Penisula, South Austrlia. *Australian Journal of Earth Sciences* **48**, 331-345.

VASSALLO, J. J., & WILSON, C. J. (2002). Palaeoproterozoic Regional-scale Non-Coaxial Deformation: An Example From Eastern Peninsula, South Australia. *Journal of Structuaral Geology* **24** , 1-24.

WARK, D. A., & WATSON, E. B. (2006). TitaniQ: a titanium-in-quartz geothermometer. *Contributions to Mineralogy and Petrology* ***152***, 743-754.

WEBB, A. W., THOMSON, B. P., BLISSETT, A. H., DALY, S. J., FLINT, R. B., & PARKER, A. J. (1986). Geochronology of the Gawler Craton, South Australia. *Australian Journal of Earth Sciences* **33** , 119-143.

WILLIAMS, P. J., BARTON, M. D., JOHNSON, D. A., FONTBOTE, L., & HALLER, A. D. (2005). Iron Oxide Copper- Gold Deposits: Geology, Space- Time Distribution, and Possible Modes of Origin. *Economic Geology 100th Anniversary Volume* , 371-405.

WYBORN, L. A., PAGE, R. W., & PARKER, A. J. (1987). Geochemical and Geochronological Signatures in Australia Proterozoic Igneous Rocks. *Geological Society, London, Special Publications* **33** , 377-394.

Table.1- Raw chlorite compositional data

	RJ001_001	RJ001_002	RJ001_003	RJ001_004	RJ001_005	RJ001_007
SiO_2	27.6831	28.0126	29.1392	27.4478	28.6278	27.523
TiO_2	0.0002	0.0673	0.2736	0.17	0.1357	0.026
Al_2O_3	18.9172	16.4143	16.7632	16.8897	15.9135	15.6165
FeO	26.8997	24.8492	24.5097	25.1395	25.2944	24.4565
MnO	0.5878	0.5527	0.5673	0.4725	0.7254	0.4359
MgO	12.3208	12.8931	13.8037	13.4234	12.8674	12.1508
CaO	0.0955	0.225	0.0963	0.0654	0.1377	0.2265
Na_2O	0.1294	0.1215	0.1533	0.0763	0.0737	0.0981
K_2O	0.0957	0.115	0.1345	0.1022	0.2225	0.1214

	RJ001_008	RJ010_001	RJ010_003	RJ010_004	RJ010_005	RJ010_006
SiO_2	28.3446	25.755	28.9619	28.3822	28.4041	28.3906
TiO_2	1.4971	0.0179	0.0002	0.0325	0.0502	0.012
Al_2O_3	15.9024	16.6845	18.6793	17.677	19.2458	18.3178
FeO	25.1264	19.9684	17.4392	18.4421	12.0133	20.2398
MnO	0.5461	0.2351	0.417	0.4223	0.4215	0.1516
MgO	13.0659	16.3991	20.8691	18.8669	24.1402	18.4615
CaO	0.1978	0.0738	0.0314	0.0329	0.0157	0.0002
Na_2O	0.0587	0.1239	0.0489	0.1705	0.0436	0.0669
K_2O	0.0298	0.1234	0.0249	0.0712	0.0055	0.2616

	RJ010_009	RJ010_010	RJ010_011	RJ010_012	RJ010_015	RJ010_016
SiO_2	28.318	29.5205	27.2548	27.3437	28.9519	30.2173
TiO_2	0.012	0.0098	0.0478	0.0478	0.0181	0.0395
Al_2O_3	18.6209	19.4609	19.6796	19.1081	18.4435	18.4679
FeO	20.8468	12.4559	21.166	21.8883	18.9575	9.3289
MnO	0.3399	0.5105	0.3529	0.2115	0.5479	0.604
MgO	18.7582	24.8651	16.6156	17.4286	19.5906	26.8578
CaO	0.0782	0.0078	0.076	0.0546	0.0083	0.0531
Na_2O	0.2361	0.024	0.0121	0.0099	0.0021	0.0981
K_2O	0.0086	0.0001	0.3684	0.0247	0.0594	0.0692

	RJ010_017	RJ010_018	RJ010_019	RJ010_021	RJ010_022	RJ010_023
SiO_2	25.2399	28.473	27.5125	28.3559	29.0916	29.1373
TiO_2	0.018	0.0002	0.0491	0.0782	0.0002	0.0458
Al_2O_3	17.1836	18.129	19.0287	18.6385	18.8126	18.9044
FeO	17.7303	15.6346	20.795	19.4634	19.27	19.0385
MnO	0.3306	0.32	0.2761	0.3682	0.2772	0.1691
MgO	16.0314	22.2291	18.0543	19.3532	19.649	19.2531
CaO	0.1083	0.0458	0.0418	0.0285	0.0402	0.0747
Na_2O	0.1875	0.1251	0.0667	0.1166	0.0173	0.0651
K_2O	0.0991	0.139	0.0387	0.1144	0.0389	0.337

	RJ010_024	RJ010_025	RJ010_027	RJ012_004	RJ012_005	RJ012_006
SiO_2	29.8045	34.4419	28.239	26.764	26.8608	26.6443
TiO_2	0.0121	0.0327	0.0216	0.0002	0.0002	0.0552
Al_2O_3	19.1536	18.3249	18.3925	17.5594	17.7289	17.4434
FeO	18.7905	18.2297	20.0898	28.0015	28.674	27.8445
MnO	0.1591	0.2241	0.1755	0.4275	0.4438	0.4541
MgO	19.3397	18.8119	18.6249	13.3682	13.4986	13.6522
CaO	0.0755	0.0366	0.0517	0.3089	0.2654	0.0433
Na_2O	0.097	0.0062	0.1032	0.0667	0.0801	0.0322
K_2O	0.1298	0.0445	0.0582	0.0446	0.018	0.0796

	RJ012_009	RJ012_012	RJ012_013	RJ012_014	RJ012_015	RJ012_016
SiO_2	26.6776	25.5323	26.2754	27.3365	26.2043	27.1535
TiO_2	0.0082	0.1138	0.0481	0.046	0.0776	0.0129
Al_2O_3	18.4221	19.7868	19.1732	17.7096	19.5618	17.4331
FeO	27.8107	28.449	28.3261	26.9068	27.854	28.2734
MnO	0.3152	0.3412	0.4076	0.4321	0.2952	0.3281
MgO	13.7208	12.856	12.88	14.1551	12.8933	13.4868
CaO	0.0982	0.0381	0.0261	0.032	0.0344	0.0495
Na_2O	0.0003	0.0003	0.0106	0.0003	0.0822	0.0296
K_2O	0.068	0.0138	0.0138	0.049	0.0308	0.051

	RJ012_023_1	RJ012_023_2	RJ012_023_3	RJ012_025_1	RJ012_025_2	RJ012_026
SiO_2	26.3584	27.339	26.9834	27.3536	28.6926	27.0397
TiO_2	0.1126	0.0401	0.2233	0.0247	0.0449	0.0494
Al_2O_3	18.2159	17.8042	18.3148	17.5301	17.949	17.5628
FeO	28.9672	27.0171	28.4633	28.2937	27.0045	28.2106
MnO	0.3708	0.4124	0.2553	0.2654	0.3428	0.3583
MgO	12.7187	14.1029	13.2505	13.9897	13.8487	13.6164
CaO	0.0425	0.0392	0.0302	0.0287	0.0466	0.0468
Na_2O	0.0761	0.0247	0.0574	0.0147	0.0267	0.0622
K_2O	0.035	0.0107	0.0754	0.0362	0.0277	0.0361

	RJ012_028	RJ012_029	RJ012_030	RJ012_031	RJ012_032	RJ012_040
SiO_2	26.9057	26.5159	29.4913	27.693	26.9094	25.7726
TiO_2	0.0002	1.0536	0.0307	0.052	0.0716	3.2913
Al_2O_3	17.5013	17.7758	16.7333	16.9011	18.0148	17.9268
FeO	28.1793	27.1225	26.325	26.5671	28.8614	26.6166
MnO	0.4543	0.3621	0.2266	0.1764	0.3711	0.3593
MgO	13.2263	12.8925	13.957	14.4723	13.3684	12.1199
CaO	0.1935	0.0393	0.068	0.0577	0.057	0.0509
Na_2O	0.0642	0.1475	0.0304	0.0338	0.02	0.173
K_2O	0.0701	0.0223	0.0149	0.0331	0.0435	0.0752

	RJ012_046	RJ012_047	RJ015_001	RJ015_002	RJ015_004	RJ015_005
SiO_2	25.888	27.2857	26.647	27.8813	27.3642	27.473
TiO_2	0.073	0.079	0.0595	0.0249	0.0592	0.0213
Al_2O_3	19.1373	17.3378	19.8727	17.5506	16.599	17.2021
FeO	27.0992	27.2207	23.4726	25.3058	25.4832	24.9612
MnO	0.4054	0.3391	0.3047	0.2739	0.2701	0.2938
MgO	12.9877	13.7593	13.9959	15.4274	14.3413	14.3976
CaO	0.0713	0.0979	0.0976	0.1434	0.2143	0.2453
Na_2O	0.0003	0.0777	0.1028	0.0341	0.0658	0.1162
K_2O	0.0001	0.0149	0.0064	0.0428	0.0448	0.0513

	RJ015_006_1	RJ015_006_2	RJ015_006_3	RJ015_009_1	RJ015_009_3	RJ015_009_4
SiO_2	27.4581	27.3739	26.9992	26.8851	25.1489	24.6159
TiO_2	0.0556	0.0674	0.2059	0.0283	0.0378	0.615
Al_2O_3	17.731	17.709	17.4716	18.2771	20.0414	19.2093
FeO	25.9679	25.9761	25.259	26.2435	25.8895	27.6666
MnO	0.1967	0.2167	0.2635	0.263	0.3796	0.2219
MgO	14.4934	14.3515	13.8212	13.4094	13.078	11.0782
CaO	0.0982	0.092	0.117	0.062	0.0458	0.0303
Na_2O	0.0308	0.0116	0.0164	0.0906	0.0132	0.0465
K_2O	0.0214	0.0181	0.0192	0.0267	0.0085	0.0276

	RJ015_010	RJ015_011	RJ015_012	RJ015_013	RJ015_014	RJ015_015
SiO_2	27.7037	28.4515	25.9859	26.5676	26.2033	27.3543
TiO_2	0.0059	0.0047	0.0342	0.0002	0.1885	0.0462
Al_2O_3	16.8466	15.9323	19.3857	19.0659	19.1726	17.3148
FeO	24.9858	25.4506	26.2538	26.369	27.6709	25.1008
MnO	0.3308	0.2738	0.3563	0.3032	0.3757	0.314
MgO	16.0963	16.0473	13.8506	13.8767	13.6667	15.434
CaO	0.0203	0.0249	0.0668	0.0311	0.0043	0.0423
Na_2O	0.0003	0.0003	0.0175	0.0159	0.0003	0.052
K_2O	0.0471	0.0053	0.0001	0.0001	0.0341	0.0267

	RJ015_016	RJ015_017	RJ015_018_1	RJ015_018_2	RJ015_018_3	RJ015_019_1
SiO_2	25.7064	25.9014	25.1568	24.8168	25.061	26.4626
TiO_2	0.0002	0.0541	0.0211	0.0002	0.0047	4.7833
Al_2O_3	19.5991	19.228	20.1976	20.4528	21.0377	16.1111
FeO	27.5385	28.0128	28.0697	27.0947	28.597	24.0106
MnO	0.2656	0.2455	0.1425	0.3755	0.2586	0.1607
MgO	12.016	12.4129	10.7525	12.7552	11.6456	14.1133
CaO	0.0781	0.121	0.1335	0.0434	0.0002	0.1545
Na_2O	0.0441	0.0612	0.0877	0.0709	0.0513	0.0349
K_2O	0.0245	0.0967	0.0404	0.0596	0.0372	0.2218

	RJ015_019_2	RJ015_020	RJ015_021	RJ015_022	RJ015_023	RJ015_024
SiO_2	28.3376	24.5301	26.3555	25.8304	27.1948	25.4684
TiO_2	0.0309	0.0002	0.0556	0.0071	0.0002	0.0635
Al_2O_3	18.0877	18.8825	17.8457	20.1828	18.6319	19.6487
FeO	24.1487	24.6451	25.5551	26.919	26.0254	28.1781
MnO	0.3385	0.3065	0.28	0.4156	0.2636	0.1991
MgO	16.1167	12.0089	13.5654	12.2506	14.5792	12.4989
CaO	0.0537	0.1671	0.1569	0.1183	0.1424	0.0273
Na_2O	0.0124	0.1572	0.0238	0.2308	0.0366	0.0003
K_2O	0.0001	0.0001	0.0128	0.0001	0.0363	0.0106

	RJ015_025	RJ015_027	RJ015_028	RJ015_029	RJ015_030	RJ010_001
SiO_2	28.1931	27.0119	26.5214	27.1628	27.4369	26.8022
TiO_2	0.0606	0.0662	0.0555	0.0425	0.0604	0.013
Al_2O_3	16.4915	17.8883	18.7406	18.8705	17.0747	19.0611
FeO	24.7063	26.2682	26.5331	26.8159	25.8874	27.4455
MnO	0.1939	0.2133	0.2765	0.2264	0.297	0.2296
MgO	15.3277	14.0648	14.158	13.5799	15.7558	13.8831
CaO	0.1129	0.1131	0.0488	0.0882	0.0399	0.0877
Na_2O	0.0623	0.0821	0.0095	0.057	0.0003	0.0442
K_2O	0.0278	0.0032	0.0001	0.0309	0.0267	0.0001

	RJ010_002	RJ010_004	RJ010_005	RJ010_007	RJ010_009	RJ010_010
SiO_2	26.8193	27.0863	27.2851	27.1548	26.1974	25.7181
TiO_2	0.0212	0.6859	0.1004	0.0932	0.0494	0.1385
Al_2O_3	18.7731	18.4974	18.2818	17.7465	17.933	18.9282
FeO	27.5268	28.7099	27.4455	26.9681	27.4502	28.6532
MnO	0.2825	0.3719	0.253	0.2528	0.3686	0.3909
MgO	12.2836	13.6163	14.0325	13.6353	13.0427	11.8996
CaO	0.0826	0.0818	0.1305	0.047	0.0498	0.068
Na_2O	0.327	0.0266	0.0317	0.0454	0.0326	0.0551
K_2O	0.0383	0.0001	0.0001	0.0053	0.0001	0.0212

	RJ010_012	RJ010_018	RJ010_024	RJ010_027	RJ010_029	RJ010_030
SiO_2	26.2536	26.72	25.2642	28.2495	25.7237	26.8192
TiO_2	0.263	0.2069	0.115	0.0331	0.2131	0.0259
Al_2O_3	17.6078	18.5812	18.3115	17.6924	18.773	18.1097
FeO	26.7986	26.2056	28.0637	27.4823	27.5482	27.9478
MnO	0.2628	0.3067	0.4042	0.3563	0.3986	0.2625
MgO	13.5677	13.4162	11.7604	14.2109	13.0688	13.4514
CaO	0.1365	0.1275	0.0172	0.0783	0.1995	0.0644
Na_2O	0.0048	0.0294	0.042	0.1573	0.0003	0.0075
K_2O	0.0011	0.0128	0.0021	0.0821	0.0001	0.0351

	RJ010_031	RJ010_032	RJ010_033	RJ010_035	RJ010_036	RJ010_037
SiO_2	26.2063	27.2367	28.2051	26.7809	26.9688	26.5546
TiO_2	0.2964	0.0165	0.0153	0.1085	0.1634	0.2657
Al_2O_3	19.1234	18.2271	17.3649	17.74	17.1218	17.9307
FeO	28.4962	28.6966	28.0432	27.264	28.6321	28.6112
MnO	0.3453	0.3088	0.3958	0.3527	0.4711	0.3717
MgO	12.8341	13.6169	13.4623	13.7501	13.2248	12.7639
CaO	0.0519	0.0486	0.0473	0.0609	0.1091	0.1074
Na_2O	0.0322	0.0731	0.3623	0.0532	0.0072	0.033
K_2O	0.0138	0.0106	0.0192	0.0309	0.0106	0.034

	RJ010_038	RJ010_039	RJ010_040	RJ010_041	RJ010_042	RJ010_043
SiO_2	26.2019	26.6043	26.6167	26.0764	26.424	26.6758
TiO_2	0.0282	0.0577	0.047	0.1132	0.2556	0.0047
Al_2O_3	18.4828	17.3509	17.4249	18.132	18.6759	17.7735
FeO	28.1226	27.9648	28.7357	27.0282	27.8425	27.1979
MnO	0.2656	0.2923	0.3815	0.2993	0.3057	0.2861
MgO	12.5023	13.1561	13.108	12.7862	12.936	13.3728
CaO	0.0622	0.0622	0.2367	0.1185	0.0878	0.0575
Na_2O	0.0507	0.0361	0.0586	0.0392	0.0133	0.0239
K_2O	0.0064	0.0043	0.0255	0.0234	0.0309	0.0309

	RJ010_045	RJ010_046	RJ010_047	RJ010_048	RJ010_049	RJ010_050
SiO_2	27.2416	26.9213	26.5536	27.6109	26.8161	26.1247
TiO_2	0.0377	0.0685	0.039	0.0391	0.0732	0.0295
Al_2O_3	17.6518	17.0833	17.0051	17.9502	17.5094	17.2969
FeO	27.4486	26.6797	25.7425	26.0883	26.9404	26.9197
MnO	0.2429	0.2663	0.2566	0.207	0.2429	0.2959
MgO	13.6321	13.4171	13.4109	14.4346	13.4245	13.1957
CaO	0.0489	0.0736	0.1102	0.0417	0.0635	0.045
Na_2O	0.0159	0.0875	0.0342	0.0048	0.0251	0.0003
K_2O	0.0288	0.1589	0.079	0.0267	0.0288	0.0085

Table 1: Raw chlorite compositional data as determined by electron microprobe (in oxide %). Chlorite was analysed for use in chlorite thermometry which requires knowledge of Si, Al, Fe and Mg concentrations. Included here is subset of complete data showing elements involved in temperature-controlled cation exchange, as well as Ca, Na and K which indicate contamination of other sheet silicate if total greater than 0.5%.

Table.2- -ICPMS trace element in quartz data

A1ST-07.1	Na23	Al27	Si29	Cl37	K39	Ca43	Ti47	Ti48	Ti49	Fe57	Cu63
spot1	47.13	33.01	467439.4	-	3.86	47.18	4.34	0.241	3.25	-	0.462
spot2	273.59	97.08	467439.4	-	30.51	289.81	4.62	0.351	3.41	16.19	0.819
spot3	47.42	29.4	467439.4	-	170.06	1211.89	5.01	0.751	3.05	29.14	1.8
spot4	96.79	62.38	467439.4	-	16.7	96.87	4.69	0.264	3.55	4.24	1.72
spot5	1.1	52.23	467439.4	-	-	-	4.59	0.23	3.51	-	1.3
spot6	297.93	2116.44	467439.4	-	11.23	61.11	9.37	0.772	8.59	-	1.55
spot7	284.33	109.1	467439.4	-	48.85	329.29	4.86	0.43	6.35	7.98	1.33
spot8	969.64	2610.72	467439.3	-	637.44	905.11	8.16	1.077	6.91	21.32	1.55
spot9	650.78	2219.7	467439.4	-	617.52	135.6	8.8	0.714	6.8	3.12	1.91
spot10	9.3	76.31	467439.4	-	1.87	-	4.37	0.0809	2.75		1.129

A1ST-07.2	Na23	Al27	Si29	Cl37	K39	Ca43	Ti47	Ti48	Ti49	Fe57	Cu63
spot11	105.46	66.75	467439.4	-	15.96	167.5	5.31	0.4	4.35	12.62	16.25
spot12	154.74	44.2	467439.3	-	25.82	248.06	4.21	0.143	3.14	1.4	0.774
spot13	113.79	42.29	467439.3	-	12.69	77	4.07	0.192	3.51	6.6	3.98
spot14	441.05	736.24	467439.3	-	240.37	212.67	5.36	0.428	4.62	11.35	1.22
spot15	295.01	68.11	467439.3	-	26.69	115.83	3.82	0.208	3.06	-	0.568
spot16	74.62	1365.09	467439.3	-	520.32	512.03	6.41	0.725	6.6	7.26	1.33
spot17	71.87	87.58	467439.3	-	13.48	72.13	4.08	0.189	3.7	-	0.846
spot18	19.58	97.22	467439.3	-	2.72	50.78	3.86	0.0877	2.93	2.06	0.821
spot19	930.43	2564.74	467439.3	-	769.17	344.1	7.9	0.706	6.99	6.59	1.58
spot20	127.63	97.2	467439.3	-	25.34	82.6	4.54	0.189	2.53	7.48	4.64

A1ST-01.1	Na23	Al27	Si29	Cl37	K39	Ca43	Ti47	Ti48	Ti49	Fe57	Cu63
spot2	391.35	866.33	467439.4	-	1365.72	88.31	5.75	0.461	4.87	3.05	2.08
spot4	219.26	997.26	467439.4	-	641.82	-	4.58	0.27	3.86	7.1	1.13
spot6	102.05	942.88	467439.4	-	61.26	40.08	4.31	0.171	3.83	-	0.71
spot7	73.93	387.01	467439.4	-	34.82	87.28	4.48	0.317	5.79	-	1.94
spot8	168.76	769.42	467439.4	-	255.84	158.55	5.02	0.252	4.25	11.27	2.6
spot9	405.75	2270.89	467439.4	-	512.84	176.84	8.48	0.677	7.76	25.76	3.56

A1ST-01.2	Na23	Al27	Si29	Cl37	K39	Ca43	Ti47	Ti48	Ti49	Fe57	Cu63
Stop1	424.9	2101.6	467439.4	-	626.25	277.48	7.44	0.661	6.66	38.89	12.99
Stop3	23.87	346.47	467439.4	-	9.94	44.98	5.1	0.161	4.3	-	1.3
Stop4	21.15	316.25	467439.4	-	5.27	53.71	4.63	0.237	4.17	1.72	1.04
Stop6	98.64	836.83	467439.4	-	39.57	136.4	5.64	0.379	5.06	1.8	1.12
Stop7	236.22	707.1	467439.4	-	31.86	286.01	6.16	0.495	4.83	3.13	1.34
Stop8	173.21	611.52	467439.4	-	38.21	76.05	5.21	0.306	4.21	1.99	0.76
Stop9	85.55	717.73	467439.4	-	20.85	44.73	6.01	0.326	4.89	1.7	0.77
Stop10	34.84	1409.57	467439.4	-	4.9	83.52	8.77	0.77	8.21	-	1.29

A1ST-01.3	Na23	Al27	Si29	Cl37	K39	Ca43	Ti47	Ti48	Ti49	Fe57	Cu63
spot11	157.87	1612.68	467439.4	-	123.69	85.42	9.97	0.919	9.82	2.05	26.65
spot12	183.96	181.21	467439.4	-	21.18	84.6	3.82	0.144	3.21	-	3.89

A1ST-04.1	Na23	Al27	Si29	Cl37	K39	Ca43	Ti47	Ti48	Ti49	Fe57	Cu63
Spot1	97.52	1607.69	467439.4	-	378.85	42.93	6.49	0.985	5.58	8.98	-
Spot2	445.08	1851.02	467439.4	-	308.49	81.82	6.48	0.756	<4.12	51.16	2.33
Spot3	63.28	101.32	467439.4	-	18.06	99.59	2.75	0.165	<4.54	182.14	-
Spot4	68.74	96.5	467439.4	-	17.58	87.21	2.64	0.172	<4.33	20.98	-
Spot5	185.85	330.72	467439.3	-	68.88	27.04	4.73	0.569	2.48	-	3.55
Spot6	522.15	1963.9	467439.3	-	305.91	10.46	4.91	0.909	2.62	49.28	2.25
Spot7	302.06	1434.64	467439.4	-	505.54	34.83	5.93	0.417	3.47	27.07	
Spot8	49.71	18.53	467439.4	-	34.55	65.1	3.17	0.295	2.68	-	1.43
Spot9	36.3	31.28	467439.4	-	35.61	91.81	2.42	0.155	<1.91	-	
Spot10	316.45	1938.57	467439.4	-	271.72	32.51	4.45	0.588	3.03	-	1.31

A1ST-04-2	Na23	Al27	Si29	Cl37	K39	Ca43	Ti47	Ti48	Ti49	Fe57	Cu63
Spot11	201.37	422.94	467439.3	-	79.88	333.62	4.05	0.214	2.21	42.15	3.61
Spot13	213.86	546.22	467439.3	-	96.87	306.1	3.43	0.62	4.65	36.03	2.71
Spot14	382.3	1139.41	467439.3	-	302.61	305.41	5.07	0.59	2.6	35.14	3.85
Spot15	262.51	787.72	467439.4	-	151.53	337.07	4.88	0.5	3.58	37.95	2.36
Spot16	134.91	75.54	467439.4	-	36.86	331.19	3.39	0.248	2.48	37.11	1.14
Spot17	145.07	106.7	467439.4	-	42.35	351.02	3.65	0.278	2.69	38.28	6.19
Spot18	565.43	2200.35	467439.4	-	602.96	306.65	6.35	0.82	4.89	32.67	4.14
Spot20	65.41	98.38	467439.4	-	53.61	1006.14	3.82	0.8	2.5	32.59	2.78

A1ST-06.1	Na23	Al27	Si29	Cl37	K39	Ca43	Ti47	Ti48	Ti49	Fe57	Cu63
Spot1	26.15	294.34	467439.4	-	13.15	271.73	1.58	0.184	2.47	11.83	-
Spot2	90.3	25.91	467439.4	-	145.78	370.66	3.17	0.229	1.75	10.25	0.46
Spot3	49.97	14.23	467439.3	-	172.24	181.61	4.28	0.179	1.86	13.55	0.89
Spot5	64.59	2511.52	467439.4	-	802.49	331.11	4.48	0.596	4.66	11.29	-
Spot8	72.75	420.08	467439.3	-	16.3	104.89	2.24	0.18	1.17	8.18	-
Spot10	167.48	759.9	467439.3	-	109.27	136.86	3.02	0.279	1.58	12.46	0.86

A1ST-06.2	Na23	Al27	Si29	Cl37	K39	Ca43	Ti47	Ti48	Ti49	Fe57	Cu63
Spot11	56.72	183.43	467439.4	-	82.29	302.92	2.01	0.253	1.63	25.97	-
Spot12	20.93	43.7	467439.4	-	18.7	255.04	2.97	0.331	3.27	9.53	2.53
Spot13	53.08	1815.26	467439.4	-	228.66	305.18	3.36	0.426	2.53	9.64	2.28
Spot14	185	629.24	467439.4	-	81.43	132.57	3.75	0.397	3.21	8.96	1.91
Spot15	46.09	1170.23	467439.4	-	316.89	129.65	4.33	0.468	4.46	9.51	6.09
Spot16	158.44	46.45	467439.3	-	210.33	148.73	4.99	0.577	3.42	7.82	4.67
Spot17	166.67	849.46	467439.4	-	125.49	644.91	4.16	0.63	2.04	9.75	3.09
Spot18	54.57	56.19	467439.4	-	36.4	119.46	4.36	0.486	4.12	11.44	2.32
Spot19	340.57	2181.85	467439.3	-	933.24	211.48	3.91	0.644	6.71	19.76	4.36
Spot20	349.39	1621.09	467439.3	-	461.12	144.86	5.64	0.417	3.52	14.04	4.57

Table 2: LA-ICPMS trace element in quartz dataset with the minimum detection limit filtered (in ppm). Blank spaces indicate value was below detection limit. Ti was the element targeted to calculate palaeotemperature using TitaniQ method.

STABLE ISOTOPE RESULTS

RAFTER
GNS SCIENCE

SIL ID Number	Sample ID	Minerals	$\delta^{34}S$ Value	std. dev.
95927	OO4	Chalcopyrite	-10.5	0.2
95928	006	Chalcopyrite	-8.9	0.0
95929	#A11	Pyrite	-8.0	—
95930	#18	Chalcopyrite	-8.9	0.1
95931	OO5	Pyrite	-1.2	0.1
95932	#9	Chalcopyrite	-5.4	0.1
95933	#17	Chalcopyrite	-8.8	0.1
95934	#19	Chalcopyrite	-9.4	0.2
95935	#21	Chalcopyrite	-7.3	0.1
95936	#A18	Chalcopyrite	-8.6	0.1
95937	PBS	Chalcopyrite	-8.5	0.0
95938	#11	Chalcopyrite	-7.8	0.0
95939	#1	Pyrite	-7.9	0.1

Table 3: Summary of δ34S (‰ CDT) of sulphide samples from the Moola Prospect Samples differentiated by sulphide type.

Sample-
A1St_001

	p/s/pps	host	Tf	Trex/vit	Te	TmHH	Tmice	Th
1	p	Quartz	-50	-53	-37	-20	-13.6	178
2	p	Quartz	-67	-55	-35	-29	-15.8	192
3	p	Quartz	-60.5	-	-35	-23	-13.3	182
4	p	Quartz	-65	-	-38	-27	-13.5	186
5	p	Quartz	-62	-52	-41	-36	-14.3	188
6	p	Quartz		-	-37	-21	-	194
7	p	Quartz	-55	-	-42	-22	-13.6	179

	p/s/pps	host	Tf	Trex/vit	Te	TmHH	Tmice	Th
1	p	Quartz	-70	-	-45.8	-27.3	-15.2	159.5
2	p	Quartz	-	-	-55	-29.5	-14.7	162.7
3	p	Quartz	-	-	-51	-31	-14.1	166
4	p	Quartz	-	-	-53	-33.7	-15.3	188
5	p	Quartz	-	-	-48	-37.6	-13.7	178
6	p	Quartz	-	-	-46	-39	-14.5	164.5
7	p	Quartz	-	-	-42	-42.8	-12.8	181.8

	p/s/pps	host	Tf	Trex/vit	Te	TmHH	Tmice	Th
1	p	Quartz	-	-	-44.8	-27.8	-14.4	156
2	p	Quartz	-	-	-44	-29.2	-14.6	176
3	p	Quartz	-	-	-45.2	-31.4	-14.7	180
4	p	Quartz	-	-	-44.9	-41	-15.2	162
5	p	Quartz	-	-	-47.8	-33.9	-14.3	175
6	p	Quartz	-	-	-43	-32.5	-15.2	168
7	p	Quartz	-	-	-	-	-	178

	p/s/pps	host	Tf	Trex/vit	Te	TmHH	Tmice	Th
1	p	Quartz	-	-70	-55.3	-	-16	130.9
2	p	Quartz	-	-65	-53.8	-32.6	-13	139.1
3	p	Quartz	-	-72.5	-42	-21	-13.5	143
4	p	Quartz	-	-	-38.9	-	-14.8	148
5	p	Quartz	-	-	-41	-44	-13.7	148.9
6	p	Quartz	-	-	-39.8	-41.8	-14.9	146
7	p	Quartz	-	-	-39.8		-15.8	145

Table 4: Summary of the Fluid inclusion data, including both high and low temperature data. Units for all values °C.

Table.5- TitaniQ thermometry calculated temperatures

A1ST-1.1	Ti47	TitaniQ
spot1	-	-
spot2	5.75	488.8148
spot3	-	-
spot4	4.58	473.8482
spot5	-	-
spot6	4.31	469.9499
spot7	4.48	472.4271
spot8	5.02	479.8116
spot9	8.48	515.8098
spot10	-	-

A1ST-07.1	Ti47	TitaniQ
spot1	4.34	470.3928
spot2	4.62	474.4094
spot3	5.01	479.6809
spot4	4.69	475.382
spot5	4.59	473.9889
spot6	9.37	523.0561
spot7	4.86	477.695
spot8	8.16	513.052
spot9	8.8	518.4838
spot10	4.37	470.8333

A1ST-1.2	Ti47	TitaniQ
spot11	7.44	506.5075
spot12	-	-
spot13	5.1	480.8491
spot14	4.63	474.5491
spot15	-	-
spot16	5.64	487.5208
spot17	6.16	493.465
spot18	5.21	482.2539
spot19	6.01	491.7941
spot20	8.77	518.2365

A1ST-7.2	Ti47	TitaniQ
spot11	5.31	483.5099
spot12	4.21	468.4546
spot13	4.07	466.3111
spot14	5.36	484.1306
spot15	3.82	462.3263
spot16	6.41	496.1769
spot17	4.08	466.4662
spot18	3.86	462.9781
spot19	7.9	510.7454
spot20	4.54	473.2829

A1ST-1.3	Ti47	TitaniQ
spot21	9.97	527.6301
spot22	3.82	462.3263

A1ST-04.1	Ti47	TitaniQ
Spot1	6.49	497.0263
Spot2	6.48	496.9206
Spot3	2.75	442.3376
Spot4	2.64	439.9305
Spot5	4.73	475.9324
Spot6	4.91	478.3625
Spot7	5.93	490.8889
Spot8	3.17	450.8472
Spot9	2.42	434.8532
Spot10	4.45	471.9957

A1ST-06.1	Ti47	TitaniQ
Spot1	1.58	410.9857
Spot2	3.17	450.8472
Spot3	4.28	469.5043
Spot4	-	-
Spot5	4.48	472.4271
Spot6	-	-
Spot7	-	-
Spot8	2.24	430.4035
Spot9	-	-
Spot10	3.02	447.9223

A1ST-04.2	Ti47	TitaniQ
spot11	4.05	465.9999
spot12	-	-
spot13	3.43	455.6546
spot14	5.07	480.4616
spot15	4.88	477.9627
spot16	3.39	454.9351
spot17	3.65	459.4911
spot18	6.35	495.5341
spot19	-	-
spot20	3.82	462.3263

A1ST-06.2	Ti47	TitaniQ
Spot11	2.01	424.2595
Spot12	2.97	446.9204
Spot13	3.36	454.3909
Spot14	3.75	461.1718
Spot15	4.33	470.2455
Spot16	4.99	479.419
Spot17	4.16	467.6959
Spot18	4.36	470.6868
Spot19	3.91	463.7851
Spot20	5.64	487.5208

Table 5: TitaniQ thermometry calculated temperatures based on Ti concentration measured by LA-ICPMS. Table includes sample number as per naming of Table 2. Temperature calculations as per (Wark & Watson 2006).

Table.6- Summary of the three chlorite thermometers calculated tempertures

	Cathelineau (1988)	Kranidiotis (1987)	Jowett (1991)
RJ001_001	613.7984858	281.3052357	618.0267201
RJ001_002	526.3346006	250.2100453	530.3831142
RJ001_003	517.186921	245.6781294	520.6664577
RJ001_004	573.4774179	265.1983795	576.8610283
RJ001_005	497.4471936	241.0656375	501.9202892
RJ001_007	498.3548404	241.8011838	503.0072971
RJ001_008	541.1750339	255.0545893	545.0685177
RJ014_001	628.2002572	275.3122675	627.6803537
RJ014_003	616.4057112	264.9969988	613.2295783
RJ014_004	588.600234	258.4392179	586.797579
RJ014_005	656.1634847	270.5971801	649.3998943
RJ014_006	613.8075628	268.7160421	612.6220931
RJ014_009	638.0070114	276.9212522	636.7000788
RJ014_010	638.4651155	264.8542743	631.9012805
RJ014_011	669.9641614	289.8722781	669.4062977
RJ014_012	667.6076308	288.8404088	666.9614884
RJ014_015	603.772501	263.263346	601.7560018
RJ014_016	598.5957094	247.5515733	590.6050279
RJ014_017	634.7894391	275.7770147	633.4757553
RJ014_018	629.1966759	266.5191568	624.7461957
RJ014_019	660.7417303	285.0360214	659.4953195
RJ014_021	633.7437825	273.7859112	631.73176
RJ014_022	609.7457531	265.4565644	607.7714526
RJ014_023	606.9402439	264.6735839	605.0523684
RJ014_024	587.0719942	257.8337556	585.239483
RJ014_027	620.9540161	270.7849771	619.580406
RJ012_004	644.7055585	290.7177722	648.3199386
RJ012_005	653.2199672	293.7791618	656.8666079
RJ012_006	647.3533271	291.0979023	650.7318749
RJ012_009	670.9690762	298.7575043	674.07961
RJ012_012	741.0126247	323.4330396	744.1697626
RJ012_013	694.4085312	307.9767555	697.9481573
RJ012_014	626.3739673	282.888099	629.3864455
RJ012_015	704.5403652	310.9846998	707.8453829
RJ012_016	627.1165116	284.942538	630.900264
RJ012_023_1	674.1593088	301.9510319	678.1617454
RJ012_023_2	627.7714216	283.4924119	630.832983
RJ012_023_3	659.0326341	295.8983823	662.7138751
RJ012_025_1	631.5366945	285.7353902	634.9947889

	Cathelineau (1988)	Kranidiotis (1987)	Jowett (1991)
RJ012_025_2	577.7311736	267.3467259	581.3969746
RJ012_026	640.7234312	289.2047922	644.2878181
RJ012_028	635.3105229	287.9379074	639.1464652
RJ012_029	663.4317324	296.9626164	666.9071671
RJ012_030	511.7861611	245.0203733	515.7972974
RJ012_031	590.4339646	270.4097733	593.5011719
RJ012_032	656.07303	295.0165395	659.8214292
RJ012_040	732.843637	320.6040087	736.0163236
RJ012_046	698.3564344	308.3088585	701.4435329
RJ012_047	614.6515265	279.7688131	618.0905931
RJ015_001	669.8118773	294.8660801	671.4239076
RJ015_002	608.8579192	274.3883266	610.8574309
RJ015_004	584.2853012	267.7815826	587.1497572
RJ015_005	594.9686053	270.8420929	597.5378956
RJ015_006_1	617.52018	278.8767503	620.1431669
RJ015_006_2	616.1959116	278.629147	618.9121358
RJ015_006_3	611.2387607	277.1762974	614.0778668
RJ015_009_1	636.2971235	286.6949674	639.4499325
RJ015_009_3	737.6041342	320.2583098	739.910362
RJ015_009_4	734.9359201	323.6329653	739.0953174
RJ015_010	602.701378	271.3412971	604.3192595
RJ015_011	554.7189024	255.9416861	556.9514835
RJ015_012	706.5855874	309.2425127	708.8332061
RJ015_013	676.031027	299.2298044	678.5813191
RJ015_014	707.1405302	310.6455022	709.907641
RJ015_015	617.8229555	277.181218	619.6713451
RJ015_016	701.7586342	311.1513516	705.5547565
RJ015_017	700.0907808	310.320425	703.7811678
RJ015_018_1	722.6425504	320.3816884	727.2578813
RJ015_018_2	769.7004157	332.125934	772.2689576
RJ015_018_3	766.9721058	333.8750067	770.7040099
RJ015_019_1	699.2904801	304.8360478	700.7437059
RJ015_019_2	604.212435	271.1871174	605.5361791
RJ015_020	704.0802269	309.8875129	706.9829273
RJ015_021	641.2679914	287.6247979	644.0709941
RJ015_022	714.7976491	314.6735139	718.1418607
RJ015_023	653.0928214	290.5192646	655.3571423

	Cathelineau (1988)	Kranidiotis (1987)	Jowett (1991)
RJ015_024	726.471878	318.9867482	729.9100723
RJ015_025	560.4837538	258.1391343	562.7917768
RJ015_027	633.4459312	284.8896805	636.2525446
RJ015_028	676.7190999	299.1993465	679.1525428
RJ015_029	650.5499292	291.5526501	653.6419655
RJ015_030	624.259461	279.4894431	626.1296387
RJ010_001	677.9709862	300.6008451	680.8181881
RJ010_002	650.8154782	293.9696895	654.9066038
RJ010_004	679.8374614	302.4051639	683.1789283
RJ010_005	647.4496274	290.3547401	650.4941544
RJ010_007	626.9116394	283.800005	630.2350877
RJ010_009	659.7169002	295.7475114	663.2300982
RJ010_010	699.4691817	311.2969822	703.6731404
RJ010_012	656.7593821	293.6015717	659.7959644
RJ010_018	653.9710355	292.4773132	656.9447329
RJ010_024	691.4605706	308.4967163	695.6682615
RJ010_027	601.1368922	274.898894	604.5201618
RJ010_029	706.8888626	311.3059569	709.9778645
RJ010_030	651.3492981	292.7552058	654.8377991
RJ010_031	702.4190522	310.7891763	705.9598839
RJ010_032	652.3589483	293.3495335	655.9507168
RJ010_033	588.4231305	272.0869943	592.5146212
RJ010_035	644.5159859	289.6423565	647.6966099
RJ010_036	629.0595139	286.1752256	633.0802365
RJ010_037	658.6299114	296.5474718	662.650935
RJ010_038	668.5191636	299.8669074	672.4760738
RJ010_039	635.1917206	287.8561084	639.0104102
RJ010_040	647.9498123	292.6233984	651.8942559
RJ010_041	661.1983394	296.3157019	664.7324269
RJ010_042	677.7807919	302.1067297	681.3040817
RJ010_043	637.4093851	287.7721887	640.8575939
RJ010_045	621.2814974	282.277386	624.7993129
RJ010_046	610.0804391	278.3584761	613.60245
RJ010_047	609.7876151	277.6086996	613.0314377
RJ010_048	614.5972374	278.0756947	617.3165862
RJ010_049	625.9996856	283.7689	629.447275
RJ010_050	640.1788733	288.7402733	643.6256686

Table 6: A summary of the three cation exchange-based - by sample. All data and sample names based on microprobe data in Table 1.

Figure.1- The location of the Moola Prospect Northern Eyre Peninsula, South Australia. Represented by the mine symbol Modified from Google Maps imagery. http://maps.google.com.au/.

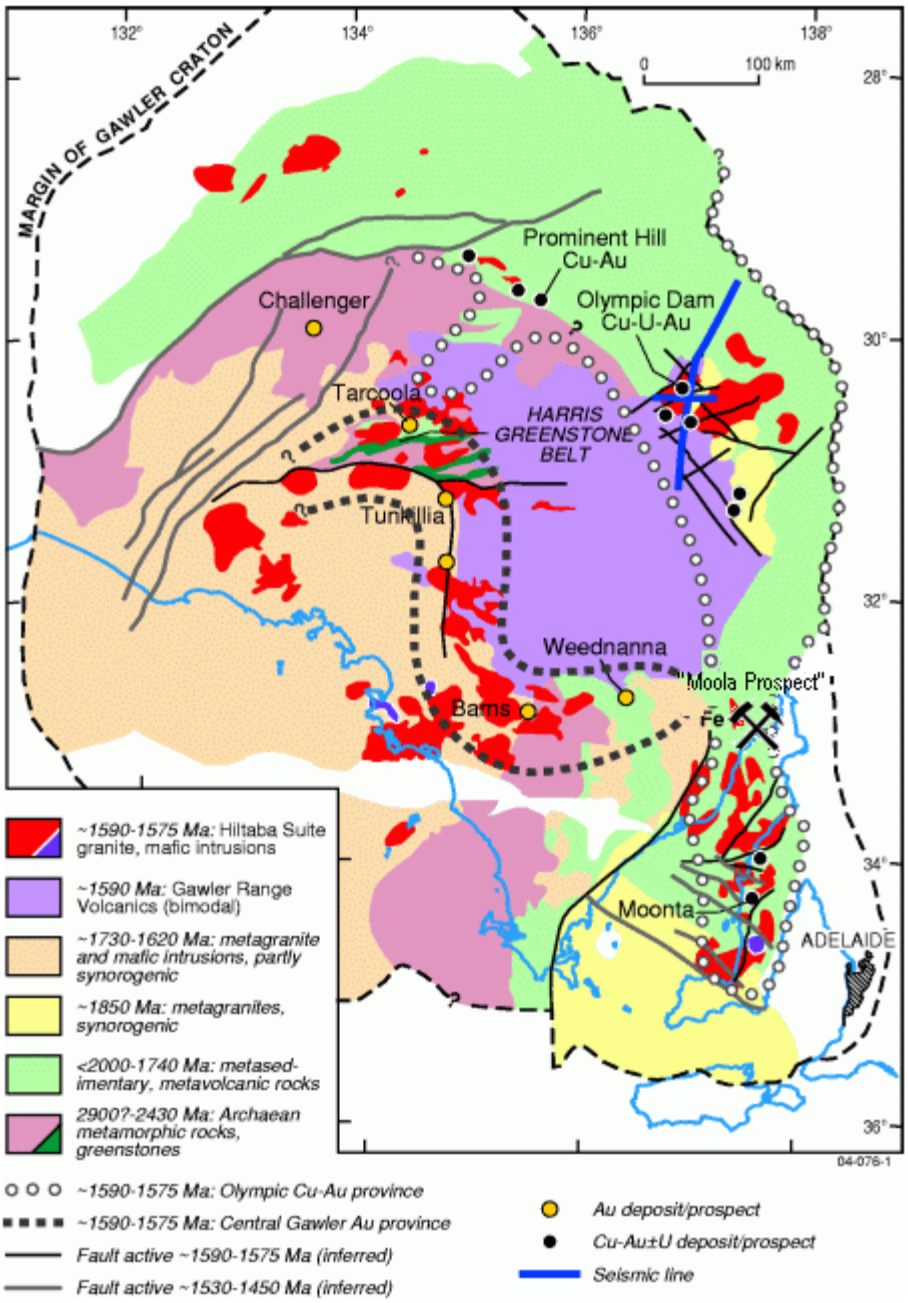

Figure.2- Outlining the extent of the Olympic Cu-Au Province with the Gawler Craton, South Australia. Modified from Skirrow R IOCG presentation during *17th Australian Geological Convention (2004)*

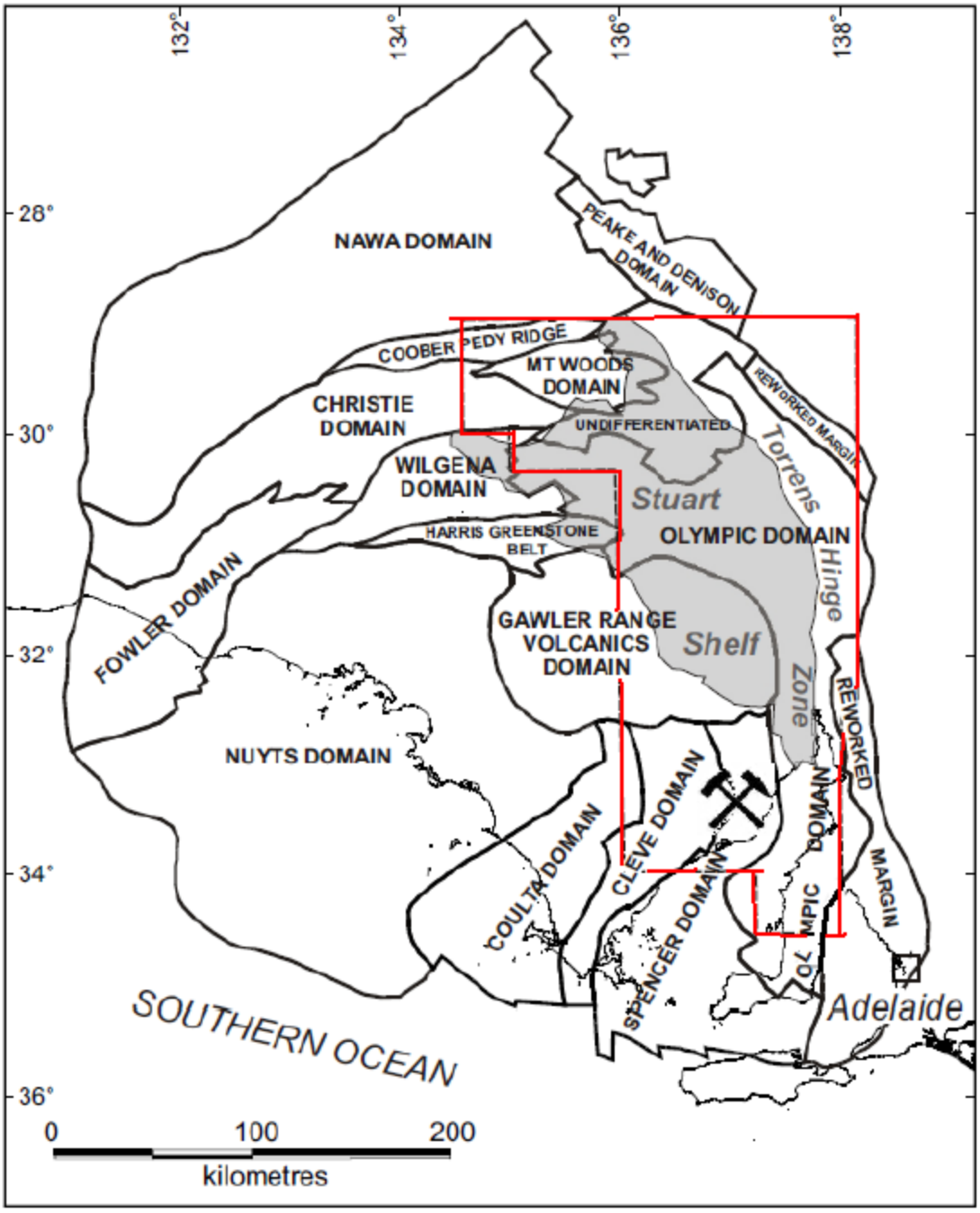

Figure.3-A map of the Tectonic domains of the Gawler Craton , with the Olympic Cu-Au Provience marked in RED. Moola Prospect is represented by the Mine Symbol and occurs within the Northern Eyre Peninsula. Modified from B.Cerlienco 2009.

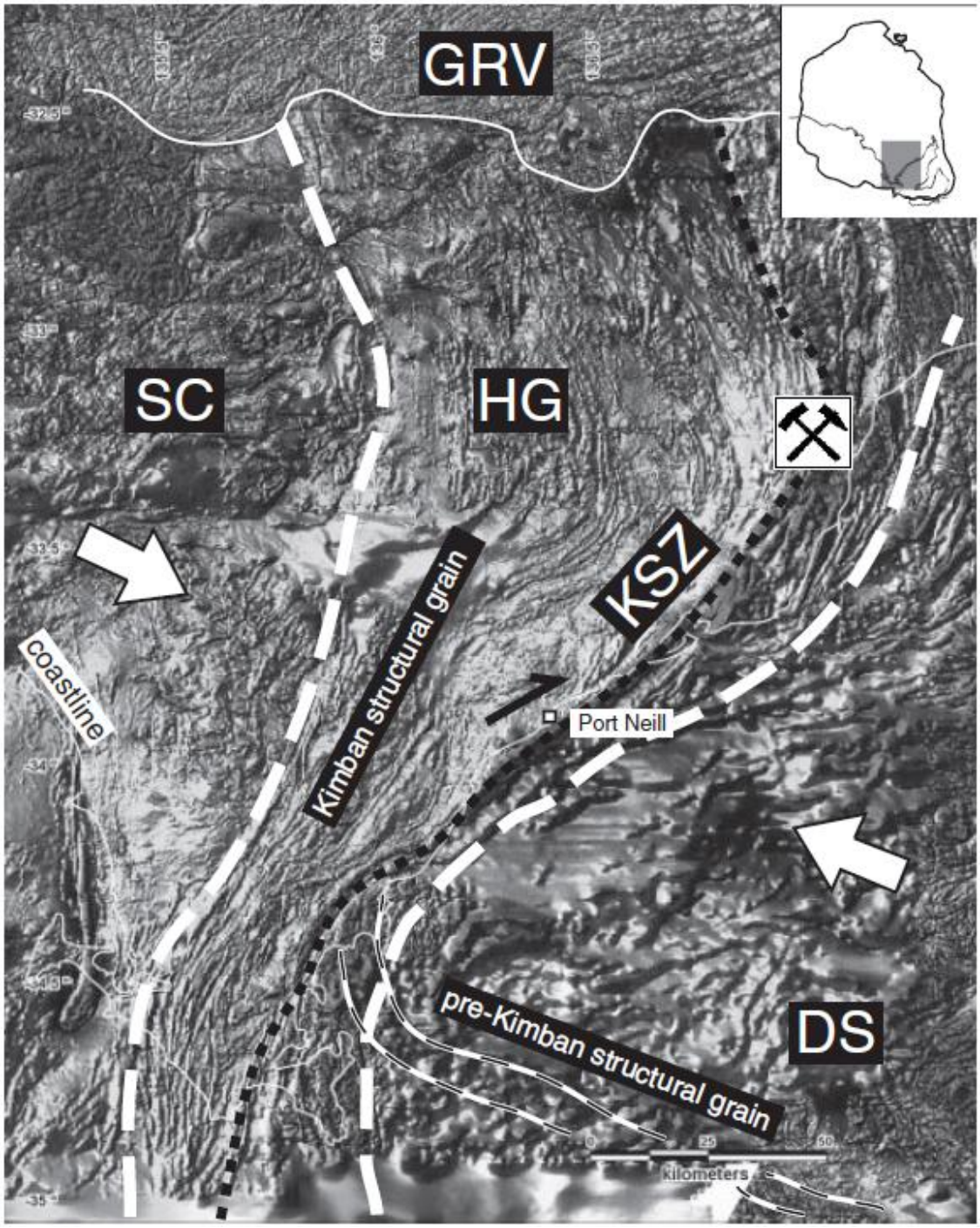

Figure.4-Regional total magnetic intensity image of the southern Eyre Peninsula showing the location of the Kalinjala shear zone and the extent of the associated deformation expressed with a 50-100 Km wide zone proximal to the shear zone (Hand et al 2007)

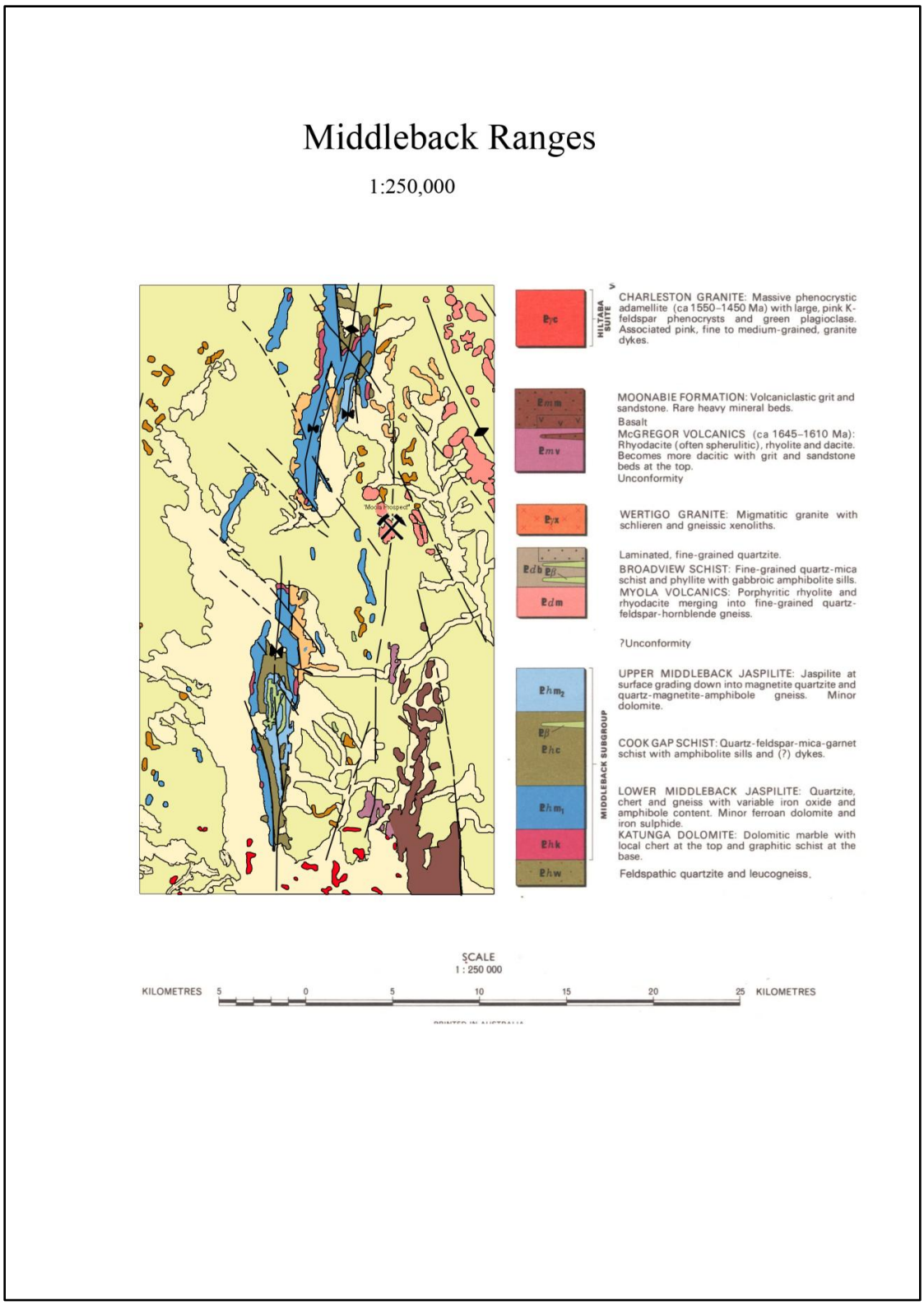

Figure.5- 1:250 000 Geological Map of the Middleback, depicting the Moola Prospect and the shear zone it is situated upon. The Moola Prospect is represented by a mine symbol. Modified from Whyalla Map sheet: Geological Survey of Australia- Department of Mines and Energy

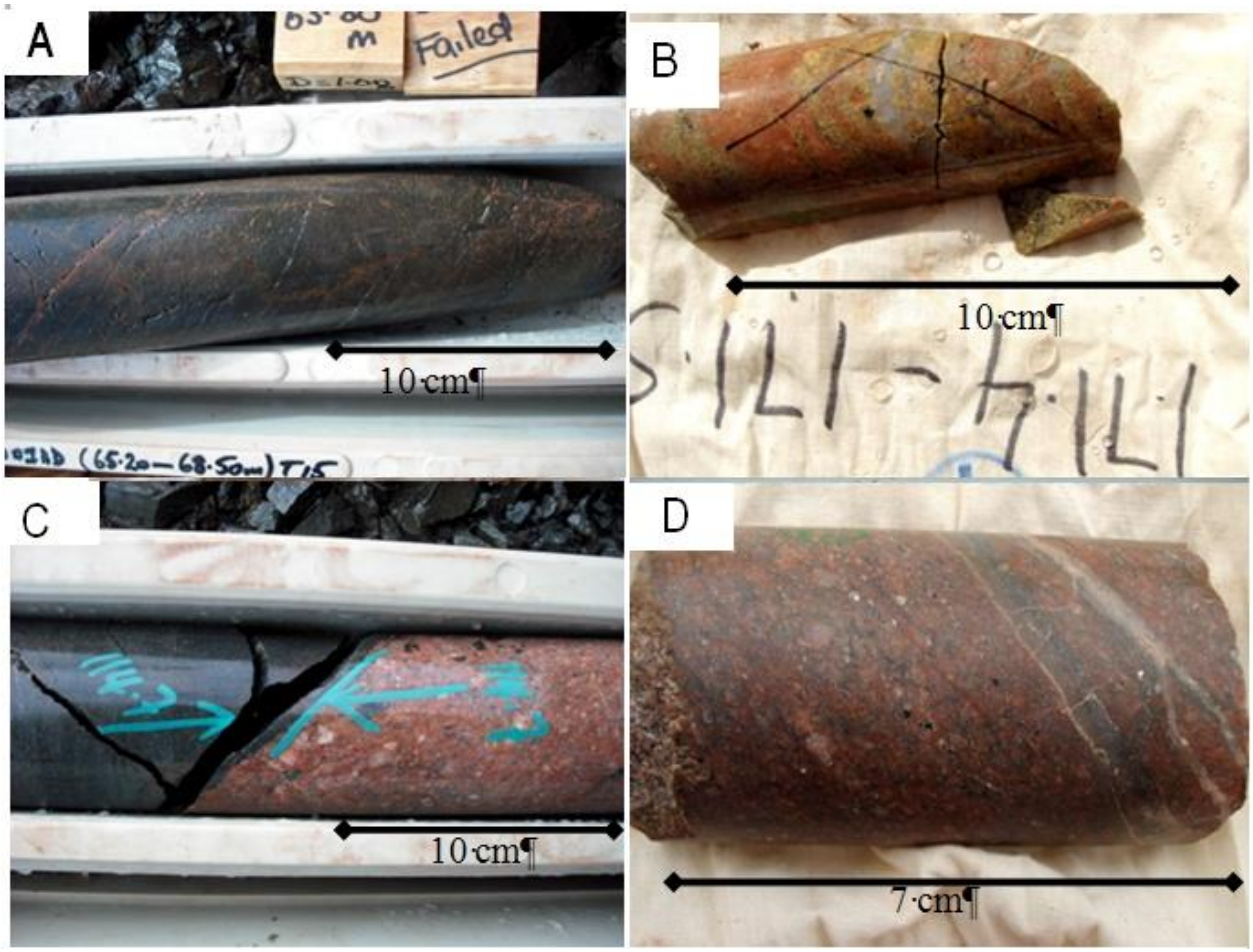
A
Failed
10 cm
B
10 cm
C
10 cm
D
7 cm

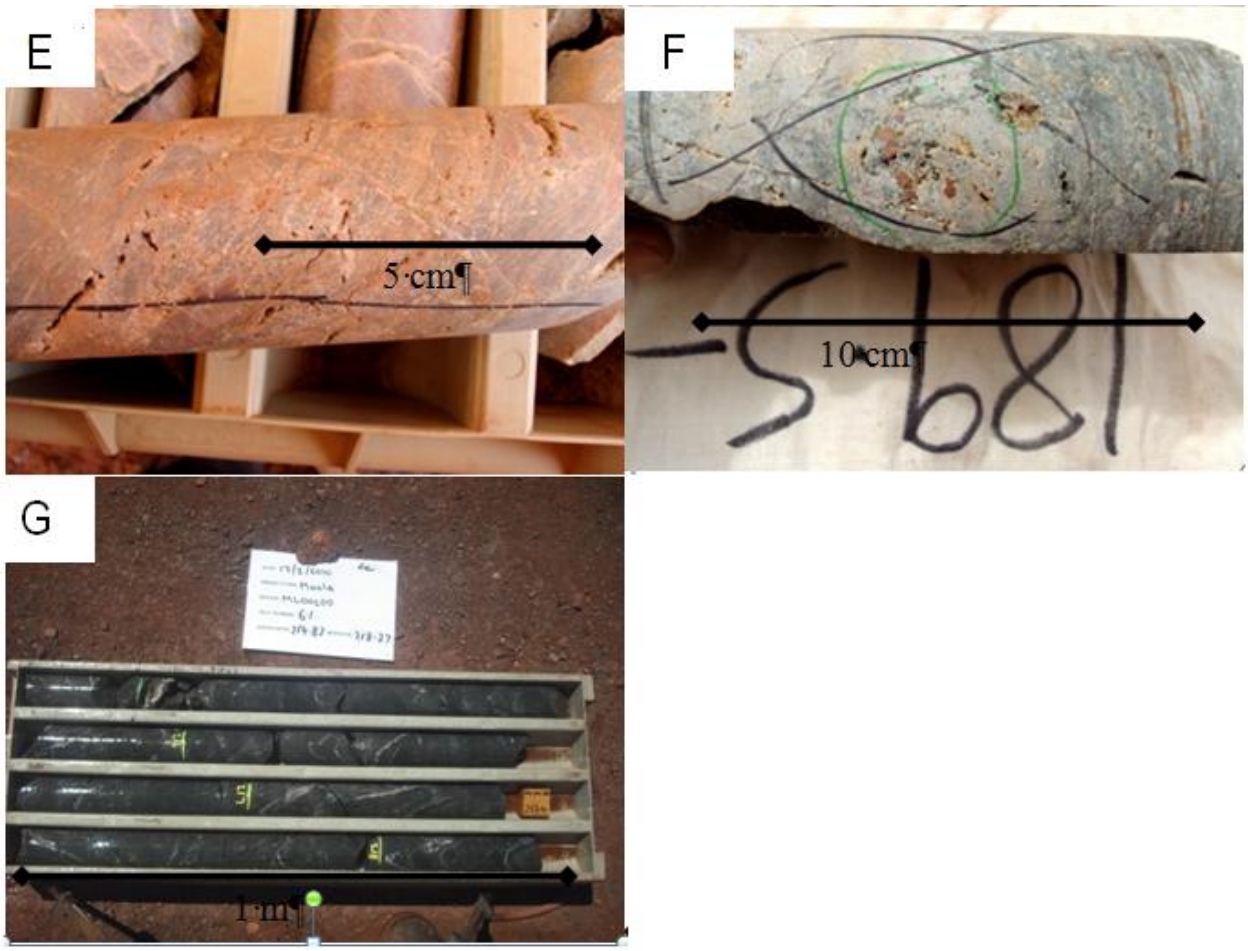

Figure 6 (Continued)- Depicts the host rock lithology for diamond drill core samples obtained from the Moola Prospect.

- (A)Slightly to moderately weathered felsic volcanic that records extencive sodic ± Potassic alteration (75.6m) (B) Highly sericite and chlorite altered fined grained felsic banded (quartz-feldspar) gneiss (171.4m). (C) Fine grained black grey, strongly magnetic amphibolite, in sharp contact with medium to coarse microgranite (114.7m)). (D) Medium to coarse micro grained pink brown microgranite (143.1m). (E) Fine grained pink rhyolite, cut by multiple fine 1-2mm quartz veins (131.4m) (F) Slightly to moderately weathered light green to green/ grey felsic fine to medium grained volcanic to volcaniclastic unit (189.5m) (G) Dark grey/ black fine grained rhyodacite with crosscutting ,large (1-2 cm) carbonate veins which are dominated by chalcopyrite mineralisation

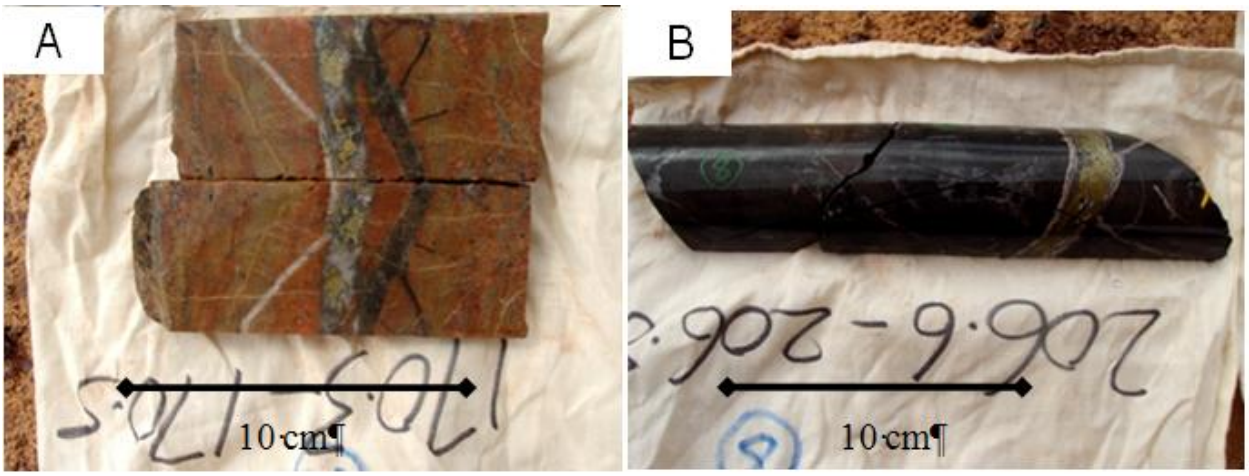

Figure.7A) Highly sericite and chlorite altered fined grained felsic banded quartz feldspar gneiss containing multiple generations of quartz-carbonate veining, with one being mineralised with chalcopyrite (170.3m) B) Dark grey/ black fine grained rhyodacite with a large (1-2 cm) carbonate vein dominated by chalcopyrite mineralisation (206.6m).

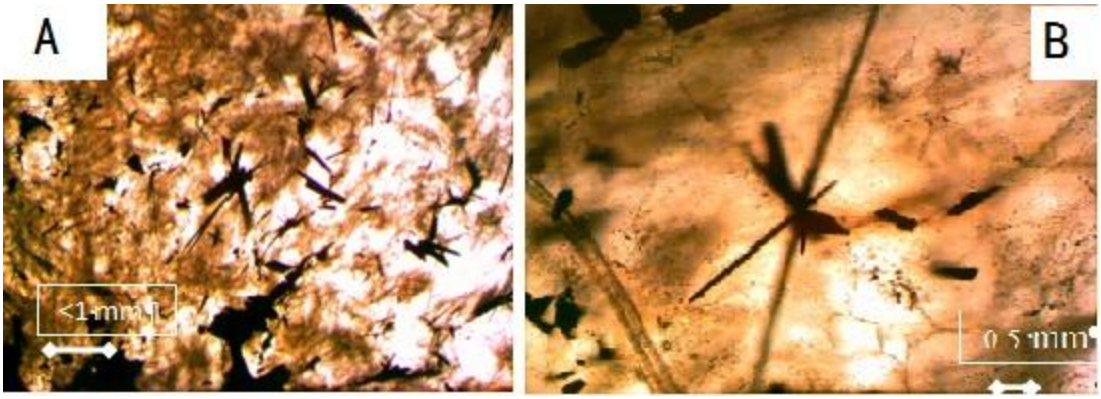

(A) Depicts fine grain rutile needles found within quartz veins which fulfills the Ti saturation requirements for TitaniqQ thermometry (B) Same rutile patch, higher magnification. NOTE due to the subsurface nature of the rutile it could not be efficiently photographed in reflected light.

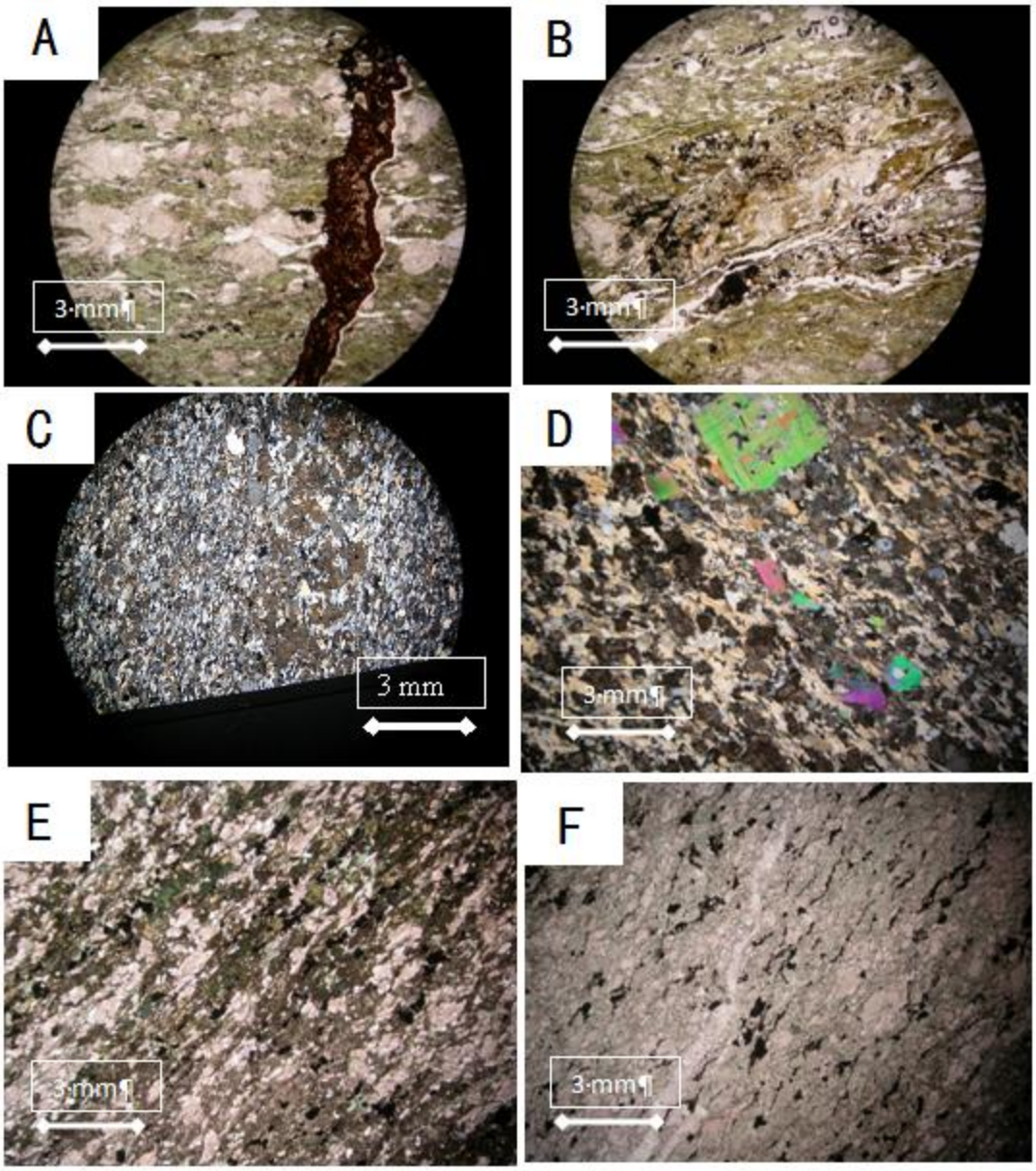
A
3·mm¶
B
3·mm¶
C
3 mm
D
3·mm¶
E
3·mm¶
F
3·mm¶

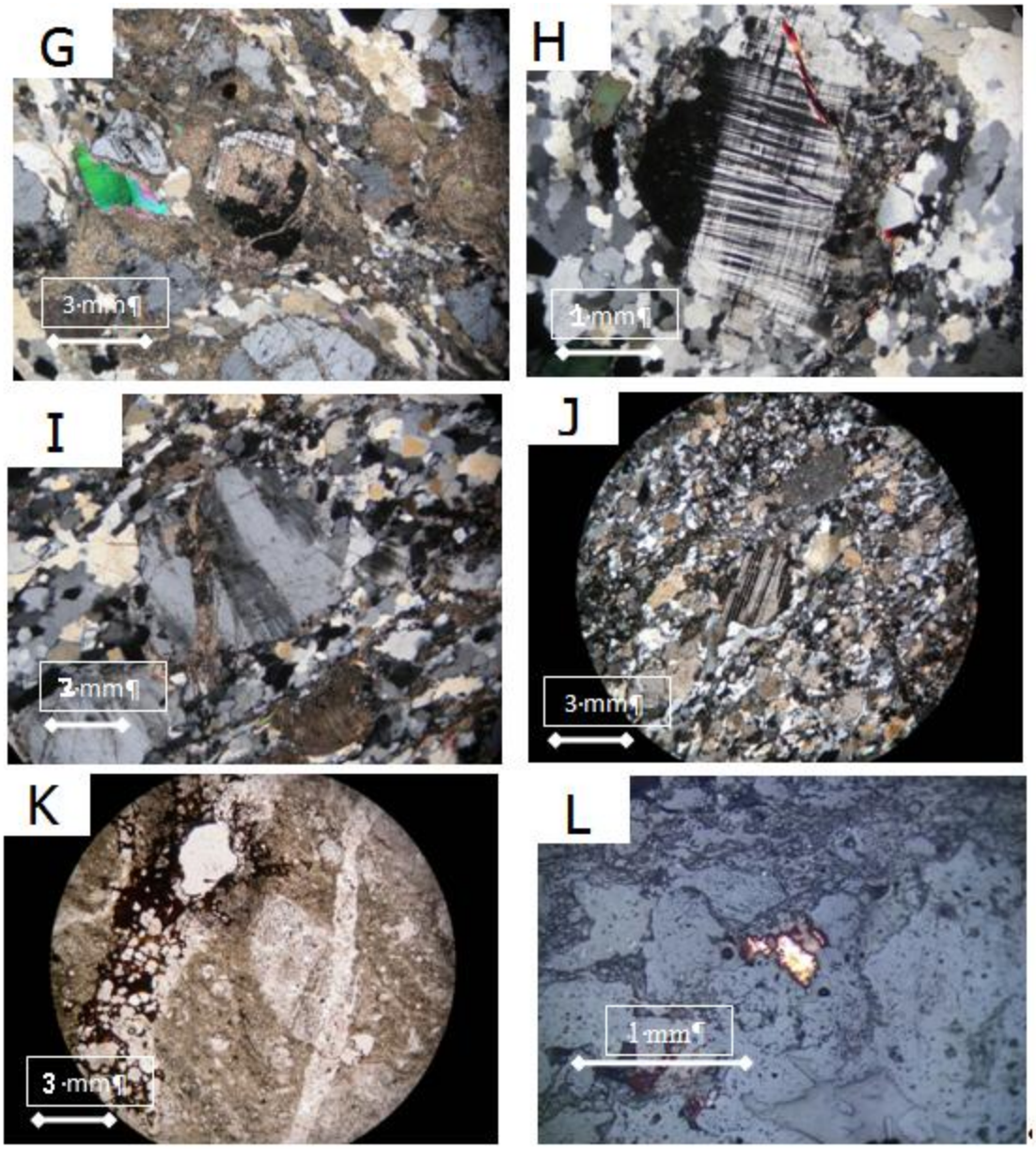
G
3·mm¶
H
1·mm¶
I
1·mm¶
J
3·mm¶
K
3·mm¶
L
1·mm¶

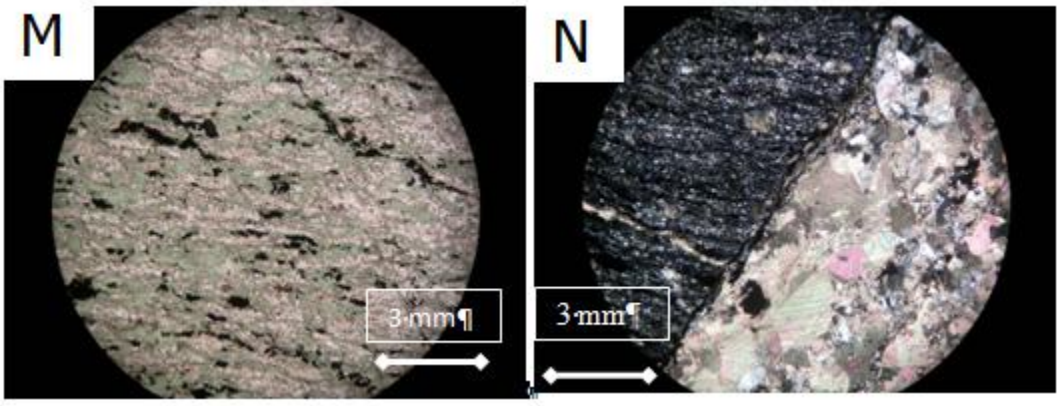

Figure 9- Depicts representative pictures of the host rock and alteration present within the Moola Prospect

- (A) Fine groundmass of chlorite and sericite altered plagioclase which forms as banding throughout, a large crosscutting vein is also depicted containing void and red clay minerals, bi-products of weathering (B) Minor epidote alteration is observed in this slide in association with chlorite and sericite, forming as banding throughout the unit. (C) Fine grained groundmass consisting of recrystallised quartz, plagioclase and sericite altered plagioclase, with larger pseudomorphed phenocrysts of plagioclase replaced by sericite. (D) fine grained groundmass of plagioclase, sericite altered plagioclase and quartz, with phenocrysts of plagioclase (albite), sericite altered plagioclase, also contains large tabular muscovite.(E) fine groundmass of plagioclase quartz and sericite altered plagioclase, with large lathes of oxides, plagioclase, sericite altered plagioclase, quartz, hornblende and chlorite. (F) Chlorite is observed replacing hornblende defining the fabric of the rock, this is localized around the transecting carbonate vein. (G) fine grained groundmass of plagioclase, sericite altered plagioclase and quartz with large phenocryst of magmatic muscovite, K-fledspar, sodic amphibole, plagioclase and sericite altered plagioclase (H) Depicts a microcline phenocryst that is typical within the granitic unit, which accompy the more common plagioclase phenocrysts (I) Fine grained groundmass consisting of recrystallised quartz, plagioclase and sericite altered plagioclase, with larger pseudomorphed phenocrysts of plagioclase replaced by sericite- x10 zoom (J) Same phenocryst depicted in (I) but at a reduced optical zoom, highlights the porphyritic nature of the phenocrysts. (K) Depicts the brecciation and extensive weathering that has affected the volcanoclastic unit. One large vein consist of void and red clay minerals, bi-products of weathering (L) Depicts supergene native copper mineralization that has been redeposited within bracciation and void space within the volcanoclastic unit. (M) Fine groundmass of plagioclase quartz and sericite altered plagioclase, with large lathes of oxides, plagioclase, sericite altered plagioclase, quartz and chlorite defining the fabric of the rock (N) Depicts the typical rhyodaite composition, heavy chlorite and sericite alteration and lathes of oxides that defines the fabric of the rock, which is being crosscut by a major carbonate vein which is characteristic of the unit.

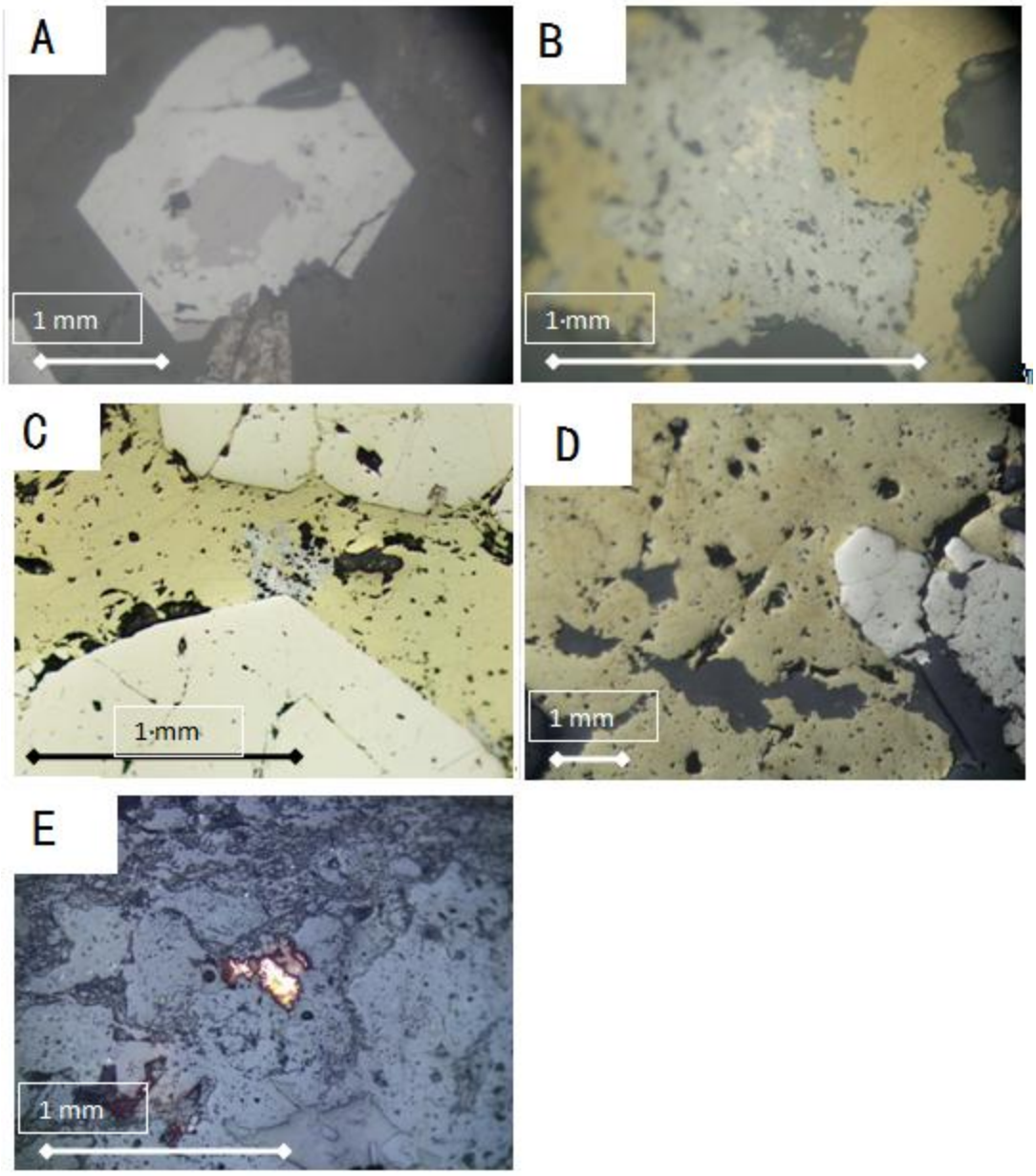

Figure 10- Depicts the transition in mineralization precipitated with the Moola Prospect.

- Martitisation of magnetite by haematite. Martititsation occurs along fractures and the rims of the magnetite (B) Tiny inclusions of pyrite within hematite depict a coprecipitation relationship between the two (C) Haematie growth on the out rim of pyrite depicting a transition from coprecipiation to pyrite dominance (D) Chalcopyrite surround and infill fractures within pyrite which depicts the tranition to chalcopyrite dominant precipitation (E) Depicts supergene native copper mineralization that has been redeposited within the bracciation and void space typical of the volcanoclastic unit.

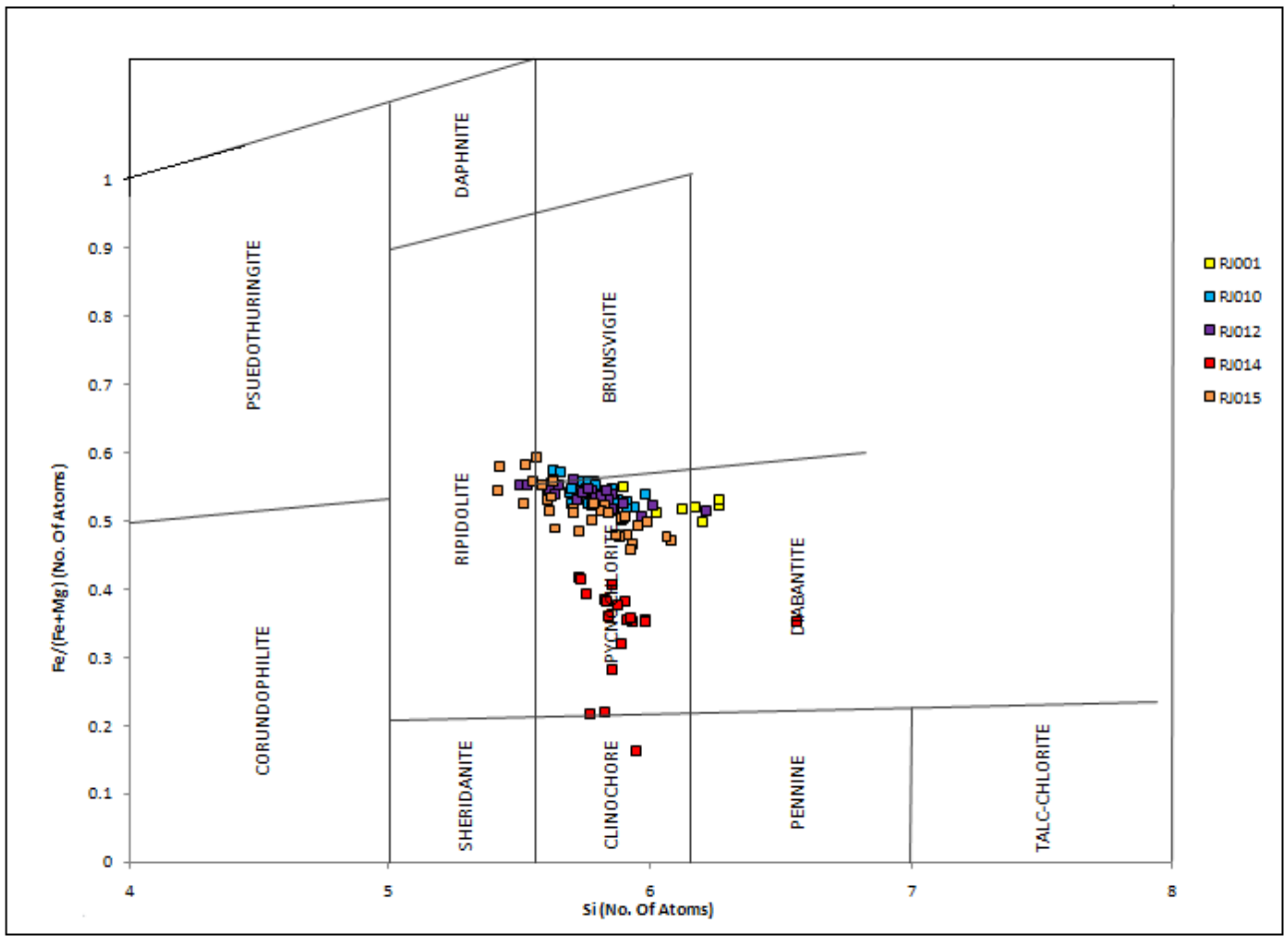

Figure.11- Classification of chlorite from The Moola Prospect based on electron microprobe data under the scheme of Hay (1954). This scheme is based on the ratio of Fe and Mg to Si atoms. Sample spots are separated by colour.

Common molecular ion interferences in ICP-MS	
Isotopes	Interference
Ti^{47}	PO^{+},
	$^{12}C^{35}Cl^{+}$
Ti^{48}	$^{32}SO^{+}$
	POH^{+}
	$^{32}S^{16}O^{+}$
	$^{34}S^{14}N^{+}$
	$^{33}S^{15}N^{+}$
TI^{49}	$^{32}SOH^{+}$
	$^{32}S^{17}O^{+}$,
	$^{35}Cl^{14}N^{+}$
	$^{31}P^{18}O+$
	$^{32}S^{16}OH$

Figure.12-Common interference ions produced by the LA-ICPMS during analysis that can cause errorous data as they are misinterpreted for Ti isotopes

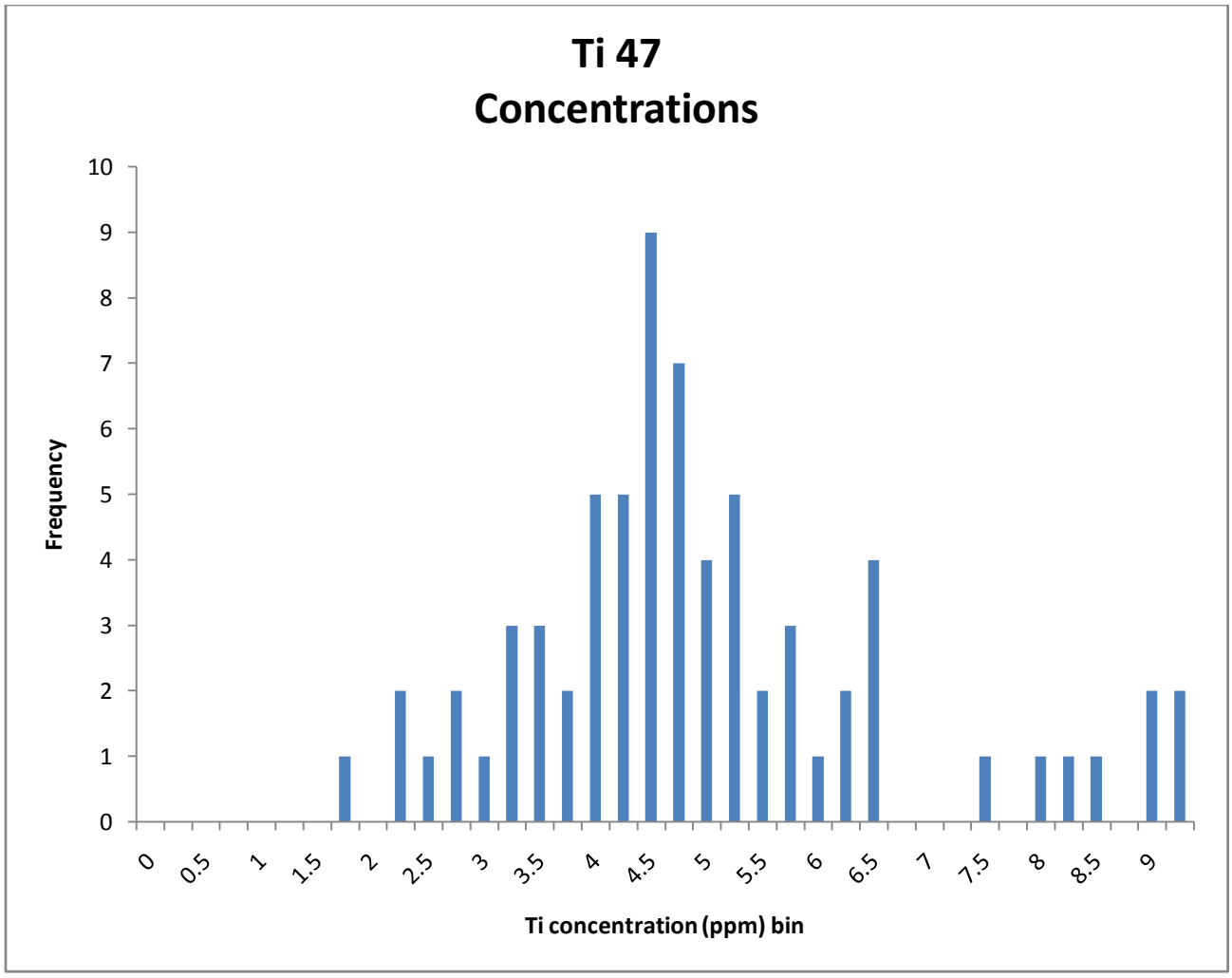

Figure 13-Titanium concentrations in quartz, obtain via LA-ICPMS analysis

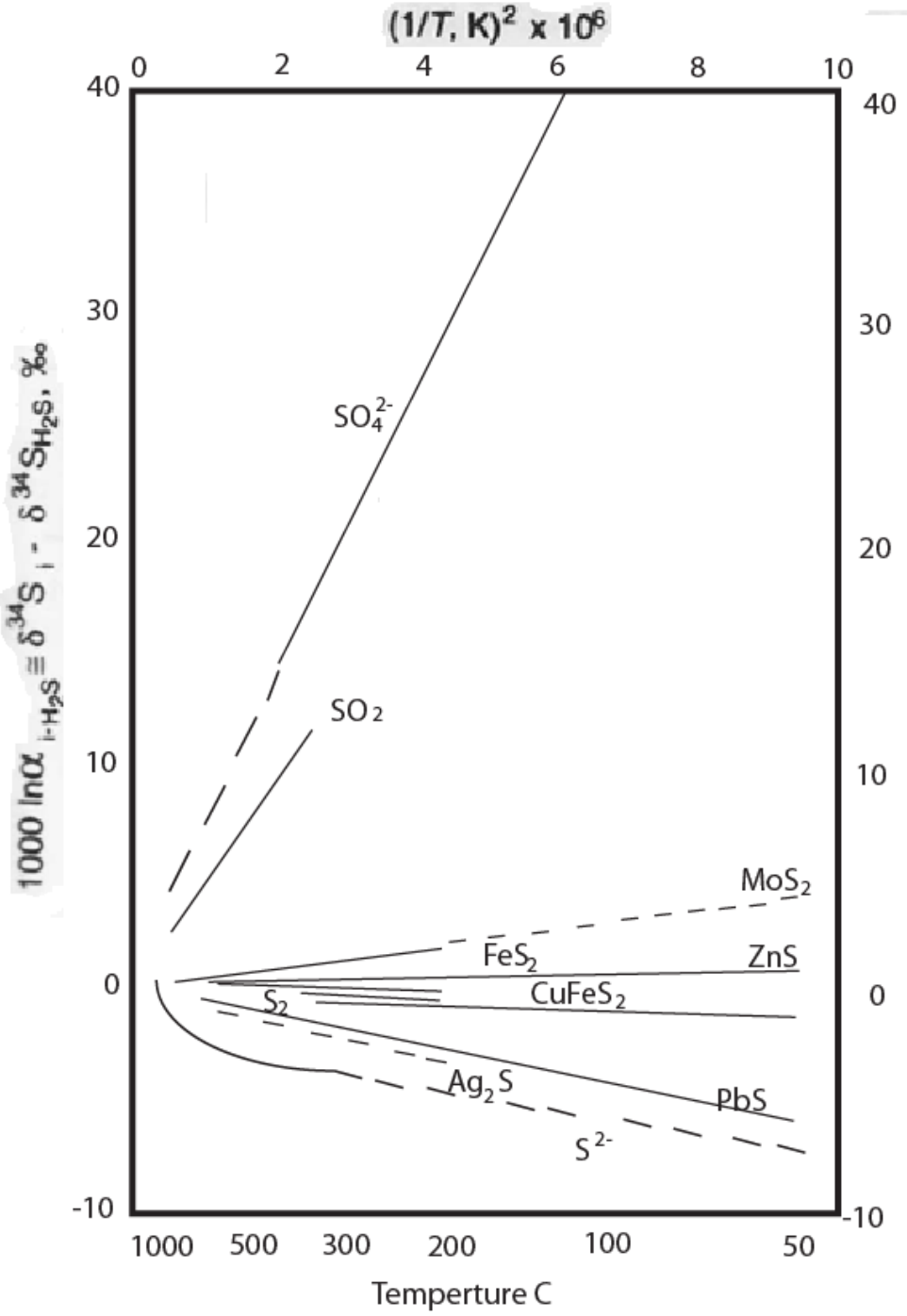

Figure 14- Depicts equilibrium isotopic fractionation between sulphur compounds in respect to temperature.

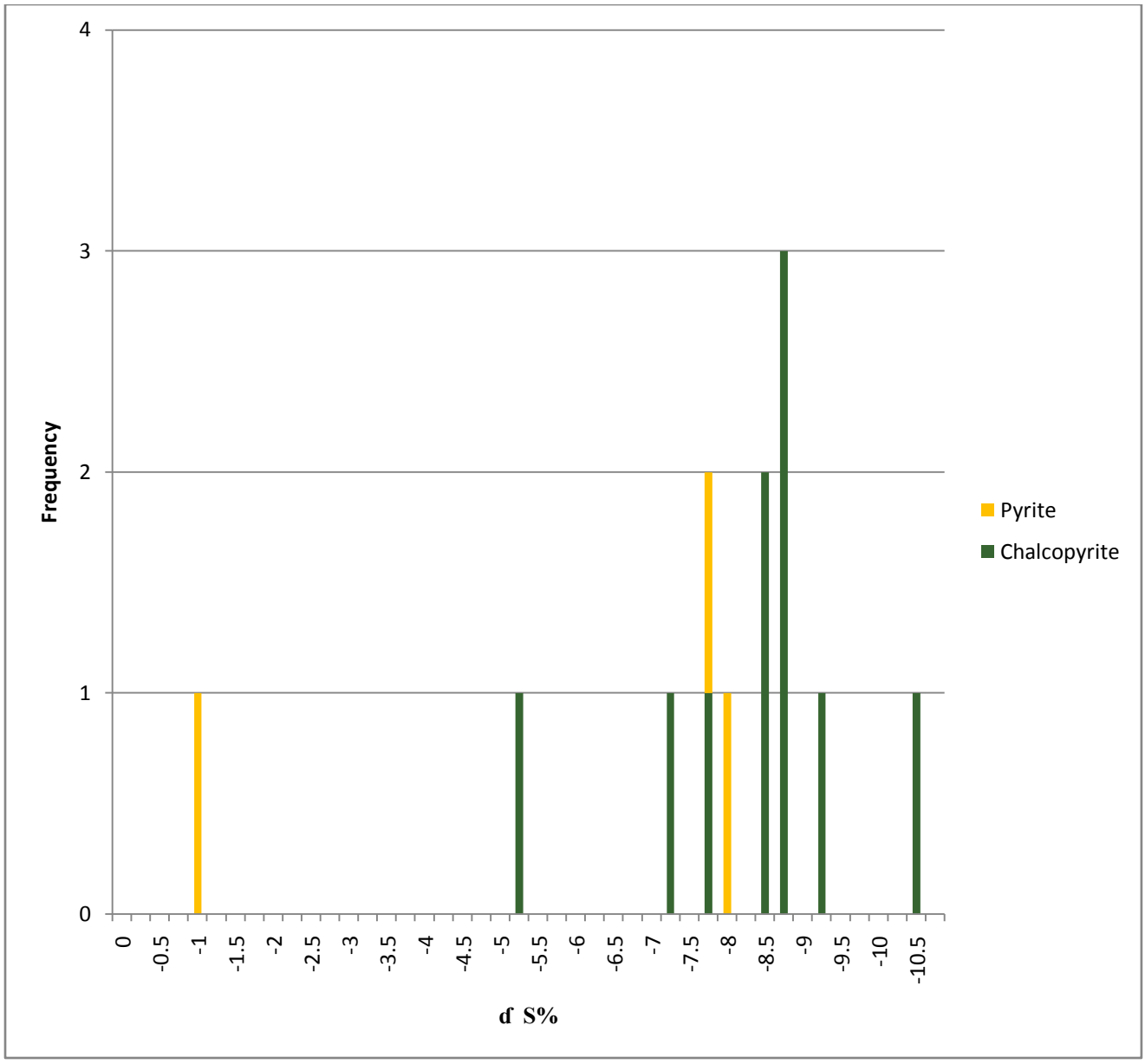

Figure 15-Histogram of sulphide (δ34S [‰CDT]) values, separating different sulphide species by colour

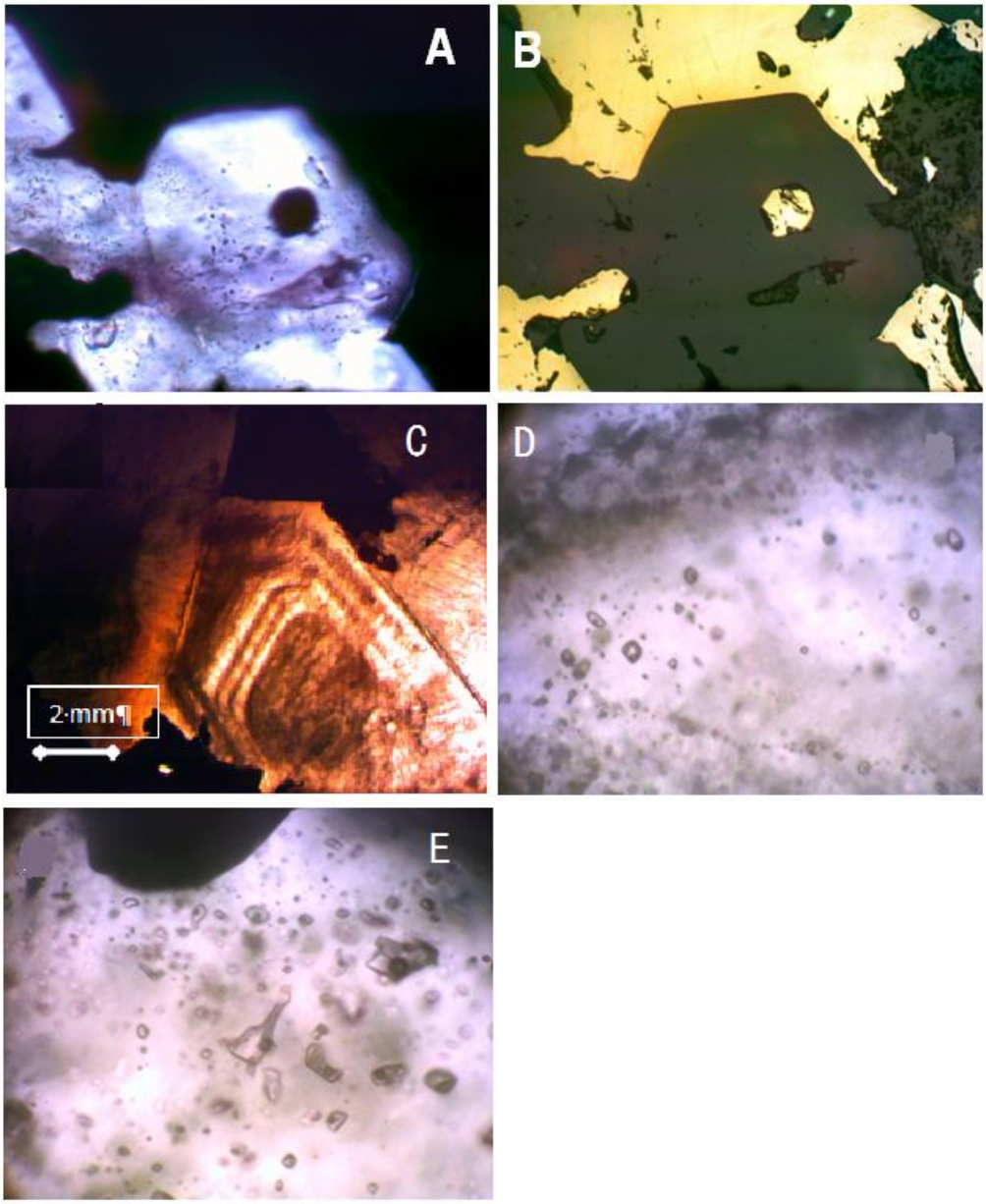

Figure 16- Depicts petrographics picture from the fluid inclusion study, showing the relationships between mineralization, quatz growth, gangue minerals and the inclusions themselves.

- (A,B)- Shows the close spatial relation between the analysised fluid inclusions and the surrounding chalcopyrite mineralization. (C) Show the growth rings of the idoiomorphic quartz and the transition from a cloudy core to a clear rim . (D) Depicts the generally smaller fluid inclusions of the outer clear rims of the quartz (10-20 µm) (E) Depicts the generally larger fluid inclusions of the inner cloudy cores of the quartz (≤ 40 µm)

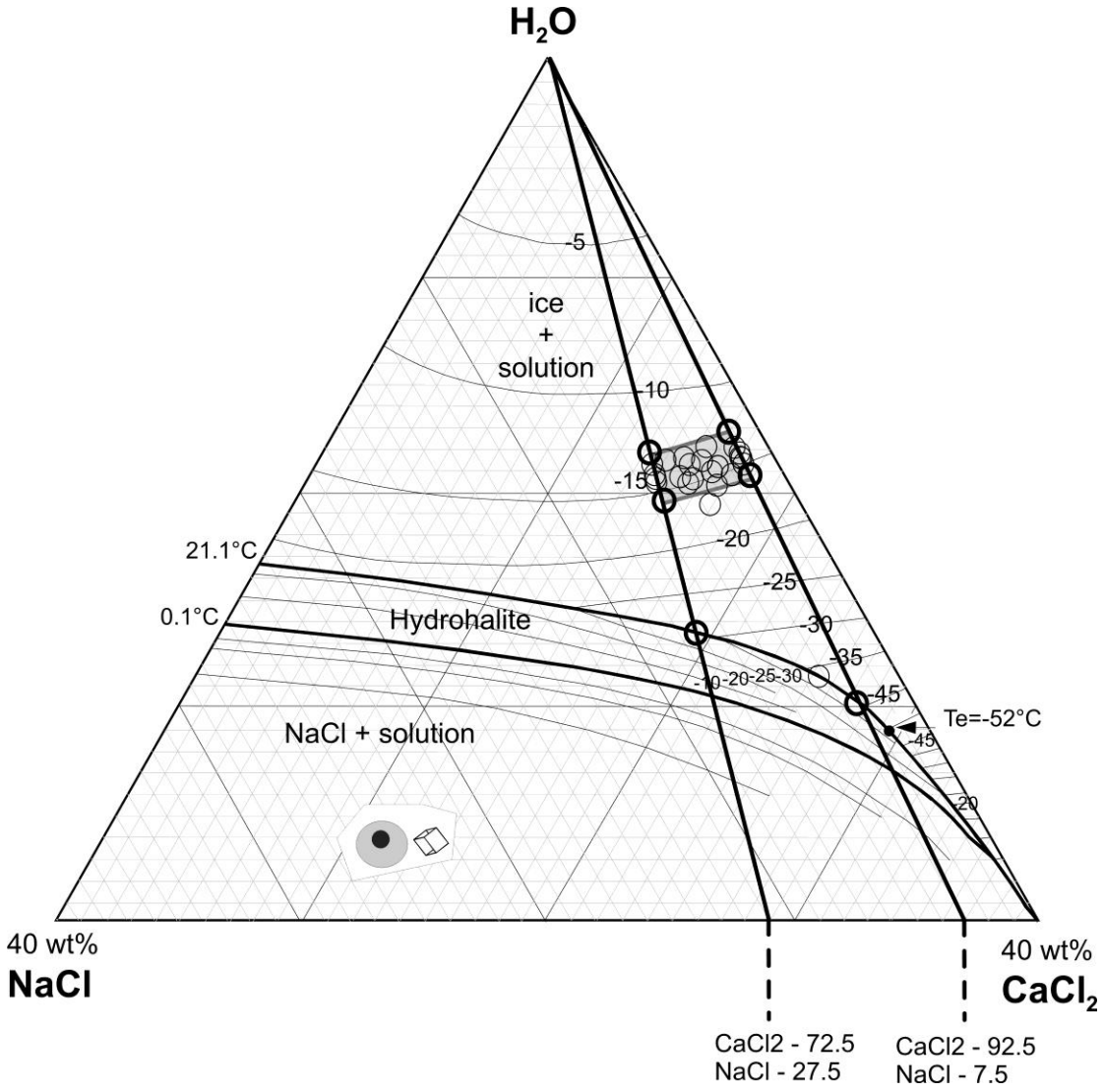

Figure.17- Relative salinity of fluid inclusions hosted with the Moola Prospect

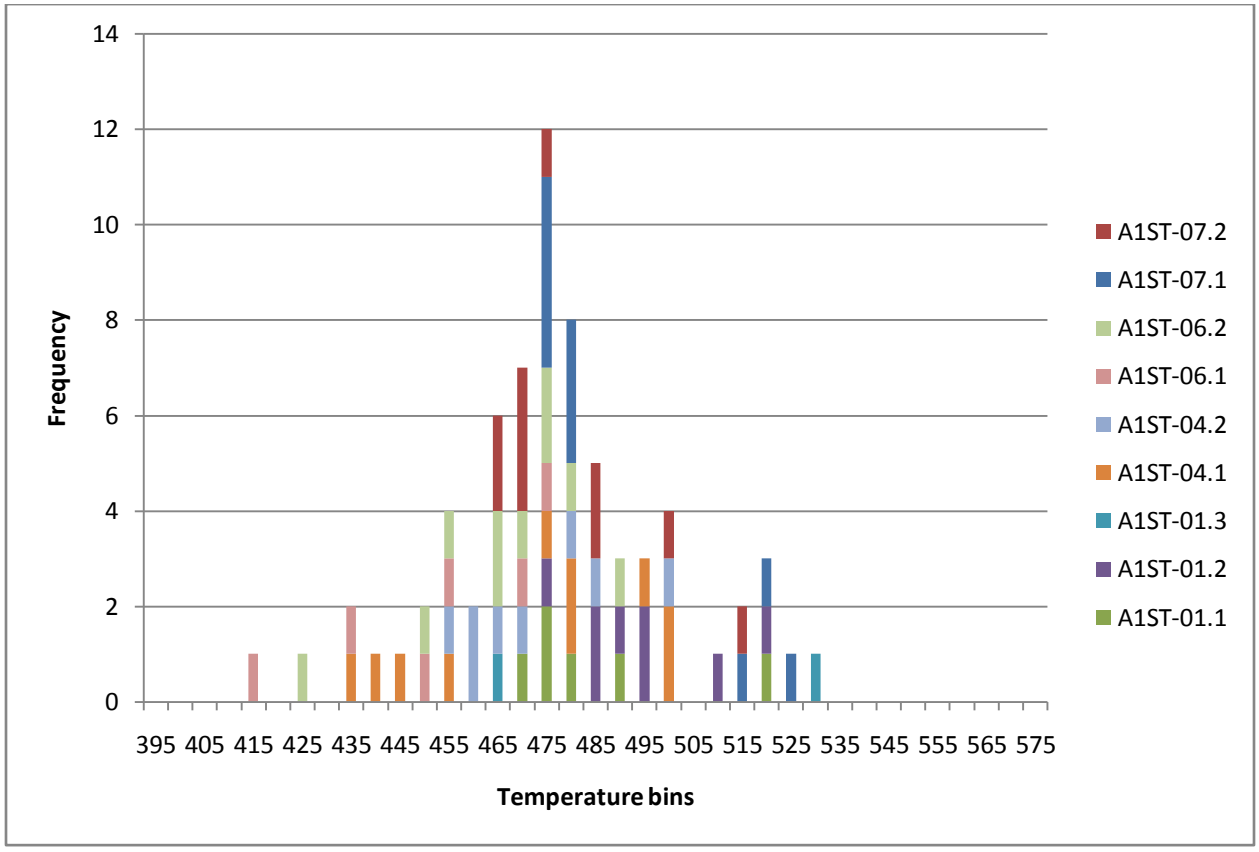

Figure.18-Histogram of the TitaniQ population from the Moola Prospect samples, showing the tempertures of each slide analysised

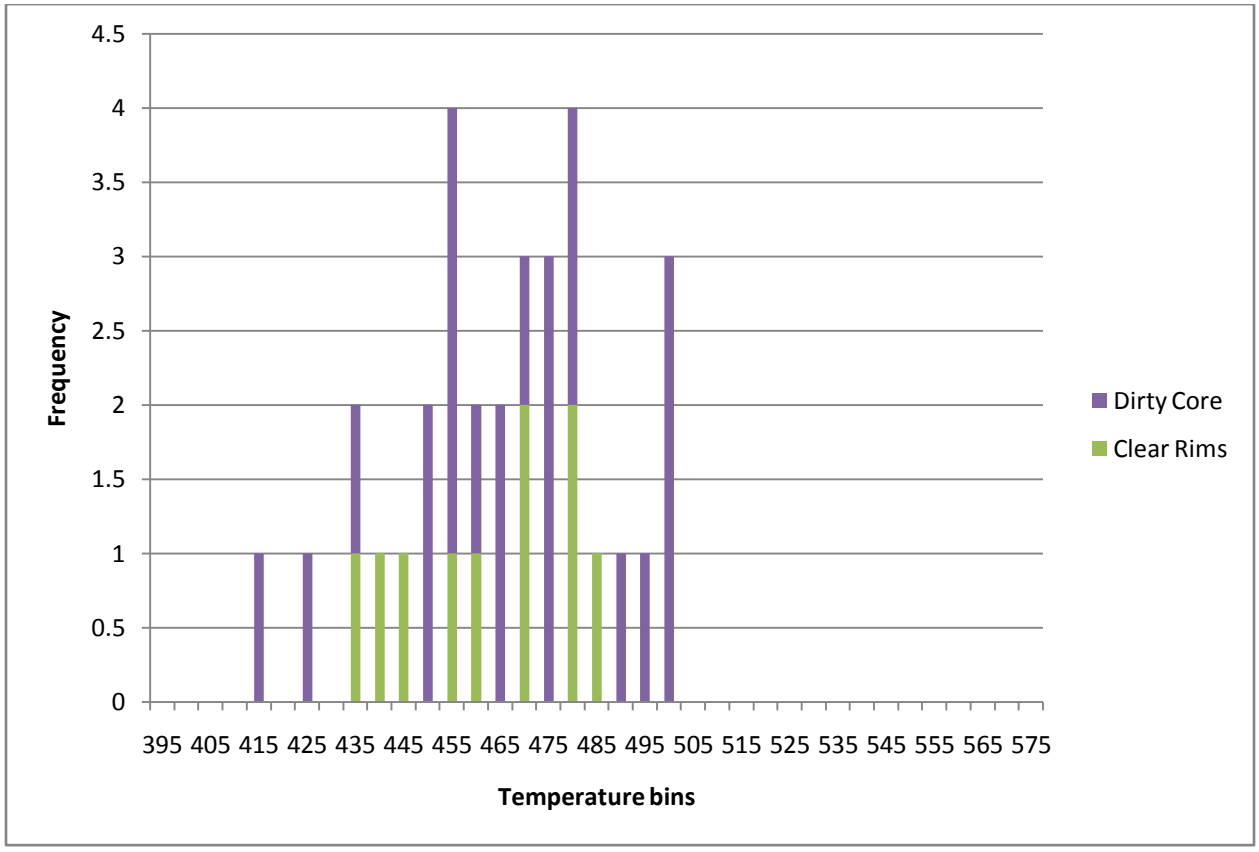

Figure 19-Temperture investigation of an identified petrographic transition in quartz- Dirty Core Vs Clear Rim

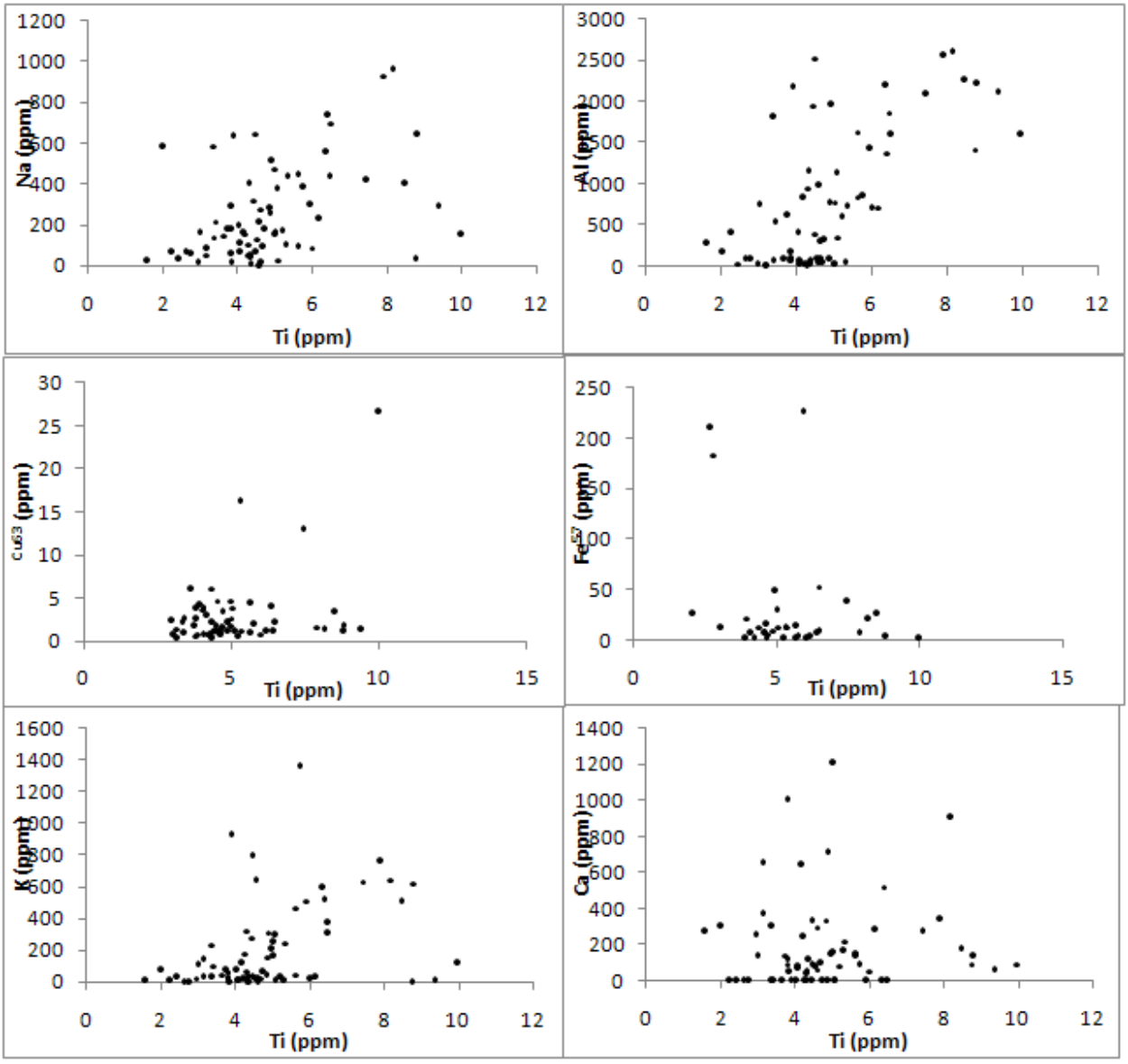

Figure 20- Elemental plots against Ti to identify any systematic link between contamination and excess Ti levels

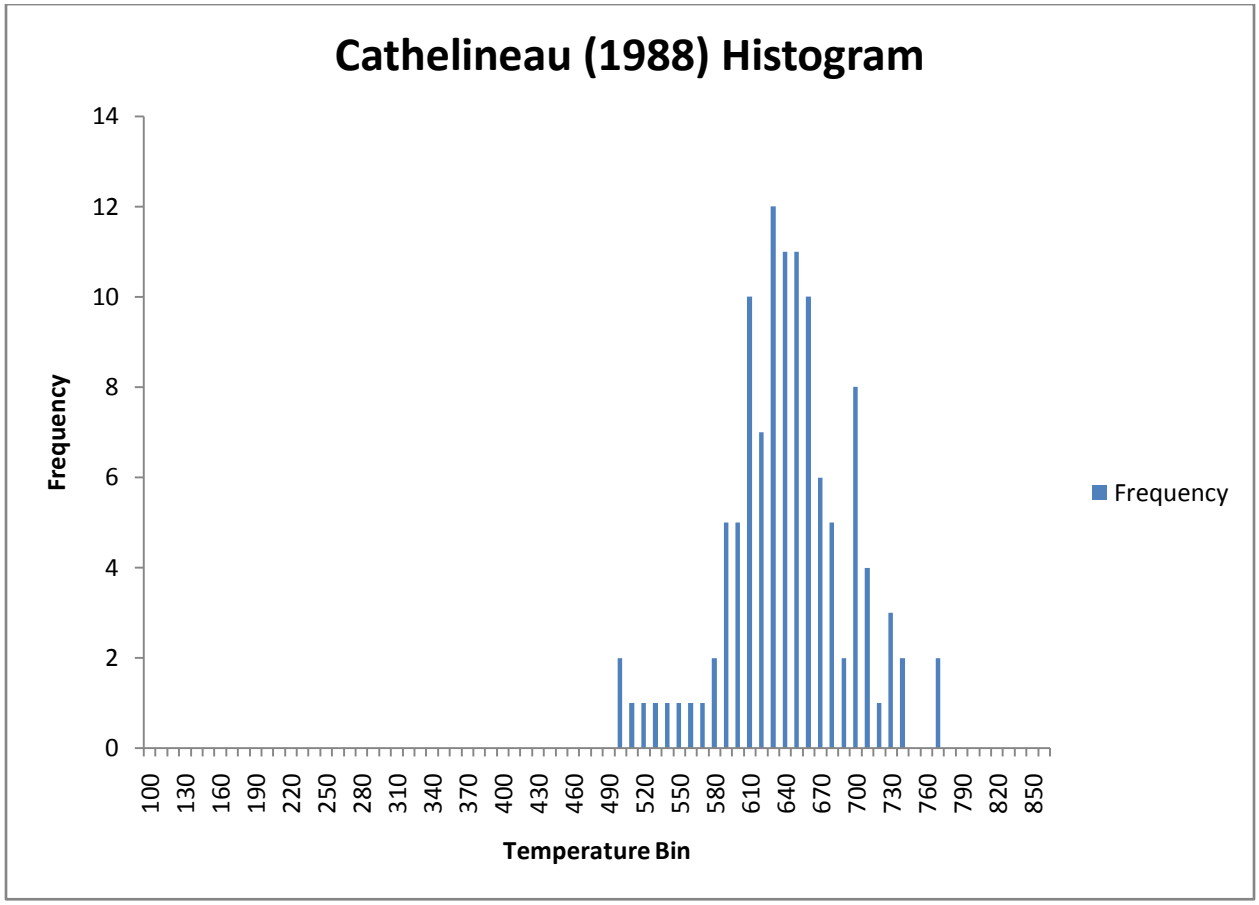

Figure 21-Temperature frequency histograms for the Cathelineau (1988) chlorite thermometer

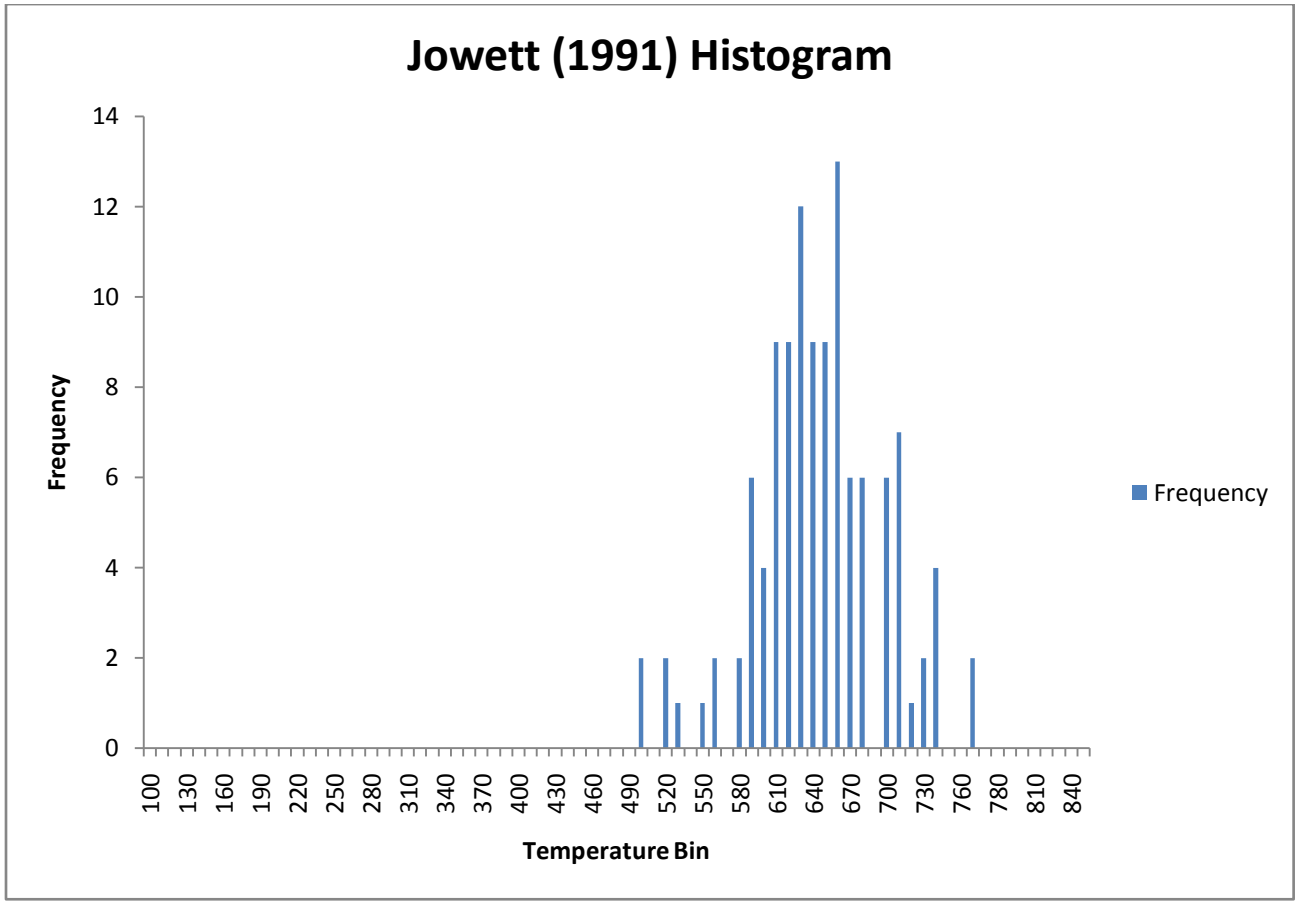

Figure 22 Temperature frequency histograms for the Jowett (1991) chlorite thermometer

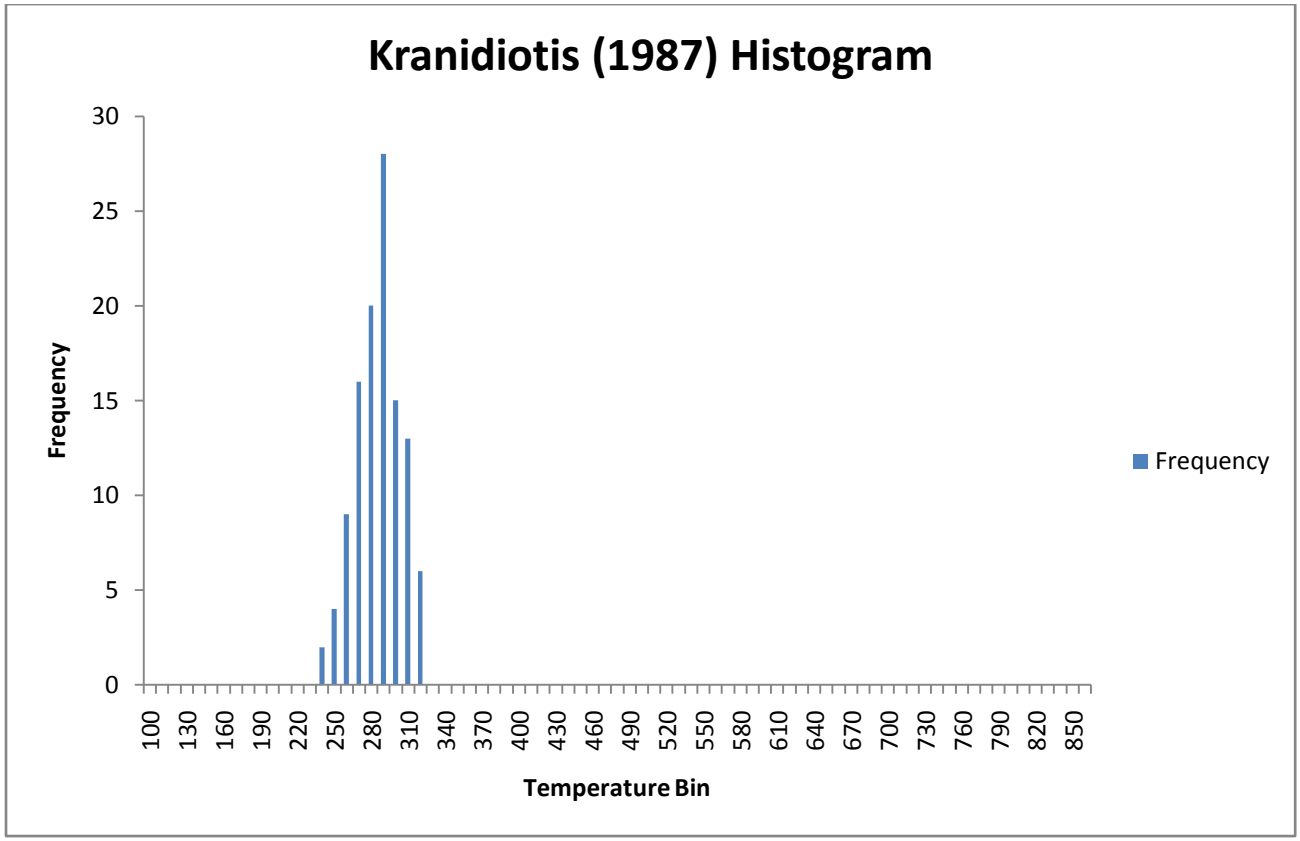

Figure 23-Temperature frequency histograms for the Kranidiotis (1987) chlorite thermometer

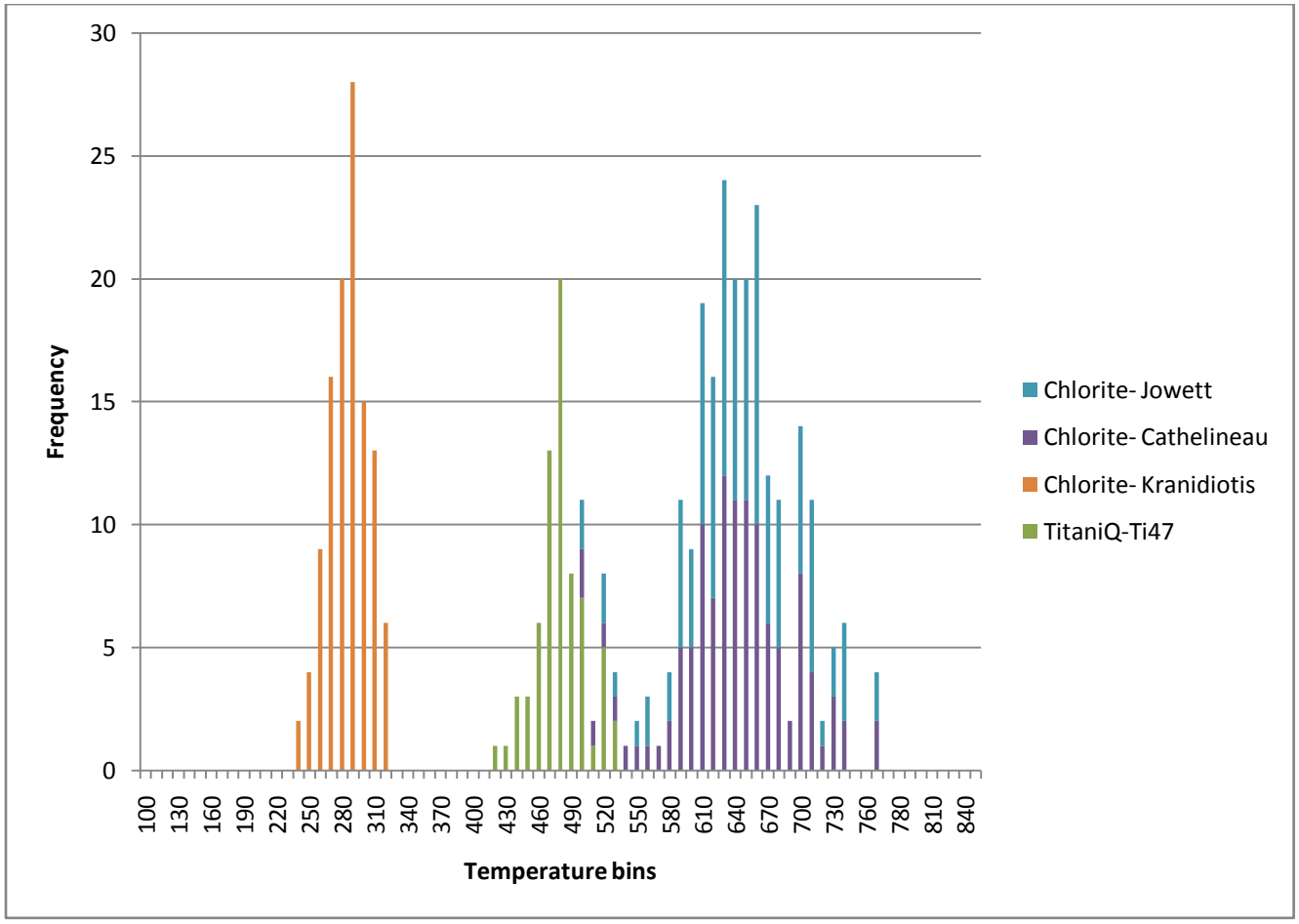

Figure.24- Graphical comparison of the TitaniQ and chlorite temperatures, showing the significant underestimation of the Jowett (1991) method and the slight agreement between the Cathelineau and Jowett thermometers

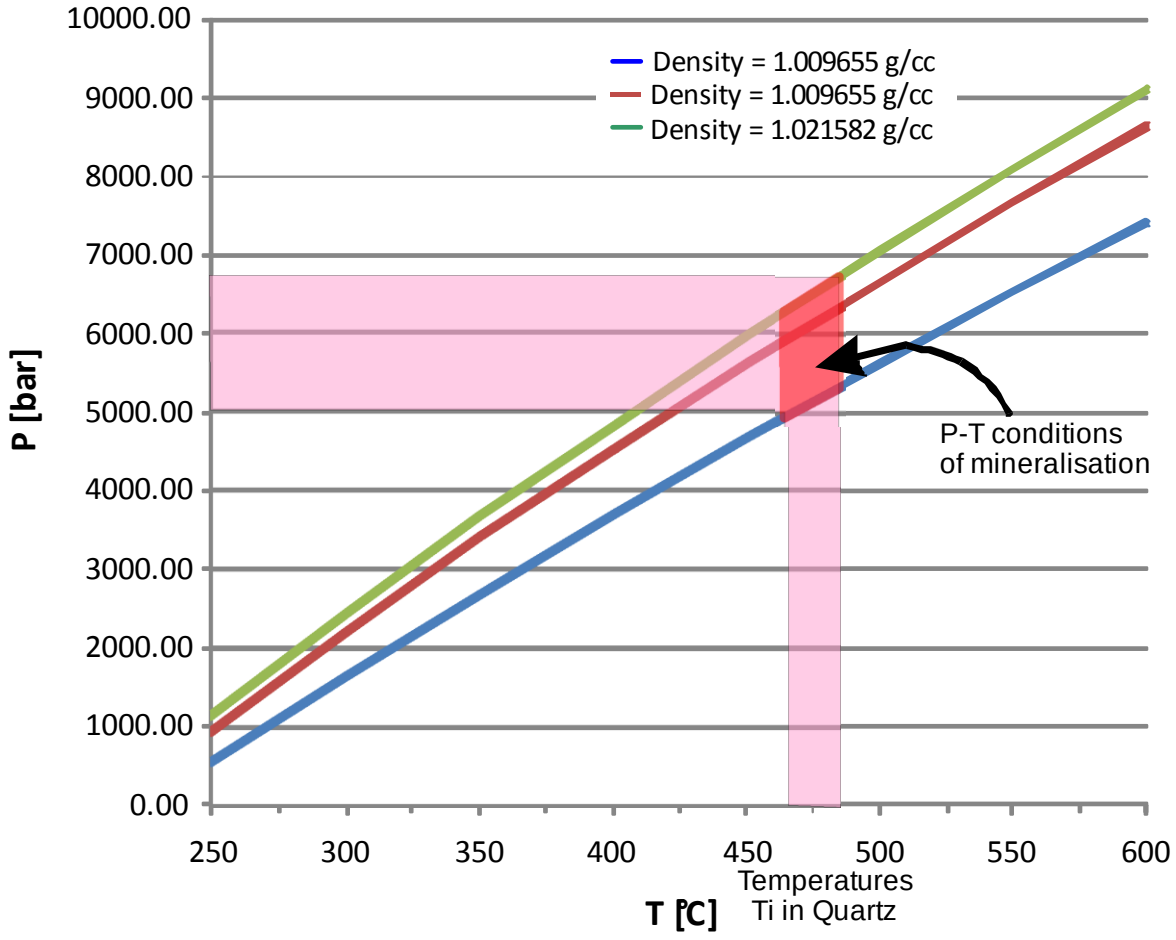

Figure 25-Reconstructed pressure conditions established by the combination of TitaniQ and Fluid Inclusion data

Figure.26- Depicts the δS^{34} ranges for several IOCG style deposits throughout the Gawler Craton and the rest of the world and shows that the Moola Prospect sulphur isotope range fits in with a magmatically derived, mantle sourse for its sulphur. Modified from Hunt et al 2007.

Hole ID: ML001
Sample Number: RJ001(Thin Section)
Depth: 75.6m
Reason for Sampling:
Representative sample of the top of the hole, investigating the style of alteration present which is forming the large red/brown veins and assess in impact of weathering on this rock.

Hand specimen Description:
: Blue/green well foliated dense rock, with bands of plagioclase + quartz and red pink alteration bands (haematite dusted feldspars or albite?) Amphibolite?

Transmitted Microscopy
└>Mineralogical and textural description

This thin section is a representative sample of the highly weathered and altered section which is prevalent at the top of the hole and appears to contain two distinct domains of simular mineralogy but different characteristics.

The first domain comprises the two distal portions of the sample which are dissected by the central, second domain. These two portions are dominated by fine→ medium grained, platy, dark green chlorite, fine grain sericite as in fill around grains and as large vein like sections along with minor occurrences of yellow strained chlorite in the proximity of the large veins prevalent in this domain, these stained areas have a notably higher birefringence then the surrounding chlorite.

Accompanying these alteration minerals are fine→ medium grained discontinuous occurrences of anhedral, quartz which occur as both small clusters and isolated grains, and minor occurrences of sub→anhedal epidote are localise within this domain and appear to be focused around the large→ medium sized vein network. These veins are prominent throughout the sample and are comprised of fine grained sericite, void and "Red Smudging" which is iron rich clay formed as a bi-product of weathering of feldspars.

The second domain is comprised of fine grained platy chlorite and sericite, the latter of which occurs in a higher concentration then the first domain. Occurrences of sub→anhedal epidote and the discontinuous quartz are still present in trace amounts, but the grain size of which are reduced from those in the first domain.

Minor occurrences of opaque minerals, most likely haematite, are seen throughout both domains they are genially fine→medium grained anhedral and share the same preferred orientation as the host rock which clearly defines the parallel linear banding as the primary fabric of the rock.

Interpretation
The protolith of this sample is difficult to deduce due to the high level of both alteration and weathering it has undergone. Multiple phases of alteration can be identified including sodic or potassic, sericite and chlorite alteration.
The sodic or postssic alteration cannot be further identified do to its extensive replacement by sericite. This phase is highly inferred from interpretations of the current petrography but is essential in explaining the presence of cluster and vein like sericite sections instead of the porpharitic phenocrysts found throughout the rest of the hole. which has been created during the production of the thin section and is in part due to the brittle composition of the alteration.

Hole ID: ML001
Sample Number: RJ002 (Thin Section)
Depth: 107.0m
Reason for Sampling:
Representative sample of the small amphobolite unit, which is strongly magnetic. The sample also contains haematite and carbonate veining within the minor brecciation present.

Hand specimen Description: Massive fine grained amphibolite unit, composed of hornblend-Biotite-Plagioclase. It is strongly magnetic (possible magnetite) and contains varying sized carbonate veins with evident haematite present (Red Dusting)

Transmitted Microscopy
↳>Mineralogical and textural description

This thin section is a representative sample of the amphiolite unit often associated with in the Myola volcanic and appears to contain two distinct domains formed via a gradation in the intensity of alteration experienced across the sample [A]. The first domain consists predominantly of coarse grained, anhedral amphiboles [B], minor occurrences of fine→ medium grained platy chlorite and opaque ore minerals, dominated by magnetite due to the magnetic nature of the sample, which is being replaced by haematite. These components are supported by a fine grained sericite matrix which shows evidence of replacing large plagioclase components of the sample. Fine→ medium grained occurrences of discontinuous anhedral, quartz also present as both small clusters and isolated grains throughout this domain.

The second domain is defined by the gradation in the intensity of alteration experience, which increases within proximity to the small carbonate vein which transects the sample [C]. The vein consists of predominantly medium grained, subhedral, carbonate and some minor occurrences of subhedral quartz, where as the surrounding area shows an increase in fine grained bladed chlorite replacing the amphiboles and an increase in the amount of fine grained sericite present. The gradation continues across the sample and results in the complete replacement of the amphibolite unit by chlorite and complete sericite replacement of the feldspars.

Interpretation

This sample is interpreted to be from an amphibolites sill which is commonly found intruding the Myola Volcanics, and from the presence of carbonate veining and chlorite alteration this sill was in place before the hydrothermal event of the area. The replacement of magnetite by haematite varies across the sample but predominantly appears to be in the advance stages. This replacement is common in IOCG style alteration although the magnetite was most probably an original component of the sample before any hydrothermal alteration occurred.

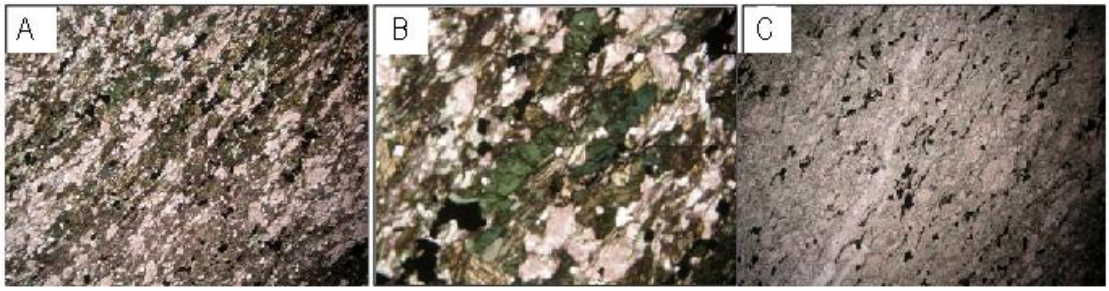

Hole ID: ML001
Sample Number: RJ006 (Thin Section)
Depth: 162.7-162.8m
Reason for Sampling:
Representative sample of highly altered, felsic volcanic unit (rhyolite), targeting apparent sericite alteration and visual amounts of disseminated pyrite and chalcopyrite.

Hand specimen Description:
Medium to fine grained pink to green, highly sericite altered volcanic rock rhyolite? with multiple stages of quartz veining with chalcopyrite and bornite? present.

Transmitted Microscopy
↳>Mineralogical and textural description

This thin section is comprised of fine→medium grained groundmass consisting of anhedral interlocking quartz and a high percentage of fine grained sericite infill which occurs between grains. Supported within the groundmass is remanent coarse grain, anhedral feldspars phenocrysts, which have undergone intense sericite alteration with a high percentage having achieved complete replacement, forming psuedomorphs [A]. Some of the phenocrsts can be identified as plagioclase as they display its characteristic simple twinning.

A large vein transects the sample consisting of coarse, subhedral interlocking recrystallised quartz along with some occurrence of coarse grained carbonate. This vein cross cuts the apparent fabric of the host rock which is created by the preferred orientation of the ground mass and the larger phenocrysts [B].

Other minor components present include trace occurrences of dark green, anhedral amphiboles, disseminated occurrences of anhedral opaques, most probably sulphides and a varying assortment of muscovite occurring as both coarse grained tabular crystals and as medium→ fine grained subhedral occurrences found around and between other grains.

The amphibole and muscovite present in the sample do not appear to have a preferred orientation and seem to exist independent of the fabric formed by the other minerals in the sample [C].

Interpretation

This sample is of the porphratic rhyolite which has undergone extensive sericite alteration followed by a quartz veining phase which cross cuts the sample and the replaced phenocrysts

Hole ID: ML001
Sample Number: RJ008-Vein (Thin Section)
Depth: 170.3-170.5m
Reason for Sampling:
Quartz vein hosting significant amount of mineralization, both pyrite and chalcopyrite, housed within felsic volcanic unit.

Hand specimen Description:
Large quartz -carbonate vein containg chalcopyrite cutting fabric of highly altered (sericite, carbonate, quartz) rhyolite.

Transmitted Microscopy
↳>Mineralogical and textural description

This thin section is dominated by a large quartz vein which houses a significant occurrence of mineralisation. The vein is hosted within a highly silious section of the rhyolite unit which is predominantly composed of medium→ coarse grained anhedral quartz and along with coarse grained subhedral feldspars [A]. The latter of which shows evidence of being replaced via sericite alteration, with some occurrences ranging from completely intact to almost fully replaced. Sericite also occurs within the extensive thin vein network, prominent in this sample, and as very fine grained infill around grains [B].

The vein housing the opaque ore minerals is dominated by medium → coarse grained interlocking quartz crystals of varying crystal habits (tabular, eqant, subhedral), which both surround and are included within the opaques, with those crystals in direct contact having a highly anhedral shape [C]. Fine grain quartz groundmass is also present in places which supports the coarse crystals.

Minor occurrences of carbonate are also present throughout the vein and within the mineralisation in the form of fine→ medium grained sudhedrel crystals, though one section of the vein does indicate a higher amount of carbonates at the centre of the vein, however this cannot be further identified due to the orientation of the sample within the vein.

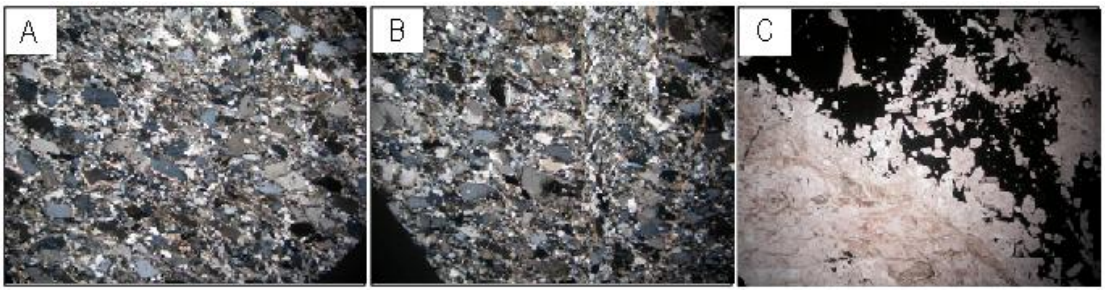

Hole ID: ML001
Sample Number: RJ008-Host Rock (Thin Section)
Depth: 170.3-170.5m
Reason for Sampling:
Larger representation of the host rock housing the mineralisation bearing quartz vein, typical highly altered felsic volcanic, definite sericite alteration present.

Hand specimen Description:
Fine to medium grained, highly sericite and chlorite altered redish to pink rock volcanic rock, with prominent multiple generations of quartz ± carbonate with chalcopyrite mineralisation.

Transmitted Microscopy
↳>Mineralogical and textural description

This thin section displays a gradational change in the composition of the sample. Going from one extent which consists of large coarse grain, subhedral feldspars phenocrysts, displaying simple twinning, housed within medium grained, subhedral quartz [A]. Sericite infill is present to a moderate degree found around grains and also within phenocryst via complete and partial replacement of the feldspar crystals.

Further across the thin section ther is a distinct increase in the amount of sericite infill between grains and replacement experience by the large phenocryst, which has lead to the complete replacement of a large percentage of them [B].

Minor isolated occurrences of sub→anhedral microcline are present and display a strong 'cross hatching' twinning, medium grained, anhedral hornblende is also present along with trace amounts of disseminated opaque minerals scatter throughout the sample.

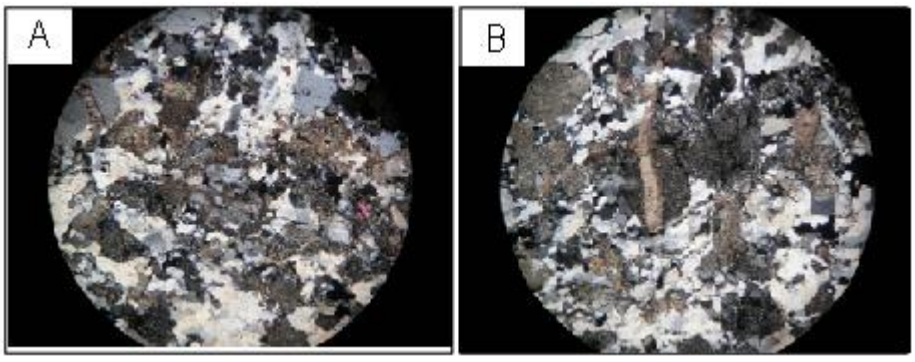

Hole ID: ML001
Sample Number: RJ009 (Thin Section)
Depth: 189.5-186.6m
Reason for Sampling:
Representative sample of the highly weathered felsic volcanoclastic section, the sample also contains minor occurrences of native copper.
(Thin and Polished section)

Hand specimen Description:
Light green/white to grey/green moderate → highly weathered felsic volcanoclastic containing native copper occurrences, void spaces with minor quartz crystal regrowth, moderate brecciation

Transmitted Microscopy
↳>Mineralogical and textural description

This thin section is a sample of the highly weathered zone containing native copper found halfway down the hole, though due to the unconsolidated state of a majority of unit this sample was chosen for its stability not that its is a representative sample.

This sample is comprised predominantly of a fine grained equant quartz and sericite matrix which hosts very fine grained platy chlorite which appears highly weathered [A] and does not match the chlorite found elsewhere in the hole. The quartz present also appears to have fine grained sericite inclusions, giving it a messy/foggy appearance.

Quartz veins ranging from 1-3mm, form a cross cutting network across the sample which is comprised of medium→ course grained subhedral quartz, with the size of the crystals being correlated to the size of the vein they are housed within [B]. In stark contrast the quartz in the veins does not contain any speckley sericite inclusions which makes identifying it easy. Accompanying the quartz within some veins is 'Red Smudging', an iron rich clay, which is a bi-product of weathering feldspars, it is found surrounding quartz grains in the vein [C].

Interpretation

The protolith of this sample can be identified as the Rhyodacite unit, as it contains remanent traces of high chlorite concentration and lack theh large sericite replaced feldspar phenocrysts characteristic of the felsic volcanic unit (Rhyolite). This section of the hole has undergone a server amount of weathering which has reduced the chlorite present to trace levels compared to its typical amounts, all mineralisation both haematite and sulphides are lacking in this section,having been re-mobilised during weathering processes and redeposited elsewhere in the area, and which is the reason behind the presence of native copper in the section.

This section is 189.5-186.6m down the hole and is interpreted as being within a fault or shear zone, which are common along the front of the ranges and which is responsible for the weathering of these rocks at depth as it allowed access of meteoric water.

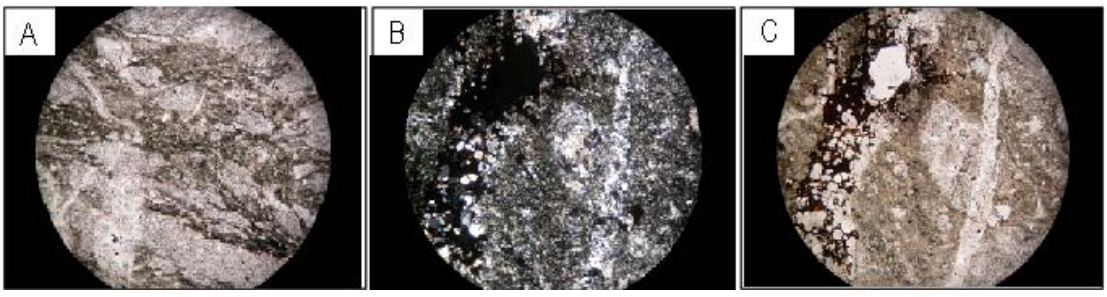

Hole ID: ML001
Sample Number: RJ010 (Thin Section)
Depth: 202.0-202.2m
Reason for Sampling:
Represnetative sample of the rhyodacite unit which contains apparently disseminated mineraslisation, only chalcopyrite.

Hand specimen Description:
Black/ blue fine grained rhyodacite with fine quartz veins with chalcopyrite. Some chalcopyrite mineralisation appears disseminate.

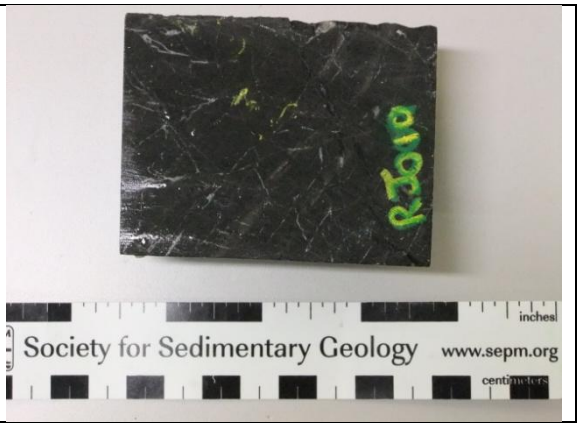

Transmitted Microscopy
↳>Mineralogical and textural description

This thin section is targeted on the rhyodacite comprised of fine grained quartz and sericite matrix which houses anhedral opaque ore minerals, most likely haematite, fine grained anhedral carnbonate along with extensive fine→ medium grained platy chlorite alteration which is extencive throughout [A].

In preserved areas these mineral appear to have a preferred orientation, except the carbonate, which define the linear fabric of the rock but in proximity of the carbonate vein network that transects the sample the fabric in both cross cut and deformed into swirled non- linear pattern [B].

The Carbonate veins present throughout the sample range form 1-3 mm and are composed of fine→ medium grained sudhedral ?carbonate along with varing amounts of fine grained to sub→anhedral quartz .

Also present within the carbonate vein is occurrences of coarse grain sub→anhedral opaques, most likely chalcopyrite.

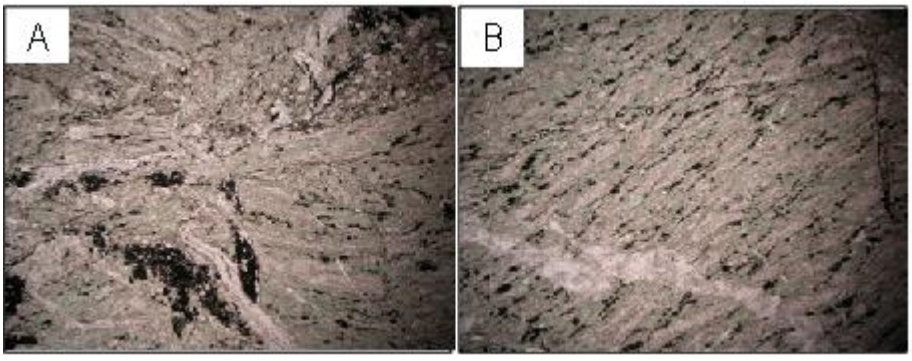

Hole ID: ML001
Sample Number: RJ012 (Thin Section)
Depth: 206.6-206.8m
Reason for Sampling:
Large carbonate vein hosting a significant amount of mineralisation, only chalcopyrite, which is housed within rhyodactite volcanic.

Hand specimen Description:
Black/ blue fine grained rhyodacite with a large carbonate vein (3-4cm) containing chalcopyrite cutting the fabric.

Transmitted Microscopy
↳>Mineralogical and textural description

This thin section is dominated by a large carbonate vein which houses a significant occurrence of mineralisation, most likely chacopyrite. The vein is hosted within the rhyodacite unit which is comprised of fine grained quartz and sericite matrix which houses anhedral opaque ore minerals, most likely haematite, along with extensive fine grained platy chlorite, ranging up to course grained in areas [A].

These components of the host rock all exhibit a preferred orientation creating the primary fabric of the rock, which is highlighted by the banding Xenoliths of the host rock which are incorporated within the primary carbonate vein [B], also contain the same fabric and composition all though they have been rotated during the formation of the vein.

The primary vein is composed predominantly of coarse→ medium grained, subhedral interlocking ?carbonate, grading to fine→ medium occurrences along the grain boundaries of the mineralisation and host rock. Instances of medium grained platy chlorite are also found within the vein and appear to occur predominantly at the outer extremities of the vein.

Secondary carbonate veins commonly cross cut the host rock fabric, the main vein and themselves, forming a vein network throughout the sample. This cross cutting along with compositional variences in the veins indicate multiple generations of carbonate veining, which is highlighted in [C] which depicts multiple cross cutting and overlapping veins Most veins are composed of both coarse and fine grained ??carbonate which are primarily anhedral, with some consisting of minor fine→ medium grained, anhedral quartz.

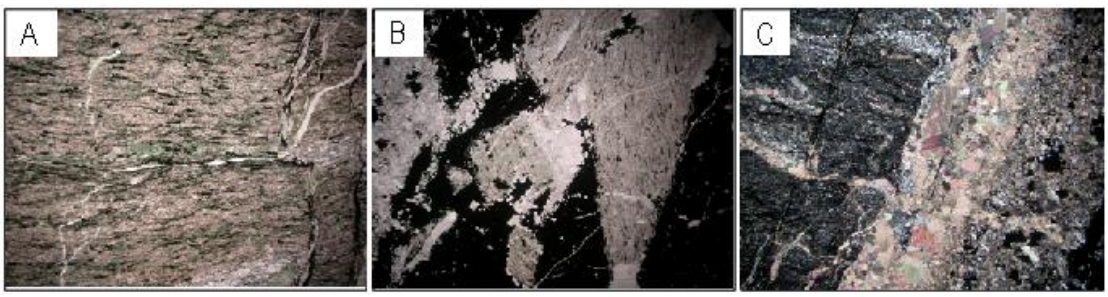

Hole ID: ML001
Sample Number: RJ013 (Thin Section)
Depth: 214.6-214.7m
Reason for Sampling:
Another representative sample of the rhyodacite unit, this time targeting a highly deformed and vein rich section.

Hand specimen Description:
Black/ blue fine grained highly deformed rhyodacite with abundant carbonate veining.

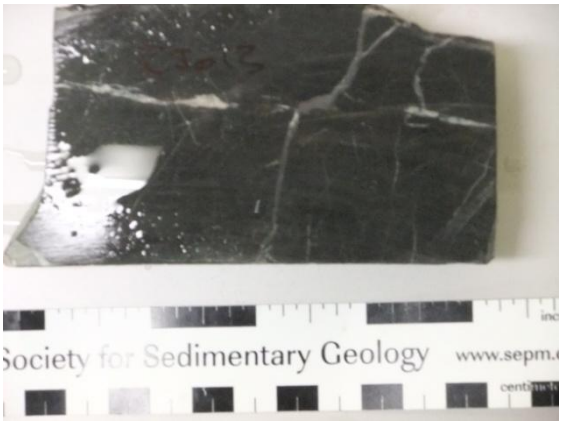

Transmitted Microscopy
↳>Mineralogical and textural description

This thin section is a representative sample of a highly deformed section of the rhyodacite unit. Similar to the rest of the unit this sample is comprised of fine grained quartz and sericite matrix which houses anhedral opaque ore minerals, most likely haematite, along with extensive fine→ medium grained platy chlorite.

These minerals all appear to have a preferred orientation, which forms the primary fabric of the rock which for a majority of the sample is a parallel linear banding which is defined predominantly by the opaques present. [A]

Due to the extensive veining and deformation experienced by the sample the fabric is not homogeneous throughout, often diverting around large veins forming localised, parallel sweeping bands. [B]

The extensive vein network present in this sample ranges between 1-3mm and are predominantly composed of course→ fine grained, subhedral, tabular carbonates with the size of the crystals being correlated to the size of the vein they are housed within [C]. Fine→ medium grained anhedral quartz is often associated within the veins, with some places appearing to have it as the dominant component of the vein. A higher percentage of anhedral opaques, most likely haematite is found concentrated around the edges of the large veins.

Cross cutting veins are very common throughout, along with the offsetting of once continuous veins which records the variant deformation history of this sample.

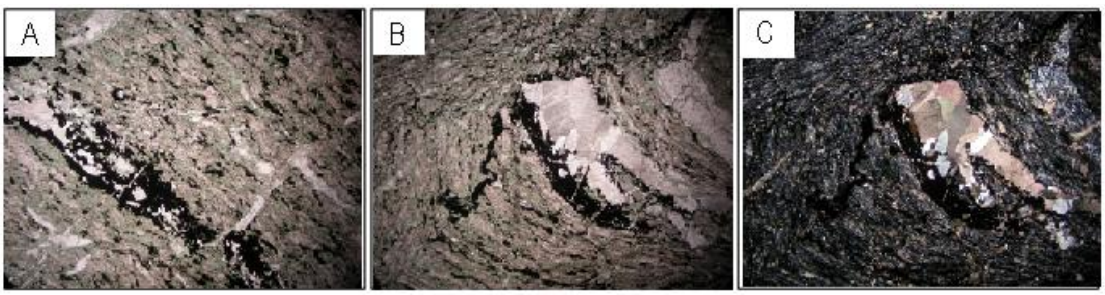

Hole ID: ML001
Sample Number: RJ014 (Thin Section)
Depth: 238.8-238.9m
Reason for Sampling:
Targeting highly heterogeneous swirling layered section which is similar in appearance to the rhyodactite units seen elsewhere but appears to have a different composition.
Hand specimen Description:
Black blue rhyodacite, interbanded with brown-red (rhyolite)

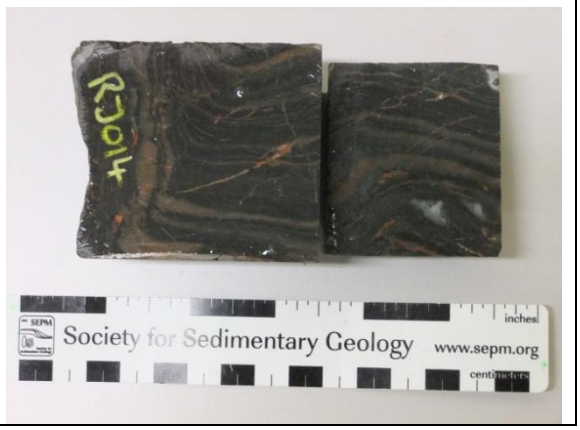

Transmitted Microscopy
↳>Mineralogical and textural description

This sample is highly heterogeneous, even differing vast amounts within its two major components, the first of which is dominated by fine grained tightly spaced, speckley opaque minerals, most likely haematite, which is supported within two differing fine grain groundmasses. The other major component of this sample is the large quartz and feldspar layering which transect the sample in a curved and sweeping pattern forming a layering texture along with the opaque dominant component.

The opaque dominated portions are supported by two distinct matrixes, fine grained quarts and fine grained sericite respectably. The quartz supported regions [A] are more tightly packed, meaning less spacing between opaque grain, then there counterpart and the quartz crystals are very fine, beyond the optical capabilities of these microscopes, and are most probably anhedral. Within this portion the opaques are fine grained, bladed and appear to have a preferred orientation which forms a, acute angle to the laying within the sample.

The sericite supported regions [B] have greater spacing between the opaque minerals and there still appears to be the same preferred orientation within the fine grained, opaques but thay have been deformed, becoming wavy and variable, seeming to follow the sericite grains. The sericite matrix is composed of fine grained anhedral occurrences but still retains some enclaves of semi altered quartz regions.

The other major component, the quartz-feldspar layering, is dominated by fine→ medium grained anhedral quartz, with some larger coarse grained recrystallised sections present within [C]. The feldspar components present are medium grain sudhedral occurrences and occur in lower quantities. Fine grained, anhedral opaques are also present within these layers, scattered throughout in trace amounts.

Other minor components within the sample include small→medium sized crosscutting veins of varying composition including chlorite, quartz, carbonates and feldspars. Chlorite is also founded as coarse →medium grained occurrences localised along the boundary of the quartz-feldspar layers.

There are also signs of deformation with the sample through the offsetting of veins and compositional layers.

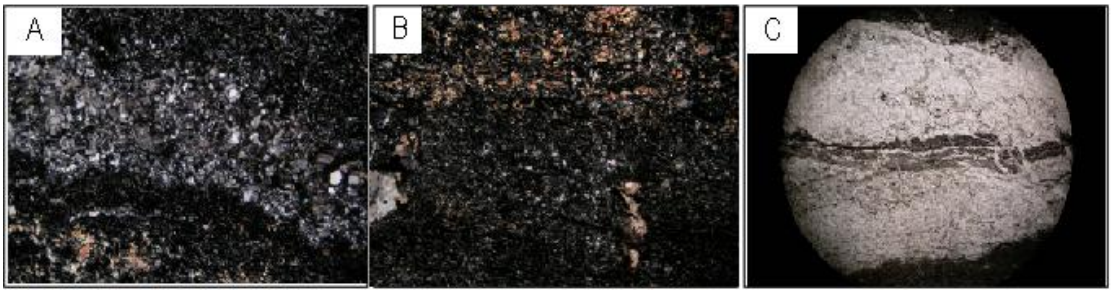

Hole ID: ML001
Sample Number: RJ015 (Thin Section)
Depth: 248.9-249.0m
Reason for Sampling:
Representative sample of the bottom of hole unit, clearly unique to units seen elsewhere in the hole, strange red pheoncrysts/components within a rhyodacite like ground mass.

Hand specimen Description:
Black blue interbanded with red orange rhyodacite/ rhyolite large 2-3cm wide quartz vein sheared by a white (opaque) carbonate vein.

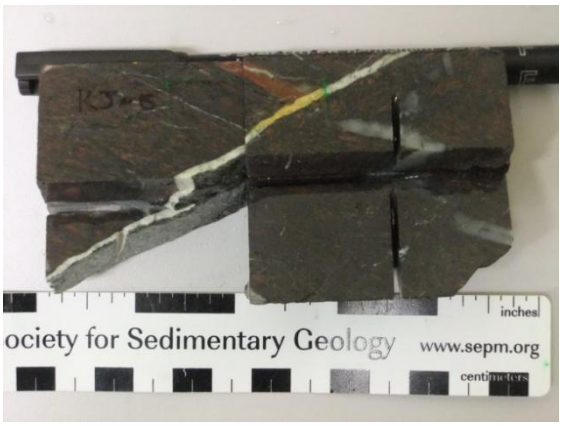

Transmitted Microscopy
↳>Mineralogical and textural description

This thin section is a representative sample of the bottom of the hole, which is comprised of a fine grained quarts and sericite matrix which houses extensive fine→ medium grained platy chlorite, anhedral opaques, mostly likely haematite and phenocrysts of feldspars which have undergone varying extents of sericite replacement, but still exhibit the characteristic simple twinning [A].

Most minerals, excluding the feldspar phenocrysts, appear to have a preferred orientation defined by the opaques and chlorite which form a rough undulating banding throughout the sample which seem to deflect around areas of heavy sericite alteration of feldspars [B]. Localised areas of disturbance indicate the fabric is not homogeneous throughout and contains areas of high deformation.

Small fractures transect the sample, with some forming into minor veins in places, which are comprised of fine grained subhedral carbonate. These fractures/veins often cross cut each other forming offsets of once continuous features [C]. Chlorite appears to have an affinity to these fractures/veins forming around the edges or appearing in greater concentrations in proximity to them.

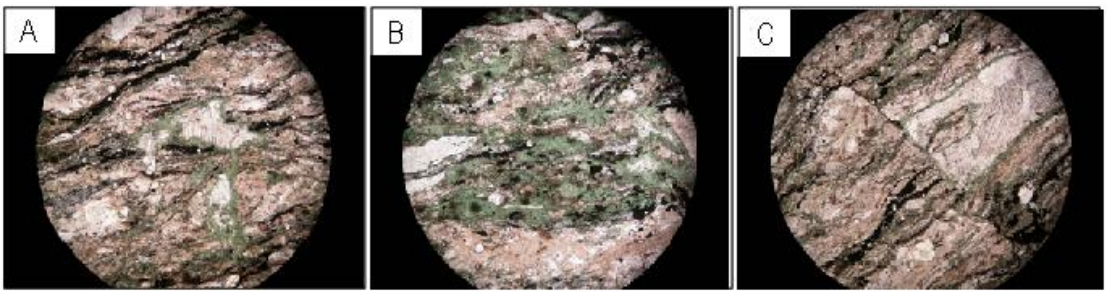

Hole ID: ML001 **Sample Number:** OS001(Thin Section) **Depth:** 212.44-212.51m **Reason for Sampling:** Representative sample of the banded felsic unit, targeting a all major lithology component for identification and classification. **Hand specimen Description:**	

Transmitted Microscopy

└>Mineralogical and textural description

This thin section is a representative sample of the banded felsic unit which is characterized by three major domains which repeat throughout the sample creating the banding.

The first domain is comprised of the remanent large interlocking feldspar phenocrysts which have undergorn intense brecciation and varying degrees of sericite alteration, ranging from sleight to complete replacement. These phenocrysts are hosted within fine→medium grained, anhedral, interlocking quartz, forming XX→XXmm wide bands that are repeated throughout the thin section . This section shows characteristic red staining of the sericite present, which is typical throughout the hole.

The second domain is comprised of medium grained, anhedral, quartz, accompanied by minor fine grained sericite as infill around grains. Hosted within this groundmass is a considerable amount of reminent medium→ coarse, anhedral feldspar which are evenly spaced throughout the domain and have been partially or completely replaced by sericite, to form psudomorphs . Some of these feldspars are still identifiable as being plagioclase as these occurrences still retain the characteristic simple twinning. The preferred orientation of crystals within this domain coincide with the layering of the sample, running parallel to the fabric identified in other domains.

The third domain is primarily composed of fine→ medium grained anhedral quatz and medium grained anhedral feldspars showing varing extents of sericite replacement, which are accompanied by a large amount of fine grained sericite infill around and between grains. Though the composition is predominantly the same there is some variability in the abundance of sericite present which in places can become the dominant mineral. The third domain is significantly finer grained then its counterparts and contains a trace amounts of fine grain chlorite with the sericite matrix .

A large quartz vein also transects the thin section, which is common throughout the sample. It is comprised of fine→ medium grained, interlocking anhedral quatz, which hosts solitary occurrences of fractured coarse grained anhedral feldspar, identified as both microcline and plagioclase via characteristic cross hatched and simple twinning respectably. Also present within the vein is an isolated occurrence of coarse grained platy muscovite which records evidence of deformation experienced by the sample in the offset between its two halves , which has been sheared apart.

Interpretation

Hole ID: ML001
Sample Number: OS003 (Thin Section)
Depth:
Reason for Sampling:
Representative sample of felsic volcanic unit which appears to have banding of highly sericite alteration areas.

Hand specimen Description:
Fine grained sericite and chlorite altered, interlayered grey-pink felsic gneiss.

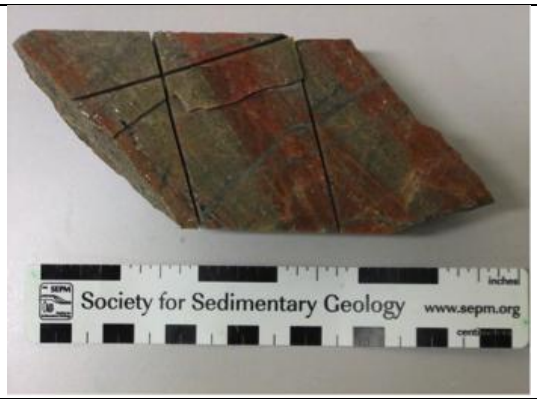

Transmitted Microscopy
↳>Mineralogical and textural description

This thin section is comprised of fine→medium grained groundmass consisting of anhedral interlocking quartz and a high percentage of fine grained sericite infill which occurs between grains. Supported within the matrix is remanent coarse grain, anhedral feldspars phenocrysts, which have undergone intense sericite alteration with a high percentage having achieved complete replacement, forming psuedomorphs . Some of the phenocrsts can be identified as plagioclase as they display its characteristic simple twinning.

Both the ground mass and the larger phenosrictes appear to have a preferred orientation forming a fabric across the sample , also present is distinct zonation in some areas of the sample highlighted by a red discolouration of sericite in plain polar light even though the mineralogy is the same.

A large vein transects the sample consisting of fine grained quartz and sericite matrix which supports medium grained elongate, rectangular quartz which appears to have no preferred orientation. This vein completely cross cuts the fabric of the host rock.

Other minor components present include medium grained platy muscovite which occurs scattered throughout the sample, scattered disseminated opaques, most probably sulphides, and trace occurrences of dark green, anhedral amphiboles.

The amphibole and muscovite present in the sample do not appear to have a preferred orientation and seem to exist independent of the fabric formed by the other minerals in the sample .

Interpretation

This sample is of the felsic gneiss unit which is defined by a subtle change in the groundmass quartz shape from subhedral, equant to elongate and a general decrease in grain size. Extensive alteration of the feldspar for sericite is the defining feature in hand specimen with the banding of larger phenocryst standing out. Compositionally this sample is the same as rhyolite units found throughout the hole.

Hole ID: ML001
Sample Number: OS004 (Thin Section)
Depth: 82.98-83.10m
Reason for Sampling:
Representative sample of the intrusive granite unit, targeted to get composition.

Hand specimen Description:
Medium grained porphryritic pinkish microgranite.

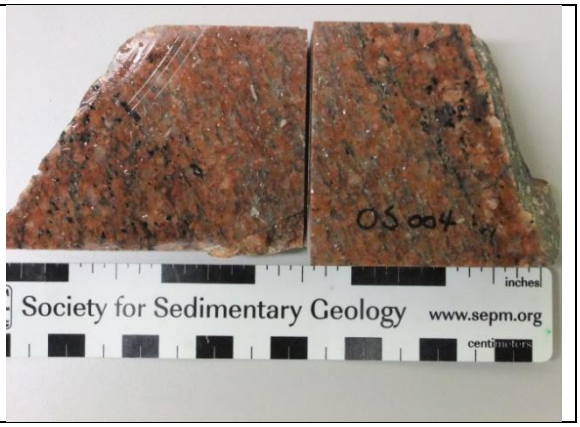

Transmitted Microscopy
↳>Mineralogical and textural description

This thin section is a representative sample of the granite unit present within the drill core. It is composed of large coarse grained sub→andhedral feldspar phenocrysts, which form a porphyritic texture. Both plagioclase and microcline comprise the phenocrysts, displaying their characteristic simple and cross hatched twinning respectively , they are also effected by varying stages of fine grained sericite alteration, ranging from none to fully replaced psudomorphs.. Perthite exsolution patterns are also found within some phenocrysts, formed via the intergrowth of potassium rich and sodium rich feldspars.

Fine grained sericte is also found within the surrounding groundmass, which is predominantly comprised of anhedral, medium grained, interlocking quartz.

Other minor components present include subhedral and tabular, dark green amphiboles along with coarse grained magmatic muscovite which occur as large isolated tabular grains, infill and some as inclusions within the feldspar phenocrysts.

Interpretation

Typical granite composition and texture which has undergone extensive sericite alteration of the plagioclase and K-Feldspar phenocrysts, ranging from partial to full replacement.